

NAGOYA UNIVERSITY

DOCTORAL THESIS

**High-Efficiency Cutting with
Spindle Speed Variation**

Author:

Soohyun Nam

Supervisor:

Dr. Eiji Shamoto

*A thesis submitted in fulfilment of the requirements
for the degree of Doctor of Engineering*

in the

Manufacturing Engineering Research Group
Graduate Department of Aerospace Engineering

Declaration of Authorship

I, Soohyun Nam, declare that this thesis titled. “High-Efficiency Cutting with Spindle Speed Variation” and the work presented in it are my own. I confirm that:

- This work was done wholly or mainly while in candidature for a research degree at this University
- Where any part of this thesis has previously been submitted for a degree or any other qualification at this University or any other institution, this has been clearly stated.
- Where I have quoted from the work of others, the source is always given. With the exception of such quotations, this thesis is entirely my own work.
- I have acknowledged all main sources of help.
- Where the thesis is based on work done by myself jointly with others, I have made clear exactly what was done by others and what I have contributed myself.

Signed : Soohyun Nam

Date : 2020. 11. 25

CONTENT

Chapter 1.

Introduction

1. 1 Background	1
1. 1. 1 Chatter suppression techniques	4
1. 1. 2 Spindle speed variation (SSV)	7
1. 2 Motivation and objective	9
1. 2. 1 Motivations	9
1. 2. 2 Research objectives	10
1. 3 Real-World Data Circulation in thesis	12
1. 4 Construction of thesis	16

Chapter 2.

Proposal of Novel Chatter Stability Indices of Spindle Speed Variation

2. 1 Introduction	19
2. 2 Characteristics of chatter growth in SSV	20
2. 2. 1 Dynamic model of orthogonal cutting process	21
2. 2. 2 Chatter growth/suppression in SSV	23
2. 3 Analytical investigation of chatter stability in SSV	26
2. 3. 1 Time-domain simulation model	26
2. 3. 2 Formulation of SSV profiles and introduction of stability indices	27
2. 3. 3 Simulation conditions and profile examples	28
2. 3. 4 Simulation results and discussions	31
2. 4 Experimental verification	34
2. 4. 1 Experimental setup	34
2. 4. 2 Measurement of dynamic compliance of tool	35
2. 4. 3 Cutting experiments with CSS	38
2. 4. 4 Cutting experiments with TSSV and comparison with simulations	40
2. 5 Summary	44

Chapter 3.

Proposal of Novel Spindle Speed Variation Profile with Constant Acceleration Rate for Improvement of Chatter Stability

3. 1 Introduction	48
-------------------	----

3. 2 Proposal of CAR-SSV	49
3. 2. 1 Concept of CAR-SSV	49
3. 2. 2 Formulation of CAR-SSV profile	53
3. 3 Analytical investigations of CAR-SSV	55
3. 3. 1 Time-domain simulation model	55
3. 3. 2 Comparison with conventional SSV based on stability indices	57
3. 3. 3 Clarification of effects of CAR-SSV parameters on stability	60
3. 3. 4 Comparison with conventional SSV focusing on its applicability	63
3. 4 Experimental investigations into CAR-SSV	67
3. 4. 1 Experimental setup	67
3. 4. 2 Measurement of dynamic compliance of tool shank	68
3. 4. 3 Cutting experiments with constant spindle speed	70
3. 4. 4 Method for generating CAR-SSV profile and experimental conditions	72
3. 4. 5 Experimental results and discussions	75
3. 5 Summary	81

Chapter 4.

Proposal of ‘accelerative cutting’ for Suppression of Regenerative Chatter in Short-duration Cutting

4. 1 Introduction	85
4. 2 Accelerative cutting and its advantage	87
4. 2. 1 Limit of SSV	87
4. 2. 2 Proposal of accelerative cutting and its advantage	88
4. 3 Time-domain simulation of accelerative cutting	89
4. 3. 1 Time-domain simulation model	89
4. 3. 2 Simulation results	91
4. 4 Experimental results and discussions	94
4. 4. 1 Experimental setup and conditions	94
4. 4. 2 Results and discussions	97
4. 5 Summary	98

Chapter 5.

Real-World Data Circulation in High-Efficiency Cutting

5. 1 Real-World Data and its measurement in High-Efficiency Cutting	100
5. 2. Real-World Data Circulation in High-Efficiency Cutting	104
5. 3. Imagined future Real-World Data Circulation of researches in thesis	110

Chapter 6.	
Conclusions	114
References	118
List of Publications	126
Acknowledgements	130

Chapter 1

Introduction

1.1 Background

Metal cutting is an indispensable technology in manufacturing field because it is one of the most widely used methods for producing the products in the automotive, aerospace, and machine manufacturing industries. This technology continues to develop in parallel with advances of computers, sensors, and actuators. Hence, it is till the fundamental manufacturing technique and it expected to remain so for the next few decades [1]. However, when cutting with highly flexible workpieces and/or cutting tools such as thin-walled workpieces and long slender shaped tools, self-excited vibrations called chatter vibration is likely to occur between the tool and the workpiece during cutting. The chatter vibration is a huge obstacle in the cutting process because it causes a breakage/wear of the cutting tool and poor surface finish or even the deterioration of the machine tool life. Figure 1.1 shows chatter problem in numerous machining applications [2]. Moreover, a metal removal rate has to be reduced for the avoidance of chatter vibration, which results in a reduction of machining efficiency. In the actual manufacturing field, additional manual operations are required to clean chatter marks left on the finished surface, and it results in a decrease in productivity and an increase in production cost [3]. For this reason, significant research efforts have been made in modeling and predicting the chatter stability in cutting operations.

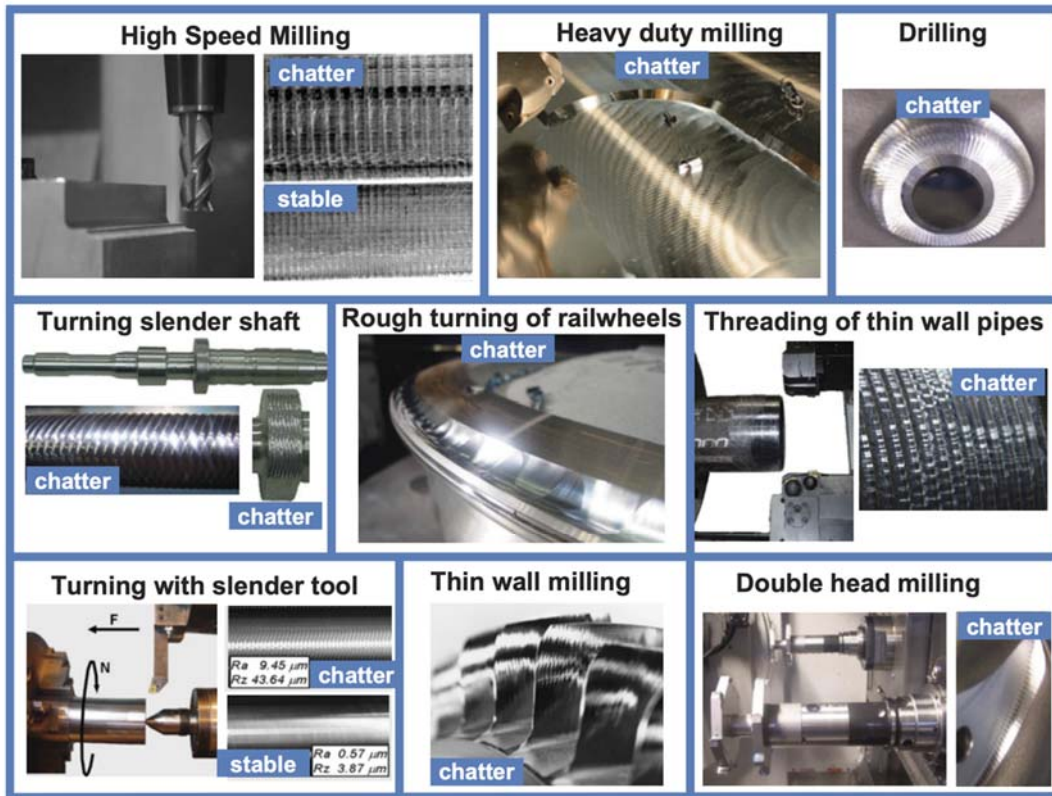


Fig. 1.1. Chatter problem in numerous machining applications [2].

The first attempts to describe the chatter vibration were made by Arnold [5], Hahn [5], and Doi et al. [6]. A comprehensive mathematical model and analysis was firstly introduced by Tobias [7]. A variable types of chatter vibrations have been studied throughout the history. The self-excited chatter vibrations may be caused by regeneration of the chip thickness [8, 9], mode-coupling phenomena [10], and excitation effect from the contact between the flank face and the workpiece, i.e., frictional chatter [11,12]. The regenerative chatter is induced by regeneration of wavy surface on the workpiece left during the previous revolution in turning or by a previous tooth in milling during it is removed in the succeeding revolution or tooth period [13]. When the phase shift between the previous and present waves makes unstable relation, the maximum chip thickness may grow exponentially while oscillating at a chatter frequency that is close to, but not equal to, a dominant structural mode in the system [14]. The mode-coupling chatter occurs when there are excitations of two-directional orthogonal modes in the plane of cut. Specifically, it occurs if the vibration in the thrust force direction generates vibration in the cutting force

direction and vice versa, and this results in simultaneous vibration in those two directions [1]. The frictional chatter occurs due to the excitation effect from the friction force when the clearance face of the tool contacts with the workpiece [1, 12], i.e., ploughing process. It is known that the frictional chatter tends to occur when the tool is worn since the contact between the clearance face and the workpiece becomes critical. However, those contact between the clearance face of the tool and workpiece can act on a decrease in the vibration of the vibratory system, i.e., process damping effect occurs, when the force is in the reverse phase with the vibration speed [12]. The process damping makes system significantly stable in the low-cutting-speed region [15, 16]. As described above, the frictional chatter and the process damping occur from the same mechanism, but they have been dealt separately and differently in the extensive of studies [12]. Hayasaka et al. [12] proposed a new consolidated model for realizing the analytical prediction of the critical stability by considering the frictional chatter and the process damping simultaneously.

Among many types of chatter vibration, the regenerative vibration most commonly occurs in the cutting process [1]. Kaneko et al. [17] and Marui et al. [18-20] provided clear evidence that the regenerative effect is dominant when compared with other types of chatter by experimental investigations. For example, Marui et al. [18-20] compared the size of the vibratory locus for the frictional chatter and the regenerative chatter, and the results denoted that the regenerative locus is approximately ten times bigger than the frictional locus. Many studies have been carried out for predicting regenerative chatter stability to avoid it. Tlustý et al. [13] presented a stability limit, i.e., the maximum cutting load can avoid the regenerative chatter, can be calculated based upon the system dynamics for orthogonal cutting. After that, Meritt et al. [21] presented stability lobe diagram (SLD) which can predict the stability limit in terms of cutting parameters such as depth of cut and spindle speed. Since it allowed an improvement in machining efficiency without the regenerative chatter by selecting the appropriate process parameters, it was a critical contribution. Extensive studies have conducted to propose SLD not only for single degree

of freedom (SDoF) turning process but also 2DoF [22]/3DoF [23] turning process and milling process [24]. The information and knowledge acquired from those studies have been used in real-world applications [12].

1.1.1 Chatter suppression techniques

In addition to the method of avoiding regenerative chatter based on SLD, chatter suppression techniques have become major concerns for achieving high productivity, high precision, and low production costs. By improving the design of the machine tool and cutting tools or by using additional devices that can disrupt regenerative effect, the chatter can be suppressed [3]. These additional devices are involving vibration absorbers [25] and friction dampers [26]. Xiao et al. [27] experimentally presented the chatter suppression effect by applying vibration cutting. Special milling tools such as variable pitch and/or helix angle tools shown in Fig. 1.2 have been developed for suppressing chatter. Since those tools have multiple time delays between the past and the present vibrations, they can disturb the regenerative effect [28-32]. In order to improve chatter stability, many studies have been conducted on the design method of those tools [30-33].

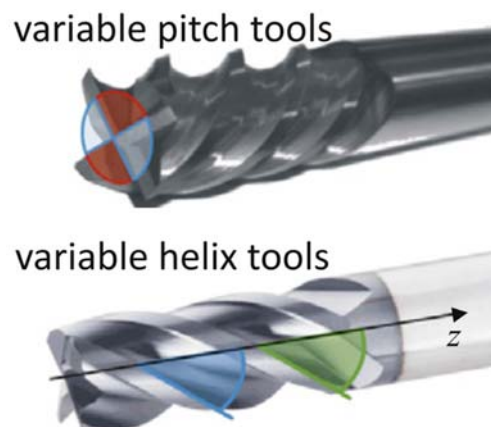


Fig. 1.2. Special milling tool for suppressing regenerative chatter [2].

Budak et al. [34] demonstrated that parallel turning shown in Fig. 1.3 (a) can increase the stability limits compared to turning operations with a single tool because of the dynamical interaction between the tools. It is described

that the stabilizing effect is especially obtained then the natural frequencies of the turning tools are close to each other. Brecher et al. [35] presented that radial angle between the tools in parallel turning shown in Fig. 1.3. (b) changes the stability limits drastically. By appropriately changing the radial angle depends on the spindle speed, the chatter can be suppressed because the regeneration between consecutive tools can be disturbed.

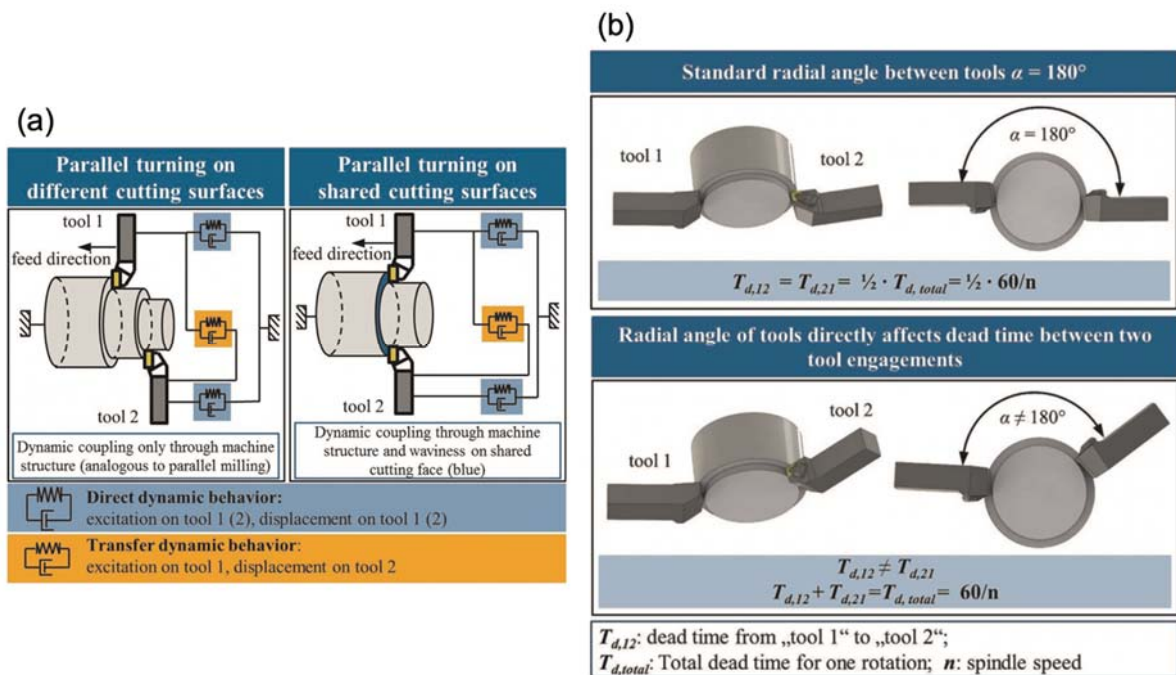


Fig. 1.3. (a) Parallel turning for chatter suppression (b) Influence of radial angle [35].

Meanwhile, when cutting the same workpiece by utilizing two or more milling tools, i.e., parallel milling process, occurs strong chatter problems [2] in case the phase shift between subsequent tooth passes makes unstable relation. Shamoto et al. [36] proposed the method to suppress the chatter in the parallel milling process by making speed difference in the two cutting tools to cancel out the regenerative effects (Fig. 1.4). The variable pitch/helix angle tools and parallel turning/milling process have the same principle of suppressing the chatter as diminishing the regenerative effect by making multiple time-delays in consecutive tooth passes.

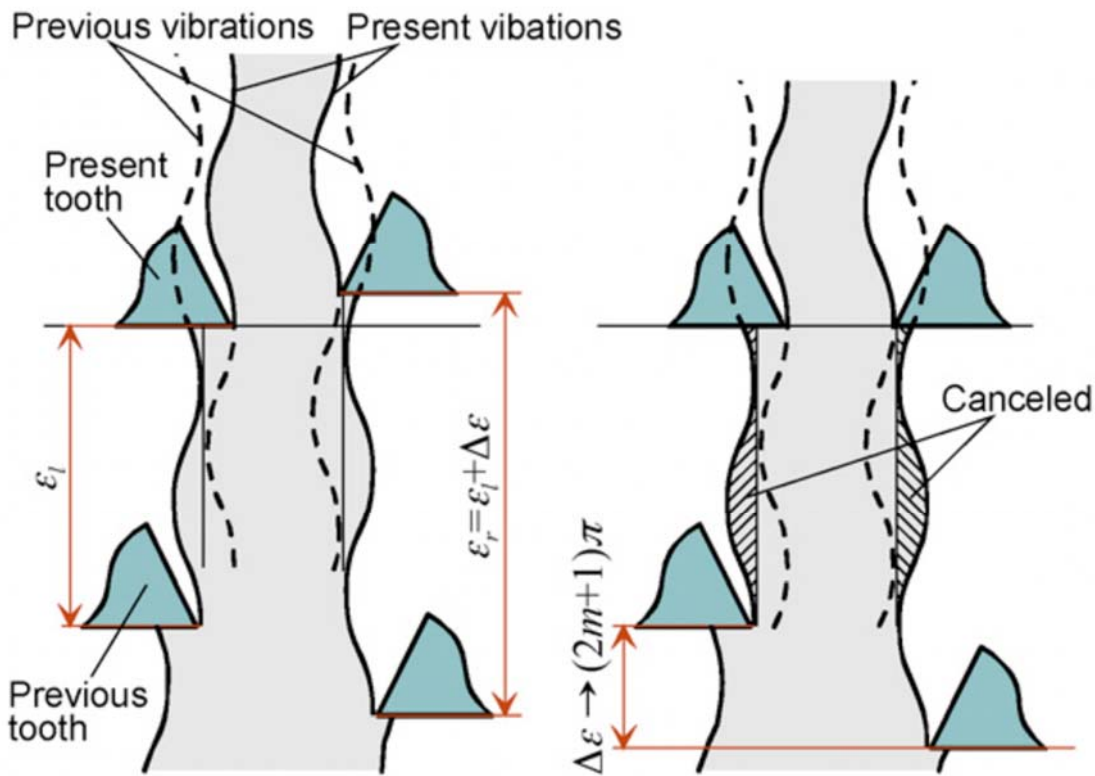


Fig. 1.4. Mechanism for suppressing chatter in parallel milling process (a) Actual cutting (b) Cutting on right side is shifted [36].

It is well known that the chatter stability depends on tool geometry and cutting conditions. Shamoto et al. [37] presented a novel strategy to optimize tool path/posture, in which can avoid chatter and increase the chatter stability. Many strategies are studied to increase the process damping. First, the process damping can be increased by lowering the spindle speed. However, this strategy causes the reduction in productivity. Second, worn tools increase the process damping in clearance face. However, this strategy reveals the increase of the static cutting loads, tool breakage, and poor surface finish due to the worn tool. Third, special edge geometries are studied so that reproduce the performance of a worn tool but cancel the disadvantages of it. Tunc et al. [38] presented that the process damping effect can be increased by cylindrical clearance geometry compared to planar clearance geometry even at higher cutting speed.

In recent years, the production of thin-walled products keeps increasing in order to reduce the weight of aircraft and automobiles. Because of the

flexibility in thin-walled products, the chatter more easily occurs compared to other products. However, it is essentially difficult to predict and suppress the chatter stability of thin-walled products because the workpiece dynamics vary with not only the material removal and the cutter location [2]. For increasing the stiffness throughout the cutting process, appropriate planning of the material removal sequence is important. Alan et al. [39] proposed strategy to maximize the stiffness during the thin-wall machining process. The waterfall machining technique which means the material removal sequence that ensures the stiffness of the thin wall to be high enough to withstand the cutting force and also to avoid chatter has been developed [40].

1.1.2 Spindle speed variation (SSV) and its limitations

Another technique for suppressing the chatter vibration is spindle speed variation (SSV), where the spindle speed is varied cyclically around a nominal speed, i.e., average speed. This technique was proposed by some authors in the seventies [41-44], and still be attracting increasing attention because of its simplicity to implement and effectiveness in chatter suppression. Since this technique can be implemented only with the spindle system without any special tools or devices, it shows high compatibility with other techniques for suppressing chatter vibration [45]. It has been understood that the chatter suppression effect of SSV can be obtained from the time-varying rotational period but constant chatter frequency in every revolution so that the disruption of the regenerative effect occurs [41-44]. Figure 1.5 shows the schematics for the specific explanation of conventional understanding with the chatter suppression effect of SSV. $n(t)$ [min^{-1}], $n(t')$ [min^{-1}], $f_c(t)$ [Hz], and $f_c(t')$ [Hz] in Fig. 1.5 represents spindle speed in one revolution before, spindle speed in present revolution, chatter frequency in one revolution before, and chatter frequency in present revolution. Note that it is assumed that $n(t)$ is lower compared to $n(t')$. In conventional studies, it has been understood that the chatter frequency generated during cutting with SSV is constant, i.e., $f_c(t) = f_c(t')$. Based on the understanding, the number of left waves by

chatter vibration on the cut surface per unit angle f_{sc} [1/rad] varies, i.e., spatial wavelength of chatter vibration $1/f_{sc}$ [rad] also varies. Therefore, the phase shift of the chatter vibration between the present and one revolution before changes, and it causes the disruption of the regenerative effect occurs.

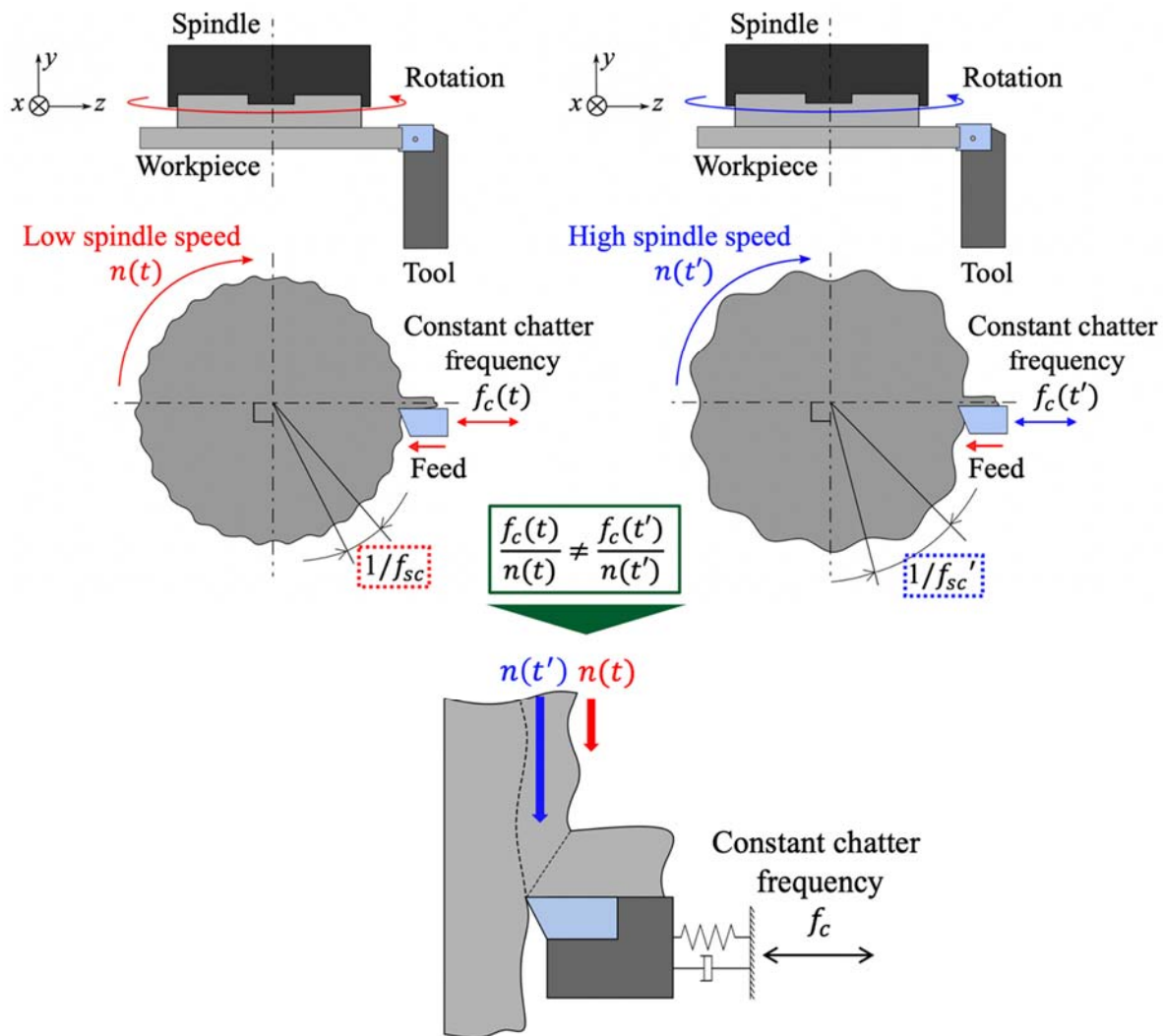


Fig. 1.5. Conventional understanding with chatter suppression effect of spindle speed variation.

There are various types of methods to vary the spindle speed such as sinusoidal [46], triangular [47], rectangular [44], and random [48] SSV. Among them, the sinusoidal SSV is most studied because of its simplicity in control of spindle motor.

1.2 Motivation and objectives of thesis

The chatter suppression effect by utilizing SSV has been verified in previous literatures [46-48] as shown in Fig. 1.6. For utilization of SSV in manufacturing sites, several companies have developed the optional function for SSV, e.g., Machining Navi L-g from OKUMA Corp., SSV function from HAAS Automation Inc., and ChatterPro from MAL Inc. However, the limitations of SSV have been reported from previous studies, and hence the wide application of SSV to actual manufacturing sites has not been realized yet. In this section, the main limitations of SSV are described, and the motivations and objectives of this thesis are presented based on the limitations.

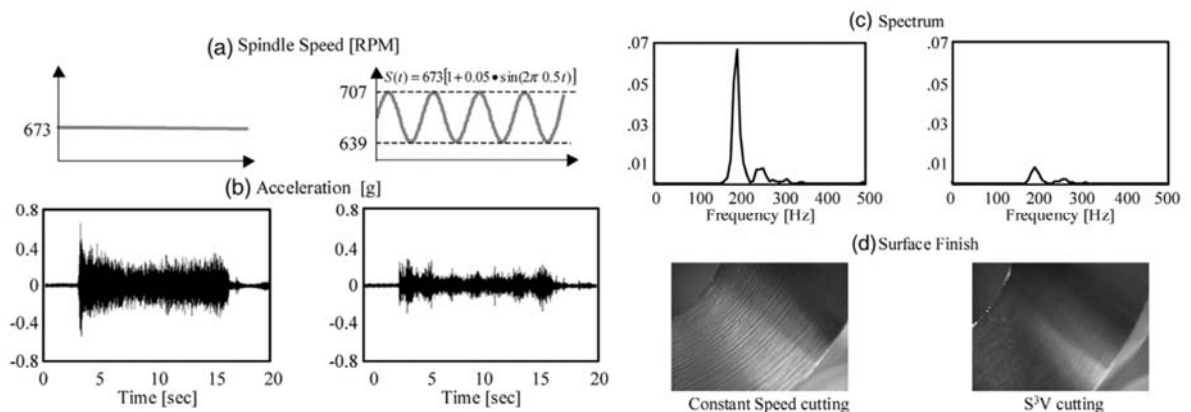


Fig. 1.6. Verified chatter suppression effect of spindle speed variation [46].

1.2.1 Motivations

Nowadays, most research works have been focused on the determination of the optimal SSV parameters involving the amplitude and period of speed variation to increase the chatter stability [2, 45]. However, it is a complex problem. According to the review paper [2], only Al-Regib [46] proposed a simplified strategy to select the proper design the parameters in sinusoidal SSV. Most other studies used complex and time-consuming stability simulations to find optimal SSV parameters [2], and hence these design methods cannot be implemented in actual manufacturing sites. In addition, it

has been investigated that the chatter suppression effect by SSV is more promising in relatively low spindle speed regions [49, 50], and hence the critical improvement in machining efficiency cannot be achieved. Furthermore, the temporal growth of chatter occurs in cutting with SSV has been reported in every SSV cycle [46, 51, 52], and the reason for this temporal instability has not been clarified. Sexton et al. [53] stated that the stability improvement by SSV often becomes modest compared to the predicted stability in the simulation. For these reasons, despite that it is well known that SSV can suppress the chatter vibration, this technique has not been sufficiently utilized yet in actual manufacturing sites. In order to realize its wide applications, not only the simple and logical methodology to determine the SSV parameters but also a general index to evaluate the stability of SSV are necessary. Moreover, an effective countermeasure to eliminate the temporal chatter growth throughout cutting with SSV should be prepared. This thesis focuses on those objectives.

1.2.2 Research objectives

To realize the high-efficiency cutting with SSV and to widely apply this technique to actual manufacturing sites by improving the limitations mentioned earlier, the author carried out researches as follows:

1. Clarification of chatter growth characteristics in SSV and proposal of novel chatter stability indices of SSV

The temporal growth of chatter occurs even if SSV is applied, and it results in uneven roughness of the cut surface, which degrades the quality of the product. However, there are no clear understandings of the temporal instability of SSV. Furthermore, since the stability of SSV varies greatly depending on the SSV parameters, it is quite a complicated problem to determine the parameters properly. These limitations are the main reason for the limited industrial application of SSV.

Therefore, not only a clear understanding of the chatter growth characteristics in SSV but also a simple and logical methodology to determine the appropriate SSV parameters for greater chatter suppression and improvement of the machining efficiency are necessary. The characteristics of the chatter growth in SSV are clarified and the chatter stability indices are newly proposed, and their validities are verified through both analytical and experimental investigations. The strategies for setting appropriate SSV parameters are also described by utilizing the proposed stability indices.

2. Proposal of novel spindle speed variation profile for improvement of chatter stability

Based on the clarified chatter growth characteristics and the proposed chatter stability indices, it is confirmed that the chatter suppression effect fluctuates in conventionally utilized SSV profiles, and hence the suppressing the chatter vibration in all sections of SSV is difficult. Especially, the stability decreases in a high-speed region, and thus remarkable improvement of machining efficiency cannot be realized.

A novel SSV profile is proposed to overcome the limitation of the conventional SSV profiles. In order to verify the effectiveness of the proposed profile, the stabilities of conventional SSV profiles and the proposed SSV profile are compared through the time-domain simulations and cutting experiments. A higher stability and applicability of the proposed SSV profile is verified from the results. By investigating the influence of the proposed SSV parameters on the stability, an appropriate strategy for setting the parameters to achieve higher stability is discussed.

3. Proposal of 'accelerative cutting' for improvement of chatter stability in short-duration cutting.

A novel speed variation method, namely 'accelerative cutting', is proposed for realizing the improvement of the chatter stability in short-duration cutting such as finishing of sealing, seating, and bearing surfaces. Due to the

large cutting width, the chatter vibration often occurs despite of the short cutting time in these cutting processes. Since the spindle speed is accelerated unidirectionally in 'accelerative cutting', there is no transient section, where changes from acceleration to deceleration or vice versa. Therefore, a sufficient speed difference can be obtained throughout the cutting. Because the maximum spindle speed is limited, the cutting method can be utilized in short-duration cutting.

Higher chatter stability in 'accelerative cutting' compared to the SSV profiles are verified through analytical and experimental investigations.

1.3 Real-World Data Circulation in thesis

Real-World Data Circulation (RWDC) is a new academic field established by Graduate Program for Real-World Data Circulation Leaders, Program for Leading Graduate Schools of Nagoya University. RWDC means the procedures of data acquisition, analysis, and implementation to the real-world. Creating new values through the interactive integration of the three procedures is the essential objective of RWDC. Extensive data in the real-world exists, and there are many data acquisition methods through observation and/or measurement utilizing sensors. Those acquired data is analyzed based on the appropriate methodology in order for identifying the mechanism of certain phenomena or effectively applying them to real-world. Consequently, it can be realized that not only a clear understanding of the real-world problem but also the creation of the new values from the new approach with a perspective of RWDC. In recent years, the combination of informatics involving the procedures of RWDC and other fields of research are getting increased such as material informatics, medical informatics, and Industry 4.0. Research that relied solely on the experiments required a long time to obtain results because numerous experiments should be conducted to reveal certain phenomena. In addition, when there are many parameters affecting a certain phenomenon, the research method that relies on experiments is even more inefficient to clarify all the relations between the parameters and that phenomenon. The

utilization of RWDC in those research fields is an effective way to solve the problem.

The author's main concern is how RWDC will be adopted for improving the circumstance of the manufacturing industry, especially related to the cutting process. The chatter suppression techniques, which are the main topic of the thesis, can be a good example of RWDC. As described in the background of this thesis, the chatter vibration is one of the biggest problems, i.e., real-world problems, at the manufacturing sites because it causes the poor cut surface and loss of productivity. For resolving the problem, the real-world data related to the cutting process such as the vibration acceleration, cutting forces, and profiles of the cut surface are acquired through the experiments as a first step. Then, they are analyzed to classify the types of chatter vibration based on the established mechanisms of chatter vibrations because the countermeasures for each type of chatter are different. Based on the classified chatter type and the corresponding cutting process, an appropriate solution is proposed, and the validity of the solution is investigated through various simulations. Finally, the proposed solution is directly applied to the machine tool, and then data acquisition and analysis are carried out again to evaluate the effectiveness of the technology. As a result, effective solutions can be implemented in the actual manufacturing sites.

Recently, the integrations between information technologies, e.g., big data, information analytics, Internet of Things (IoT), and monitoring technologies, and manufacturing technologies are encouraging the advent of the smart factory of Industry 4.0 [54]. Wang et al. [54] stated that the smart factory of Industry 4.0 is achievable by extensively applying the existing enable technologies while actively coping with the technical challenges. Shrouf et al. [55] described that it is expected the high flexibility in production volume and customization, extensive integration between customers, companies, and suppliers, and above all sustainability in the new era of industrial production. From those recent advances in the manufacturing industry have paved the way for a systematical deployment of Cyber-Physical Systems (CPS) [56].

CPS has been defined as transformative technologies for managing the interconnection between the physical systems and cyber systems [57]. For instance, the cutting process in the manufacturing sites is a real-world physical system and the monitoring techniques or chatter detection techniques are the representative examples of the cyber system. Data acquisition from the physical system is analyzed in the cyber system, and it gives a feedback to physical system through the data implementation. By iterating these procedures, the physical system can take proper action according to a certain purpose. With recent advances in the availability and affordability of sensors, data acquisition systems, and computer networks, the manufacturing fields move toward implementing high-tech applications [56]. The ever-growing usage of sensors and networked machines has resulted in the continuous generation of high-volume data, i.e., Big data. In such an environment, in order to implement CPS in the manufacturing fields and utilize it for practically improving productivity, it is essential to develop more efficient and resilient big data management techniques, inexpensive real-time data acquisition methods, and appropriate data analysis strategies. Lee et al. [56] proposed 5-level CPS structure, namely the 5C architecture, providing a step-by-step guideline for developing and deploying a CPS for manufacturing applications. Figure. 1. 7 shows the flow of 5-level CPS enabled factory with machine tools in manufacturing fields [56]. It is described sequential workflow manner, how to construct a CPS from the initial data acquisition to analytics, to the final value creation. On the other hand, in order to maximize productivity through CPS, proper analysis using acquired data is essential, and hence the comprehensive knowledge and understanding of the cutting process are required. In other words, it is predicted that the demand for collaboration between researchers in the field of manufacturing and in the field of informatics, or for researchers with both bits of knowledges, will increase.

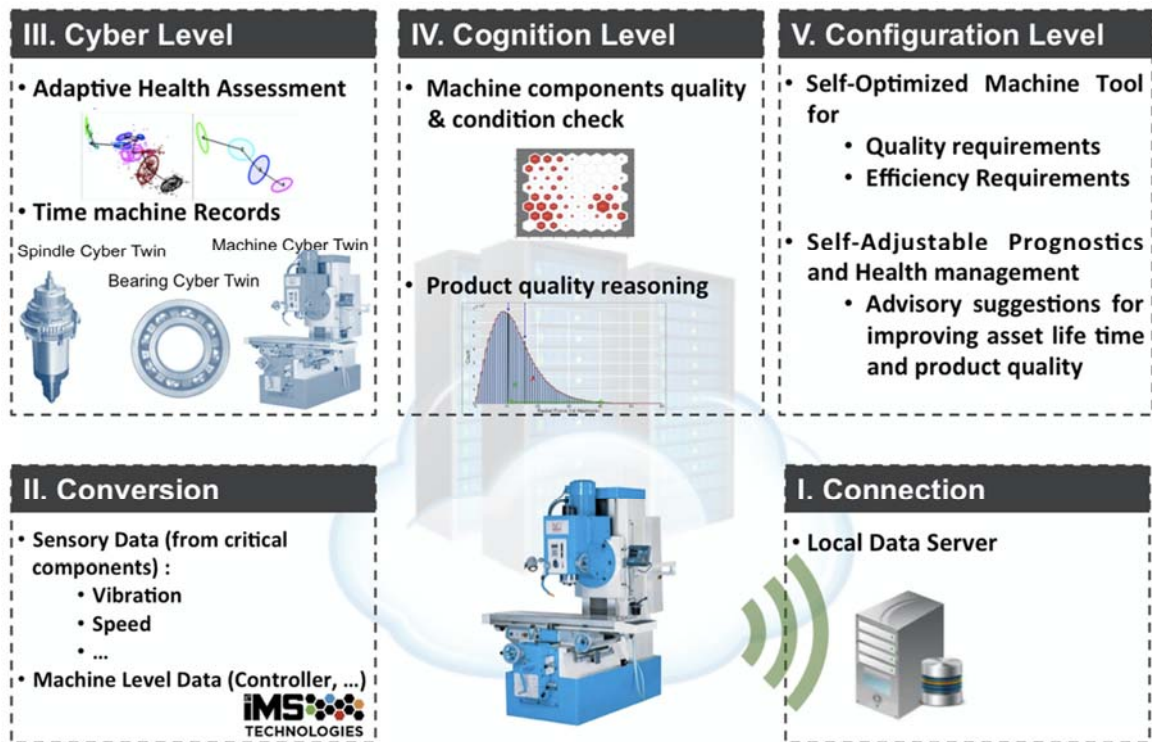


Fig. 1.7. Flow of 5-level CPS enabled factory with machine tools in manufacturing sites [56].

The author, as a researcher of Graduate Program for Real-World Data Circulation Leaders, Program for Leading Graduate Schools of Nagoya University, tried to study how RWDC can contribute to the realization of CPS in the cutting process, especially in the chatter suppression issues. For instance, the acquired acceleration vibration data during the chatter in SSV was analyzed to clarify the chatter growth characteristics of SSV and to propose the simple indices to evaluate the chatter stability (Chapter 2). Moreover, for the improvement of machining efficiency in both long-duration and short-duration cutting process, the novel SSV profiles (Chapter 3) and ‘accelerative cutting’ (Chapter 4) were developed and verified its effectiveness by utilizing the time-domain simulators, i.e., cyber system of CPS, in advance of the actual cutting experiments. The validation of the proposed technologies using a simulator has the advantage of being able to investigate under unrestricted conditions and of reducing wastage of expensive workpieces in the cutting experiments. The developed technologies were implemented to the machine tool, i.e., physical system of CPS, and the effectiveness of the

technologies were evaluated by analyzing again the acquired data from the machine tool. A more specific and concrete conception for RWDC in the thesis is described in [Chapter 5](#). The novelty and contributions of the author's research in the thesis with regard to RWDC are also described.

1.4 Construction of thesis

The present thesis consists of six chapters.

[Chapter 1](#) describes the background of the various types of chatter vibrations and the introduction of chatter suppression techniques. Then, a brief overview of the researches related to spindle speed variation (SSV), which one of the chatter suppression methods are presented, and the remained challenges in SSV are described. The motivation and objectives of the thesis are also described based on the limitations of SSV which are revealed from the past researches. In order to realize the robust chatter suppression effect of SSV so that achieve high-efficiency cutting and wide application to the production site, several objectives of the thesis are set and briefly described. Moreover, Real-World Data Circulation (RWDC) in the manufacturing field, which is the state-of-art academic field for realizing Industry 4.0 is introduced.

[Chapter 2](#) presents the chatter growth characteristics in SSV and newly explains the suppression effect of SSV. Based on these, the novel chatter stability indices are proposed to evaluate the chatter stability in SSV. By utilizing the proposed chatter stability indices, the influences of SSV parameters on the stability are clarified. The validity of the proposed chatter growth characteristics and suppression effects of SSV as well as the stability indices are verified through the analytical investigations and cutting experiments.

[Chapter 3](#) describes a proposed a new SSV profile to overcome the limitation of the chatter stability improvement in conventional SSV. The concept and formulation of new SSV profile are described. The relations between the chatter stability and the proposed stability indices in conventional

SSV profiles and in proposed SSV profile are compared. The influences of the parameters of proposed SSV profile on the chatter stability are revealed. In order to verify the effectiveness of the proposed SSV profile considering its applicability to the actual industry, the machining efficiency against the thermal load of the spindle motor in the proposed SSV profile is compared with the conventional SSV profiles. Through these investigations, it is verified that the proposed SSV profile is an effective solution to overcome the limitation of conventional SSV and it can realize higher applicability to the industry.

[Chapter 4](#) describes a new speed variation method proposed to improve the chatter stability in short-duration cutting process. The concept of the new method is explained based on the limitation of all SSV profiles due to their nature. The effectiveness of the new method is verified through both analytically and experimentally.

[Chapter 5](#), the contributions of the present thesis to the Real-World Data Circulation (RWDC) are summarized. In the present thesis, various kinds of data acquisition are conducted to utilize not only in analytical investigations but also analysis of experimental results. Through the analysis of data, the proposals of the new techniques can be realized, and they allow to improve the chatter stability and high-efficiency cutting. By applying the proposed techniques to machine tool and verifying their effectiveness, the implementation of new techniques to actual manufacturing sites becomes realized in near future. These series of procedures are reinterpreted in terms of RWDC, i.e. what kind of data are acquired, how and what kind of analysis are done, and how the results are implemented to improve the chatter stability and machining efficiency, are summarized. The specific and concrete examples of RWDC in the present thesis are described, and the imagined future works of researches in this thesis are introduced related to RWDC.

Conclusions of the thesis will follow in [Chapter 6](#).

The structure of the thesis is summarized in [Fig. 1.8](#).

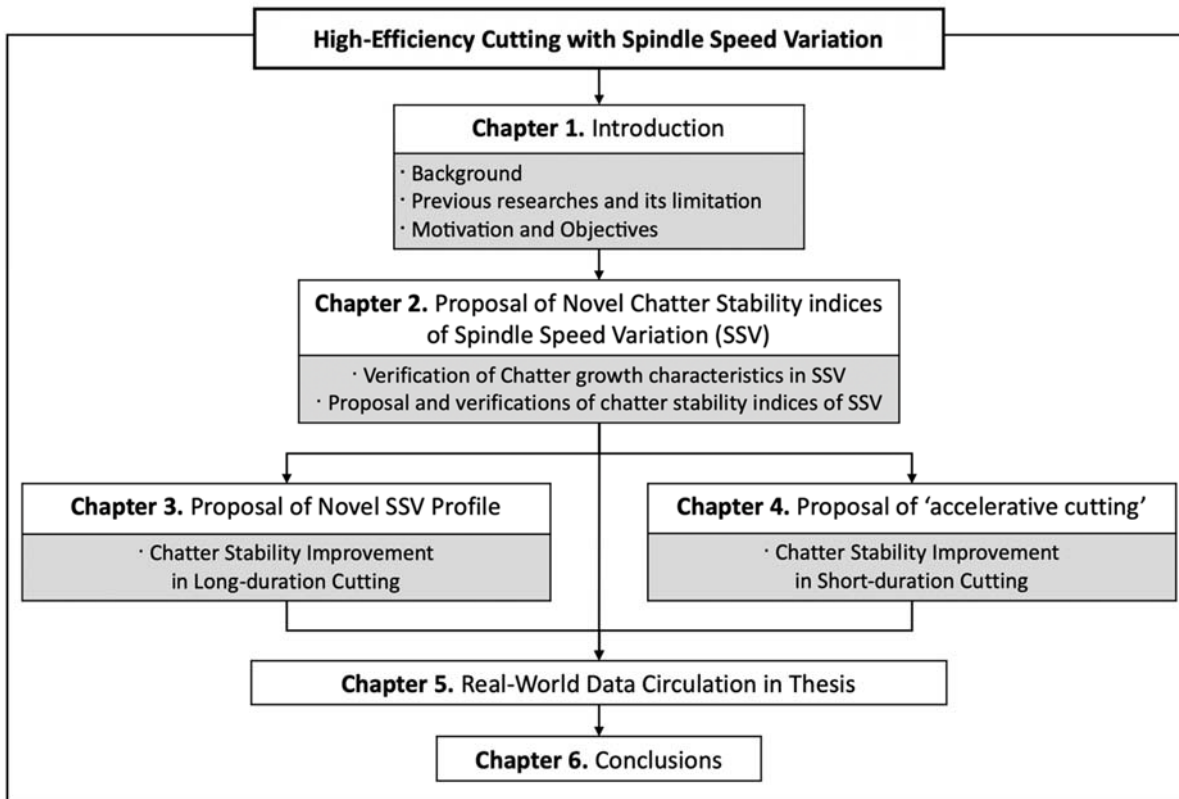


Fig. 1.8. Structure of thesis.

Chapter 2

Proposal of Novel Chatter Stability Indices of Spindle Speed Variation

2.1 Introduction

During the machining processes, the instability from the interaction between the metal cutting process and response of machine tool structure results in chatter. The chatter causes poor surface finish, excessive tool wear, and damage of the machine tool. The chatter usually occurs in conditions above a certain limit of cutting width or structural flexibility. In general, it can be avoided by lowering the cutting conditions, e.g., cutting width, but it leads to low machining efficiency. Extensive studies have been performed in order to clarify the mechanism of chatter, and it has been revealed that the self-excited vibration caused by the regenerative effect, i.e., regenerative chatter, is the most dominant machine tool chatter phenomenon [8]. The regenerative effect is caused by the previous vibration which is left on the workpiece as a wavy surface. The regenerative chatter grows up with a certain phase shift between the present and previous vibrations which causes dynamic chip load.

To suppress the regenerative chatter and to increase the stability and machining efficiency, various studies have been carried out, e.g., the selection of stable cutting conditions such as spindle speed and depth of cut [9], the optimization of tool path/posture [37], the usage of specially designed milling tools with variable pitch/helix angles [58, 59], and the optimization and the design methodology of those special tools [33, 60]. As another effective method for the suppression of the regenerative chatter without sacrificing the machining efficiency, the spindle speed variation (SSV) has been studied, where the speed is varied around the nominal spindle speed. Takemura et al. [61] analyzed its stability in the turning process by means of energy balance

and validated it through experiments. After that, numerous types of analytical methods have been proposed such as the angle domain method [62], the semidiscretization method [63], the method using the SSV frequency harmonics of chatter vibration [64], etc.

Several profiles have been proposed to vary the spindle speed such as sinusoidal, triangular, rectangular, and random profiles. It is well known that the sinusoidal spindle speed variation (SSSV) can be easily applied by the spindle speed control system with low load compared to the other profiles, hence it is the most popular technique [65]. The triangular spindle speed variation (TSSV) has also been developed to suppress the regenerative chatter (e.g., OKUMA Corp. Machining Navi L-g), and it is usefully utilized in production sites.

Meanwhile, since the stability of SSV varies greatly depending on the SSV parameters, i.e., variation amplitude, variation period, and nominal spindle speed, it is quite a complicated problem to determine the parameters properly [46, 51]. For example, in the case of the same variation amplitude, SSV yields higher stability at lower nominal speed [46, 51]. Furthermore, the temporal growth of chatter occurs even if SSV is applied [46, 51, 52]. For this problem, despite the fact that SSV is an effective technique, the industrial application has been limited because there is no simple and logical methodology to determine the parameters properly for the suppression of chatter and the improvement of the machining efficiency. Therefore, there is a need for a general index to evaluate the stability of SSV.

In this research, characteristics of the chatter growth in SSV are clarified and the chatter stability indices are newly proposed based on them. Time-domain simulations and cutting experiments are carried out, and the validity of the proposed indices and the effect of the SSV parameters on the stability are discussed.

2.2 Characteristics of chatter growth in SSV

2.2.1 Dynamic model of orthogonal cutting process

A dynamic model of a pipe-end plunging process, which can be considered as a semi-orthogonal cutting process, is shown in Fig. 2.1. It is assumed that the tool shank is flexible in the cutting (y) and feed (z) directions. In this process, the vibration in the z direction causes the fluctuation of the principal (y) and thrust (z) cutting forces.

Not only the present vibration but also the previous vibration left on the cut surface affect the present cutting; the latter one is called the regenerative effect. Those vibrations cause the uncut chip thickness fluctuation, and it results in the dynamic cutting force. Since the cutting force is proportional to the instantaneous uncut chip thickness $h(t)$ [m], which can be expressed as Eq. (2.1), the dynamic cutting forces in the principal direction f_y [N] and the thrust direction f_z [N] can be formulated as Eq. (2.2). Note that the formulation is in the Laplace domain after Eq. (2.1).

$$h(t) = h_0 + \mu z(t - \tau) - z(t) \quad (2.1)$$

$$\begin{Bmatrix} f_y \\ f_z \end{Bmatrix} = a(e^{-s\tau} - 1) \begin{bmatrix} 0 & K_y \\ 0 & K_z \end{bmatrix} \begin{Bmatrix} y \\ z \end{Bmatrix} \quad (2.2)$$

Here, h_0 [m] is the static depth of cut, i.e., feed rate of the cutting tool, μ is the overlapping factor ($\mu = 1$ in pipe-end plunging), τ [s] is the spindle period, a [m] is the cutting width, K_y [Pa] and K_z [Pa] are the specific cutting forces in the principal and thrust directions, respectively, and y [m] and z [m] are the dynamic displacements in the principal and thrust directions, respectively. Note that the static depth of cut h_0 has no effect on the dynamic cutting forces, hence it does not exist in Eq. (2.2).

The dynamic cutting forces excite the tool shank, and they cause the vibration displacements through the dynamic compliances as follows.

$$\begin{Bmatrix} y \\ z \end{Bmatrix} = \begin{bmatrix} G_{yy} & G_{yz} \\ G_{zy} & G_{zz} \end{bmatrix} \begin{Bmatrix} f_y \\ f_z \end{Bmatrix} \quad (2.3)$$

Here, G_{yy} [m/N] and G_{zz} [m/N] are the direct dynamic compliances in the principal and thrust directions, respectively, and G_{yz} [m/N] and G_{zy} [m/N] are the cross dynamic compliances between the principal and thrust directions.

Since the vibration in the principal (y) direction does not cause the dynamic uncut chip thickness, the closed-loop system with the cutting process and the equivalent dynamic compliance [66] can be represented as the block diagram shown in Fig. 2.2. Combining Eqs. (2.2) and (2.3), the following equation can be derived under critical stability at the angular chatter frequency ω_c [rad/s].

$$z(i\omega_c) = a_{lim}K_z(e^{-i\omega_c\tau} - 1)G_z(i\omega_c)z(i\omega_c). \quad (2.4)$$

Here, G_z [m/N] is the equivalent dynamic compliance, i.e., $G_z = G_{zz} + K_y/K_z \times G_{zy}$, where K_y/K_z is the cutting force ratio. The stability limit analysis is performed by solving Eq. (2.4), i.e., the critical cutting width or stability limit a_{lim} [m] and the corresponding spindle period τ [s] are calculated. As a result, a_{lim} is given as follows [67].

$$a_{lim} = -\frac{1}{2K_z\Lambda_{re}} \quad (2.5)$$

Here, Λ_{re} is the real part of the equivalent dynamic compliance.

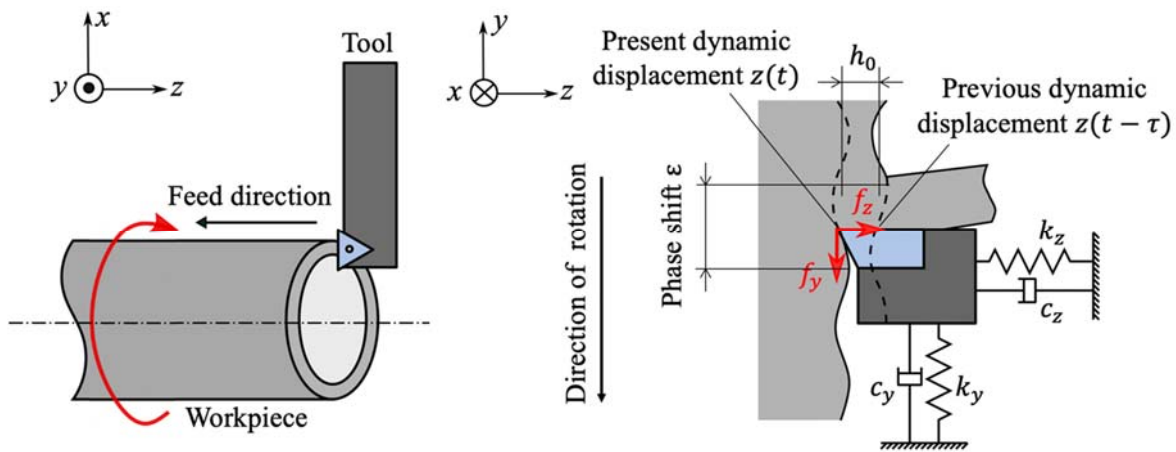


Fig. 2.1. Dynamic model of pipe-end plunging process.

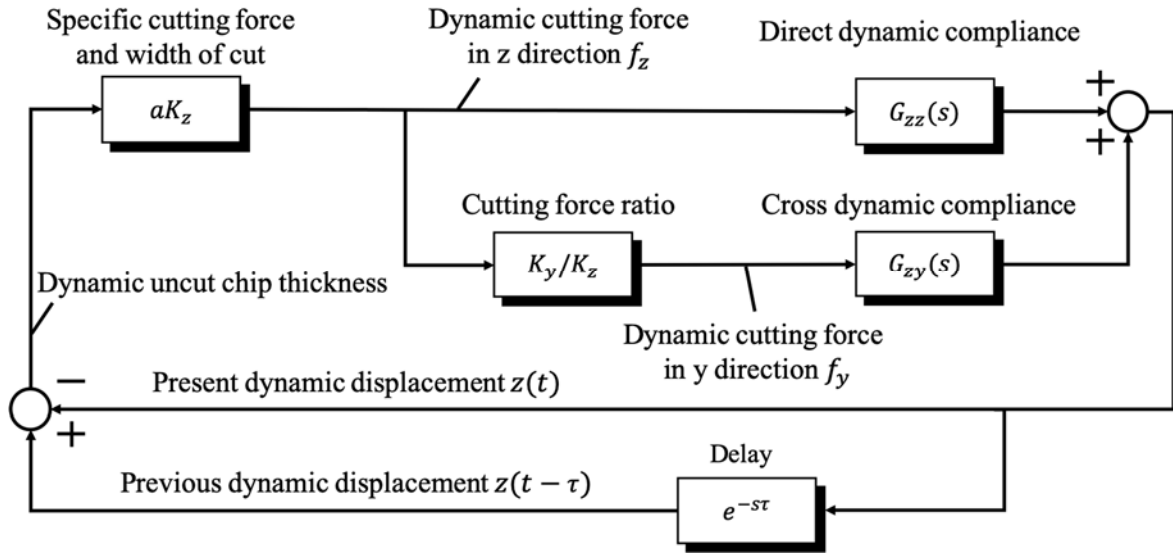


Fig. 2.2. Block diagram of pipe-end plunging process with regenerative effect.

2.2.2 Chatter growth/suppression in SSV

Due to the nature of the cutting process, the chatter is transferred to the workpiece as a wavy surface. After one revolution, the difference between the wavy surface and the present vibratory locus of the cutting edge causes the cutting force fluctuation. The regenerative chatter leaves a number of waves on the cut surface per unit angle, i.e., spatial chatter frequency f_{sc} [1/rad]. It can be expressed as Eq. (2.6), and its schematic illustration is shown in Fig. 2.3. Note that to visually imagine the concept, the figure is drawn as a plunge-turning process where the vibration waves can be seen easily, but it is the same in other cutting processes.

$$f_{sc} = \frac{60f_c(t)}{2\pi n(t)} = \frac{30f_c(t)}{\pi n(t)} \quad (2.6)$$

Here, $n(t)$ [min^{-1}] and $f_c(t)$ [Hz] are the spindle speed and the chatter frequency on the time t , respectively. From Eq. (2.6), the chatter frequency $f_c(t)$ can be described as follows.

$$f_c(t) = \frac{2\pi n(t)f_{sc}}{60} \quad (2.7)$$

In the case of CSS, $f_c(t)$ is constant since $n(t)$ is constant during the machining. Even when SSV is applied, the regenerative chatter can grow with a considerably flexible structure. It is found in this study that the regenerative

chatter generally grows at a constant spatial frequency in SSV (the first chatter growth characteristic), i.e., the time chatter frequency changes with varying spindle speed, unlike the assumption of constant time chatter frequency in previous studies [46-47, 51, 61-64]. The varied time chatter frequency can be expressed as follows.

$$f_c(t) = \frac{n(t)}{n(t - \tau(t))} f_c(t - \tau(t)) \quad (2.8)$$

Here, $\tau(t)$ [s] is the spindle period which varies depending on the spindle speed profile, $n(t - \tau(t))$ and $f_c(t - \tau(t))$ are the spindle speed and the chatter frequency at one revolution before, respectively.

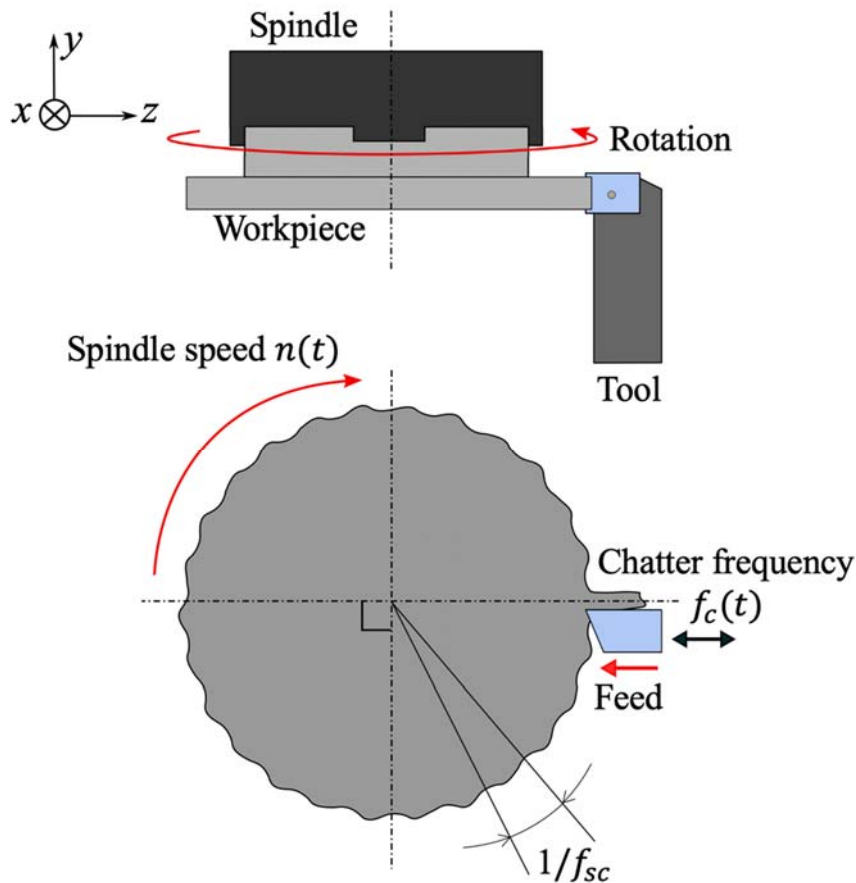


Fig. 2.3. Schematic illustration of plunge-turning process with regenerative chatter.

From Eq. (2.8), it can be noted that the time chatter frequency changes proportionally to the rate of spindle speeds in two consecutive revolutions at the same angular position, i.e., acceleration rate r_a [%], and it can be

expressed as follows [52].

$$r_a(t) = \left(\frac{n(t)}{n(t - \tau(t))} - 1 \right) \times 100 \quad (2.9)$$

Figure 2.4 shows the effect of spindle speed variation for the chatter suppression. The chatter vibration tends to occur near the resonance, where the magnitude of the dynamic compliance of the vibratory structure is large. As described above, the initial chatter frequency changes in SSV, and it generally causes a reduction of the magnitude of the dynamic compliance as shown in Fig 2.4. Note that larger the change of chatter frequency, i.e., larger r_a , the larger the reduction of magnitude of dynamic compliance, and the cutting becomes more stable [52]. The change of the magnitude of the dynamic compliance of the vibratory structure $G_z(i\omega_c(t))$ [m/N] and the amplitude of the present vibration $z(t)$ [m] can be expressed for intuitive understanding as follows.

$$G_z(i\omega_c(t)) = G_z \left(i \left(\left(1 + \frac{r_a(t)}{100} \right) \times \omega_c(t - \tau(t)) \right) \right) \quad (2.10)$$

$$z(t) = G_z(i\omega_c(t))f_z(t) = G_z \left(i \left(\left(1 + \frac{r_a(t)}{100} \right) \times \omega_c(t - \tau(t)) \right) \right) f_z(t) \quad (2.11)$$

It can be estimated that the chatter is likely to grow if there is a period where $|r_a|$ is small in SSV (the second chatter growth characteristic). The relation of $|r_a|$ and the chatter stability is investigated in Section. 2.3.

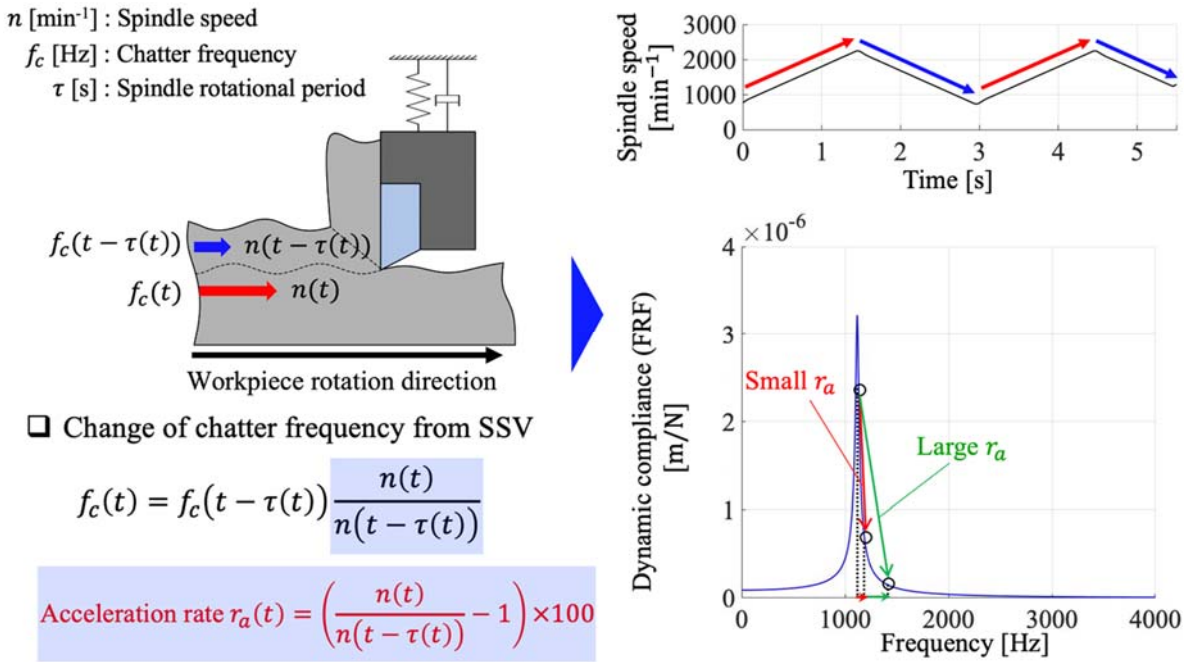


Fig. 2.4. Change of magnitude of dynamic compliance from SSV.

Next, in case of considering plural revolutions, e.g., more than two revolutions, the chatter frequency after m -revolutions at a certain angular position f_m [Hz] can be expressed as Eq. (2.12).

$$f_m = \frac{n_m}{n_{m-1}} \frac{n_{m-1}}{n_{m-2}} \dots \frac{n_1}{n_0} \times f_0 = \frac{n_m}{n_0} \times f_0 \quad (2.12)$$

Here, n_0 [min^{-1}] and f_0 [Hz] are the initial spindle speed and the initial chatter frequency, respectively. As the ratio of n_m to n_0 increases, the change of chatter frequency becomes larger and it results in larger dynamic compliance reduction, and the system becomes more stable. However, it should be noted that chatter can grow when the reduction of the dynamic compliance in each revolution is insufficient to suppress chatter. Also, the peakiness of the dynamic compliance, which increases with a decrease of the damping coefficient, as well as the cross dynamic compliance, also affect the change rate of the magnitude of the dynamic compliance, hence it can affect the degree of the chatter suppression.

2.3 Analytical investigation of chatter stability in SSV

2.3.1 Time-domain simulation model

To verify the validity of the revealed chatter growth characteristics in SSV and to investigate the relation between the acceleration rate r_a and the stability in TSSV and SSSV, time-domain simulations are carried out. A single degree of freedom (SDOF) vibratory system with orthogonal cutting shown in Fig. 2.1 is assumed. Here, the cutting tool is flexible and the regeneration occurs in the thrust direction (z). The uncut chip thickness $h(t)$ [mm] and the cutting force in the thrust direction $f_z(t)$ [N] fluctuates when chatter occurs, and each of them can be expressed as follows.

$$h(t) = h_0 + \mu z(t - \tau(t)) - z(t) \quad (2.13)$$

$$f_z(t) = K_z a h(t) \quad (2.14)$$

The response of the cutting tool to the cutting force in the SDOF system can be described as follows.

$$m\ddot{z}(t) + c\dot{z}(t) + kz(t) = K_z a (h_0 + \mu z(t - \tau(t)) - z(t)) \quad (2.15)$$

Here, m [kg] is the modal mass, c [N/(m·s)] is the modal damping coefficient, k [N/m] is the modal stiffness, and $\mu = 1$ in pipe-end plunging. Note that in the case of cutting with SSV, the spindle period $\tau(t)$ varies with time due to the time-varying spindle speed $n(t)$ [min⁻¹], and it can be searched to satisfy the following equation.

$$\int_{t-\tau(t)}^t \frac{n(t)}{60} dt = 1 \quad (2.16)$$

In the time-domain simulation, $z(t)$ is calculated by solving Eq. (2.15) directly, and the solution is approximated by the 4th order Runge-Kutta method. Here, the accumulated rotation angle $\theta(t)$ [rad], which can be expressed as Eq. (2.17), $z(t)$ and $n(t)$ are memorized at each calculation step, i.e., resolution of time-domain simulation, and they are utilized when searching the previous displacement $z(\theta(t) - 2\pi)$ and the previous spindle speed $n(\theta(t) - 2\pi)$.

$$\theta(t) = 2\pi \int_0^t \frac{n(t)}{60} dt \quad (2.17)$$

The tool jumping out of the workpiece, i.e., $h(t) = 0$, due to the vibration

is considered in the simulation. At the beginning of simulation, the cutting starts with gradually increasing static depth of cut.

2.3.2 Formulation of SSV profiles and introduction of stability indices

Since the triangular and the sinusoidal spindle speed variation, i.e., TSSV and SSSV, profiles are considered in most literatures [46-47, 51, 62-65], they are investigated in the current study. The schematics for the explanation of the spindle speed and acceleration rate profiles in TSSV and SSSV are shown in Fig. 2.5 (a) and Fig. 2.5 (b), respectively. Here, n_0 [min^{-1}] is the nominal spindle speed, T [s] is the variation period, and n_A [min^{-1}] is the variation amplitude, respectively. The variation function of TSSV $n_{tri}(t)$ [min^{-1}] can be described as follows.

$$n_{tri}(t) = \begin{cases} n_0 + n_A - \frac{4n_A}{T} \text{mod}(t, T) & \text{if } 0 \leq \text{mod}(t, T) < T/2 \\ n_0 - 3n_A + \frac{4n_A}{T} \text{mod}(t, T) & \text{if } T/2 \leq \text{mod}(t, T) < T \end{cases} \quad (2.18)$$

Here, $\text{mod}(t, T)$ denotes the modulo function.

The variation function of SSSV $n_{sin}(t)$ [min^{-1}] can be described as follows.

$$n_{sin}(t) = n_0 + n_A \sin\left(\frac{2\pi}{T}t + \frac{\pi}{2}\right) \quad (2.19)$$

As observed in Fig 2.5, the acceleration rate r_a always fluctuates with the speed variation. The r_a has a positive value in the acceleration section and has a negative value in the deceleration section. At the sections where the acceleration direction is switched, i.e., switching from acceleration to deceleration or from deceleration to acceleration, the speed difference in two consecutive revolutions is nearly zero, and the value of r_a is close to zero. Since the length of these sections should be one revolution, i.e., 2π rad, the time lengths t_1 , t_2 should satisfy the following equations.

$$\int_{\frac{T}{2}}^{\frac{T}{2}+t_1} \frac{n(t)}{60} dt = 1 \quad (2.20)$$

$$\int_T^{T+t_2} \frac{n(t)}{60} dt = 1 \quad (2.21)$$

Since r_a fluctuates in SSV, the average of absolute acceleration rate in one period of SSV $\overline{|r_a|}$ [%] is utilized as the stability index for evaluating the stability in SSV, and it can be expressed as follows.

$$\overline{|r_a|} = \frac{1}{T} \int_0^T |r_a(t)| dt = \frac{100}{T} \int_0^T \left| \left(\frac{n(t)}{n(t-\tau(t))} - 1 \right) \right| dt \quad (2.22)$$

Meanwhile, when considering the plural revolutions in a unidirectional acceleration section, the more revolutions show the larger change of the dynamic compliance since the chatter frequency also changes largely in one way, i.e., increase or decrease, as shown in Eq. (2.12). From this observation, the number of revolutions in a unidirectional acceleration section N is utilized as the second stability index for evaluating the stability in SSV, and it can be calculated from SSV parameters as follows.

$$N = \frac{n_0 T}{60 \cdot 2} = \frac{n_0 T}{120} \quad (2.23)$$

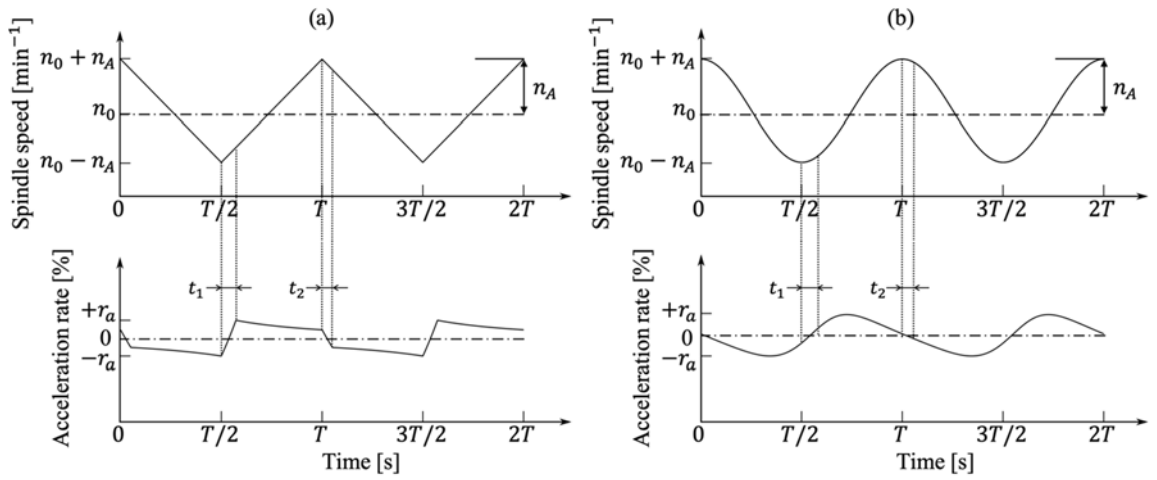


Fig. 2.5. Profiles of spindle speed and acceleration rate in (a) TSSV and (b) SSSV.

2.3.3 Simulation conditions and profile examples

The utilized parameters in the time-domain simulation are shown in Table 2.1. To investigate the validity of the proposed stability indices, i.e., $\overline{|r_a|}$ and N , the SSV parameters are determined so that TSSV and SSSV have the

same stability indices. Note that the variation amplitude ratio RVA , which is defined as the ratio of the speed variation amplitude to the nominal spindle speed n_A/n_0 , should be set lower than 1 so that the spindle speed is always higher than 0. Thus, the range of RVA is set from 0.05 to 0.80. The cutting width is gradually increased with increments of 0.1 mm, and the stability limit is found. In this simulation, the growing vibration in each period of SSV is considered as chatter.

Table 2.1. Parameters used in time-domain simulation.

Workpiece properties		
Diameter D	[mm]	70
Specific cutting force in principal direction K_y	[MPa]	1284
Specific cutting force in thrust direction K_z	[MPa]	711
Modal parameters		
Mass m	[kg]	0.2266
Damping coefficient c	[N/(m·s)]	44.19
Stiffness k	[N/m]	1.118×10^7
SSV parameters		
Nominal spindle speed n_0	[min ⁻¹]	600 - 7200
Variation period T	[s]	0.5, 1.0, 2.0
Variation amplitude ratio RVA		0.05 - 0.80
Cutting conditions		
Feed rate (static depth of cut) h_0	[mm/rev]	0.05
Increment of cutting width	[mm]	0.1

Figures 2.6(a) and 2.6(b) show examples of unstable results in TSSV and SSSV, respectively. In both profiles, the growth of chatter is observed in the transitions from the acceleration to the deceleration. On the other hand, the chatter does not grow in the transitions from the deceleration to acceleration. This can be explained as follows: the acceleration rate in the lower speed is larger than that in the higher speed, and hence the chatter suppression effect is greater in the lower speed. As a result, there is a chatter growth characteristic that it grows in the transitions from the acceleration to the deceleration where the acceleration rate $|r_a|$ is small.

The change of the chatter frequency can be observed in the short-time

Fourier transform result of vibration displacement in each graph, i.e., as the spindle speed decreases, the chatter frequency decreases in a similar way. In order to clarify the chatter growth characteristics quantitatively, the spatial frequency f_{sc} during chatter is investigated. Comparisons of the points A, B and C, D in Figure 2.6 are carried out. The spindle speeds at points of A, B and C, D are 1120 min^{-1} , 1070 min^{-1} and 1155 min^{-1} , 1110 min^{-1} , respectively. The chatter frequencies at points of A, B and C, D are 1195 Hz , 1145 Hz and 1170 Hz , 1115 Hz , respectively. Finally, the spatial frequencies at points A, B and C, D are calculated by utilizing the Eq. (2.6), and their values are 10.19, 10.22 and 9.67, 9.59, respectively. From the results, it can be confirmed that the spatial frequencies at the points A, B and C, D are nearly the same. Therefore, it can be concluded that the chatter frequency generally changes in proportion to the spindle speed, i.e., the chatter grows up at a constant spatial frequency in SSV.

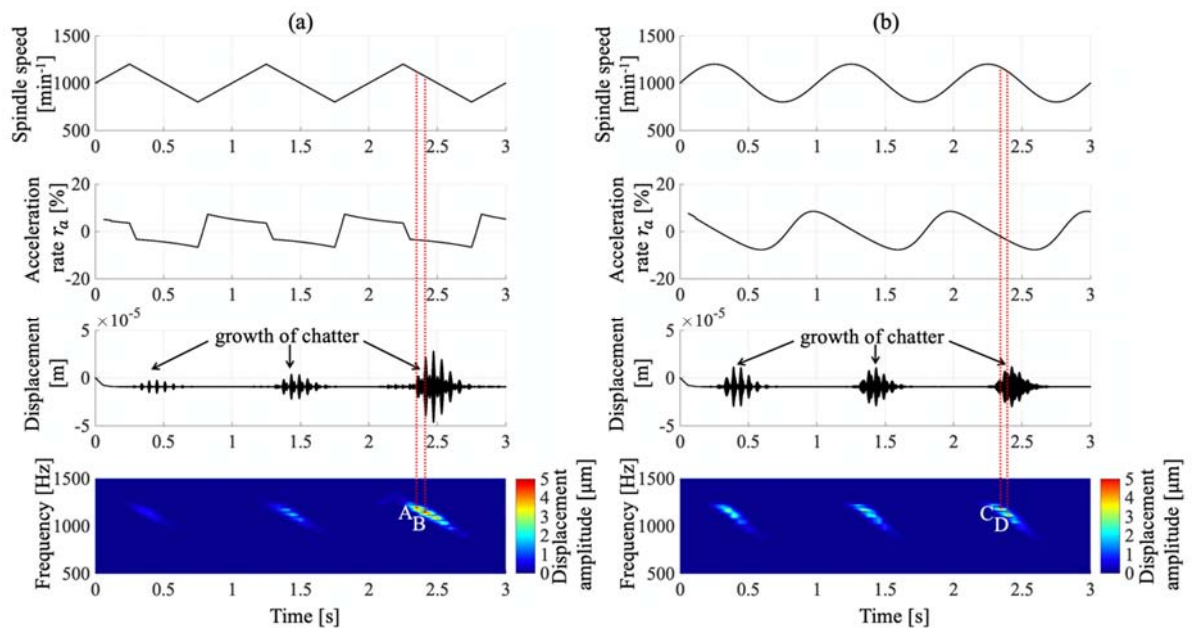


Fig. 2.6. Profile examples of spindle speed and acceleration rate, and corresponding vibration displacement and its short-time Fourier transform result of unstable condition at cutting width=2.9 mm, $n_0=1000 \text{ min}^{-1}$, $T=1.0 \text{ sec}$, and $RVA=0.2$ in (a) TSSV and (b) SSSV.

2.3.4 Simulation results and discussions

The relations between the stability limit and the proposed stability indices, i.e., $\overline{|r_a|}$ and N , in TSSV and SSSV are investigated by utilizing the time-domain simulation model. Figure 2.7 shows the simulation results under various conditions: (a) TSSV, $T=0.5$ sec (b) SSSV, $T=0.5$ sec, (c) TSSV, $T=1.0$ sec, (d) SSSV, $T=1.0$ sec, (e) TSSV, $T=2.0$ sec and (f) SSSV, $T=2.0$ sec. Since each graph represents the results obtained at a constant T , n_0 takes the proportional value with N from Eq. (2.23). The dotted lines indicate the contours where RVA is 0.2, 0.4, 0.6, and 0.8, respectively. Note that even if T and RVA are equal, the value of $\overline{|r_a|}$ decreases with an increase of n_0 or N . Finally, the magnitude of the stability limit is represented by gray scale. Figures 2.8(a) and 2.8(b) show the profile examples of spindle speed and acceleration rate which correspond to A to F marked on Figs. 2.7(c) and 2.7(d), respectively. The solid (A/D), dashed (B/E), and dotted (C/F) lines represent the profiles under the conditions of $T=1.0$ sec, $\overline{|r_a|}=10\%$, and $N=5, 15, 25$, respectively, in TSSV/SSSV. The spindle speed profiles show that the nominal spindle speed increases and RVA also increases with an increase of N . The former tendency can be confirmed in Eq. (2.23), and the latter one is needed to keep $\overline{|r_a|}$ constant. From Figs. 2.7 and 2.8, the following five remarks are found.

First, it can be confirmed from Fig. 2.7 that when N is equal, the stability limit increases with an increase of $\overline{|r_a|}$ regardless of T and the type of SSV. Hence, $\overline{|r_a|}$ is an effective index for evaluating the stability of SSV.

Second, when $\overline{|r_a|}$ is equal, the stability is the largest at a certain N , e.g., 20 in the case of $\overline{|r_a|} = 10$ in Fig. 2.7(a). The reasons for this can be considered as follows. With an increase of N , the chatter frequency changes largely as expressed in Eq. (2.12), and thus the stability increases because the dynamic compliance is greatly reduced. On the other hand, it can be observed from the profiles of r_a in Fig. 2.8 that with an increase of N the fluctuation amplitude of r_a becomes large. Consequently, $|r_a|$ becomes smaller and that section becomes longer near the transitions from acceleration

to deceleration. Therefore, a sufficient compliance reduction cannot be obtained in that section, and hence stabilization cannot be achieved at excessively large N . From these reasons, an optimal value of N exists.

Third, in the case where the values of $\overline{|r_a|}$ and N are equal in the same type of SSV, the stability limits are almost identical among different T 's (Figs. 2.7(a)-(c) or 2.7(d)-(f)). Therefore, the stability limit can be estimated in each type of SSV by utilizing the two proposed stability indices regardless of the combination of SSV parameters.

Fourth, comparing the results in TSSV and SSSV, it can be confirmed that the stability limit in SSSV is always smaller than TSSV when $\overline{|r_a|}$ and N are equal. The reason for this is considered as follows. The shape of r_a profile is different and $|r_a|$ becomes smaller in SSSV than in TSSV near the transition from acceleration to deceleration as shown in Fig. 2.8. This can be observed more clearly in Fig. 2.5. Because of this period of smaller $|r_a|$, the stability in SSSV is always smaller than TSSV. When lower RVA is desirable, e.g., tool wear may progress rapidly at high speeds for difficult-to-cut materials, SSSV (Figs. 2.7(d)-(f)) can have relatively higher $\overline{|r_a|}$ and N compared to TSSV (Figs. 2.7(a)-(c)) under equal RVA . However, the stability in TSSV is larger than that in SSSV under equal RVA even though $\overline{|r_a|}$ and N are lower. For example, stability limits under $RVA = 0.6$, $T = 2.0$ sec, and equal $\overline{|r_a|}$ or N (G-K/G'-K' shown in Figs. 2.7(c)/2.7(f)) are estimated in TSSV/SSSV by linear interpolation between neighboring stability limits. The estimated values are (3.56 mm, 3.90 mm, 4.29 mm, 4.49 mm, 4.80 mm)/(3.39 mm, 3.59 mm, 3.72 mm, 4.31 mm, 4.45 mm), and it is confirmed that the stability in TSSV is always higher than that in SSSV under equal RVA .

Fifth, when RVA and T are equal, all the graphs represent that the smaller the N , i.e., the smaller the n_0 , the higher the stability because $\overline{|r_a|}$ increases as n_0 decreases under equal RVA . In other words, the chatter suppression effect of TSSV and SSSV decreases in high-speed region, and thus it is unfortunately difficult to realize remarkable improvement of machining efficiency.

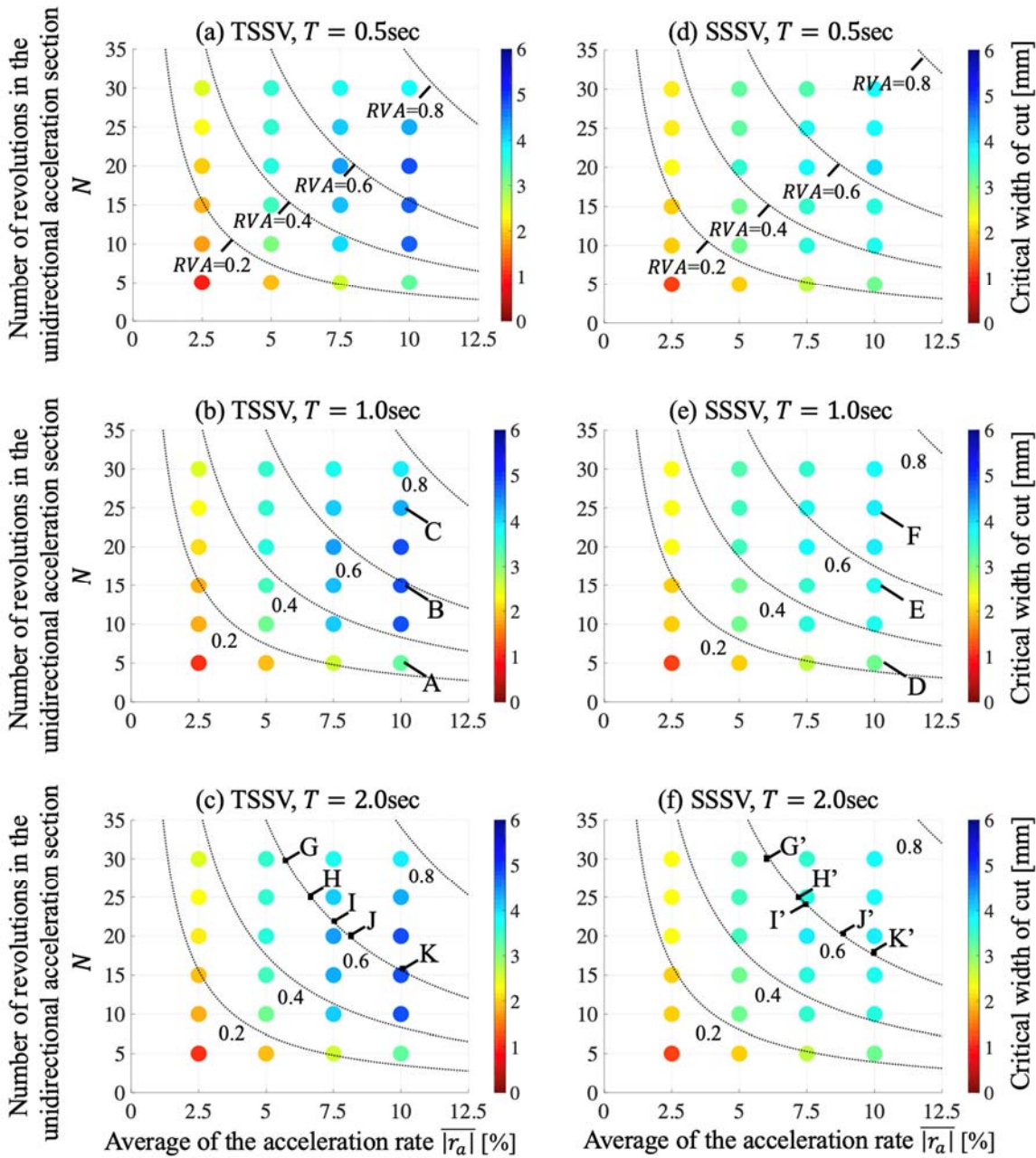


Fig. 2.7. Stability limits against the stability indices $\overline{|r_a|}$ and N under variable condition of T in TSSV and SSSV.

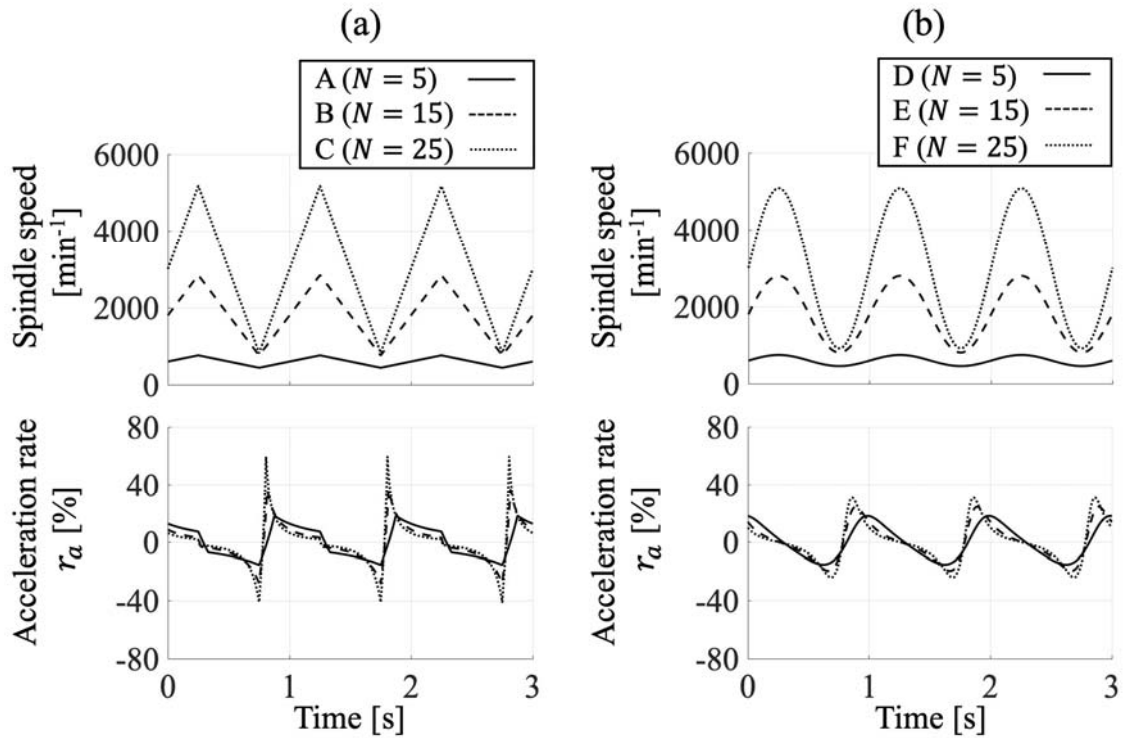


Fig. 2.8. Profile examples of spindle speed and acceleration rate under conditions of $T=1.0$ sec, $|\overline{r_a}|=10\%$, and $N=5, 15, 25$ in (a) TSSV and (b) SSSV.

2.4 Experimental verification

2.4.1 Experimental setup

A series of experiments are carried out to verify the validity of the revealed chatter growth characteristics in SSV and to confirm the effectiveness of the proposed stability indices, i.e., $|\overline{r_a}|$ and N . Figure 2.9 shows a photograph of the experimental setup for the pipe-end plunging. The experiments are conducted on a turning center (Okuma Corp., SPACETURN LB3000EX), and a pipe-shaped workpiece (brass, ISO CuZn35) is cut by a tool insert (Mitsubishi Material Corp., TCMW16T308 HTi10) mounted on a tool shank (steel, ISO C45) with a rectangular cross-section. The rake and clearance angles are 0 and 7 deg, respectively.

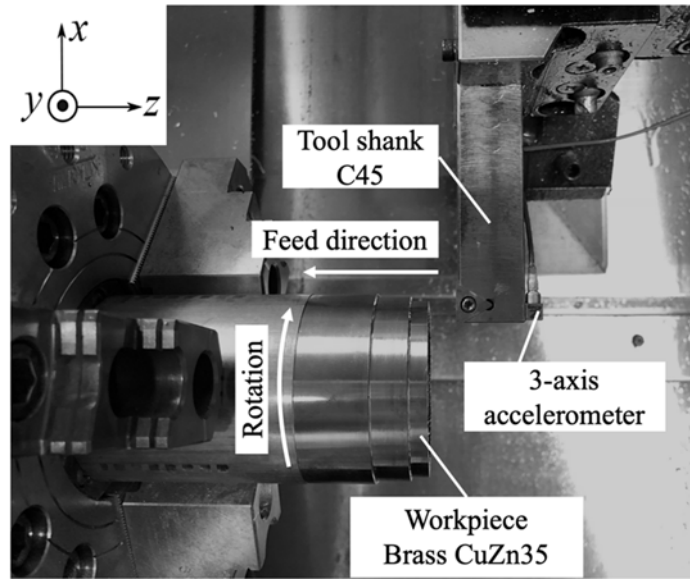


Fig. 2.9. Experimental setup for pipe-end plunging.

2.4.2 Measurement of dynamic compliance of tool

Measurement of the dynamic compliance of the tool is carried out with an impact hammer (PCB Electronics Inc., 084A14), an accelerometer (PCB Electronics Inc., 356A01), and a dummy tool insert with flat perpendicular faces for accurate force input. In order to increase the reliability of the measurement, the number of impacts for each direction is set to 10, and the average of the results is utilized in the time-domain simulations for comparison with the cutting experiments with TSSV.

The workpiece is rigid in the depth of cut (z) direction, and the projection of the tool shank is set as long as 90 mm, and thus the chatter occurs mainly due to the flexibility of the tool in the z direction. The measured dynamic compliances are shown in Fig. 2.10 where (a) shows the cross dynamic compliance and (b) shows the direct dynamic compliance. In order to use these compliances in the time-domain simulations, the modal parameters of the dynamic compliances, including the cross dynamic compliance whose phase changes complexly, are identified in the following manner. The equation of motion of the tool can be represented as follows.

$$[M] \begin{Bmatrix} \ddot{y}(t) \\ \ddot{z}(t) \end{Bmatrix} + [C] \begin{Bmatrix} \dot{y}(t) \\ \dot{z}(t) \end{Bmatrix} + [K] \begin{Bmatrix} y(t) \\ z(t) \end{Bmatrix} = \begin{Bmatrix} f_y(t) \\ f_z(t) \end{Bmatrix} \quad (2.24)$$

Here, $[M]$, $[C]$, and $[K]$ are the modal mass, damping coefficient, and stiffness matrices, and they are expressed as follows.

$$[M] = \begin{bmatrix} m_{yy} & m_{yz} \\ m_{zy} & m_{zz} \end{bmatrix}, [C] = \begin{bmatrix} c_{yy} & c_{yz} \\ c_{zy} & c_{zz} \end{bmatrix}, [K] = \begin{bmatrix} k_{yy} & k_{yz} \\ k_{zy} & k_{zz} \end{bmatrix} \quad (2.25)$$

Equation (2.24) can be represented in the s domain by taking the Laplace transform as follows.

$$([M]s^2 + [C]s + [K]) \begin{Bmatrix} y(s) \\ z(s) \end{Bmatrix} = \begin{Bmatrix} f_y(s) \\ f_z(s) \end{Bmatrix} \quad (2.26)$$

The dynamic displacements in the principal and thrust directions can be expressed as follows:

$$\begin{Bmatrix} y(s) \\ z(s) \end{Bmatrix} = ([M]s^2 + [C]s + [K])^{-1} \begin{Bmatrix} f_y(s) \\ f_z(s) \end{Bmatrix} \equiv \begin{bmatrix} G_{yy} & G_{yz} \\ G_{zy} & G_{zz} \end{bmatrix} \begin{Bmatrix} f_y(s) \\ f_z(s) \end{Bmatrix} \quad (2.27)$$

where the elements of the dynamic compliances can be expressed as follows.

$$\begin{aligned} G_{yy} &= \frac{m_{zz}s^2 + c_{zz}s + k_{zz}}{(m_{yy}s^2 + c_{yy}s + k_{yy})(m_{zz}s^2 + c_{zz}s + k_{zz}) - (m_{yz}s^2 + c_{yz}s + k_{yz})(m_{zy}s^2 + c_{zy}s + k_{zy})} \\ G_{yz} &= -\frac{m_{yz}s^2 + c_{yz}s + k_{yz}}{(m_{yy}s^2 + c_{yy}s + k_{yy})(m_{zz}s^2 + c_{zz}s + k_{zz}) - (m_{yz}s^2 + c_{yz}s + k_{yz})(m_{zy}s^2 + c_{zy}s + k_{zy})} \\ G_{zy} &= -\frac{m_{zy}s^2 + c_{zy}s + k_{zy}}{(m_{yy}s^2 + c_{yy}s + k_{yy})(m_{zz}s^2 + c_{zz}s + k_{zz}) - (m_{yz}s^2 + c_{yz}s + k_{yz})(m_{zy}s^2 + c_{zy}s + k_{zy})} \\ G_{zz} &= \frac{m_{yy}s^2 + c_{yy}s + k_{yy}}{(m_{yy}s^2 + c_{yy}s + k_{yy})(m_{zz}s^2 + c_{zz}s + k_{zz}) - (m_{yz}s^2 + c_{yz}s + k_{yz})(m_{zy}s^2 + c_{zy}s + k_{zy})} \end{aligned} \quad (2.28)$$

Therefore, the equivalent dynamic compliance in the thrust direction, i.e., $G_z(s)$, can be calculated as follows.

$$G_z(s) = \begin{Bmatrix} G_{zy} & G_{zz} \end{Bmatrix} \begin{Bmatrix} K_y/K_z \\ 1 \end{Bmatrix} = K_y/K_z \times G_{zy} + G_{zz} \quad (29)$$

The modal parameters are numerically identified by utilizing the least squares method between the measured compliances and the fitted compliances which use those parameters. The identified modal parameters are shown in Table 2.2, and the fitted compliances are shown in Fig. 2.10. Figure 2.11 shows the measured and fitted equivalent dynamic compliances, and the dotted gray lines and solid black lines in Figs. 2.10 and 2.11 represent the measured and fitted compliances, respectively.

Table 2.2. Numerically identified modal parameters.

Modal mass			
m_{yy}	[kg]		0.0748
m_{yz}	[kg]		-0.0125
m_{zy}	[kg]		-0.0124
m_{zz}	[kg]		0.1247
Modal damping coefficient			
c_{yy}	[N/(m·s)]		7.779
c_{yz}	[N/(m·s)]		35.19
c_{zy}	[N/(m·s)]		-12.60
c_{zz}	[N/(m·s)]		45.97
Modal stiffness			
k_{yy}	[N/m]		3.912×10^6
k_{yz}	[N/m]		-4.678×10^1
k_{zy}	[N/m]		-6.700×10^5
k_{zz}	[N/m]		1.063×10^7

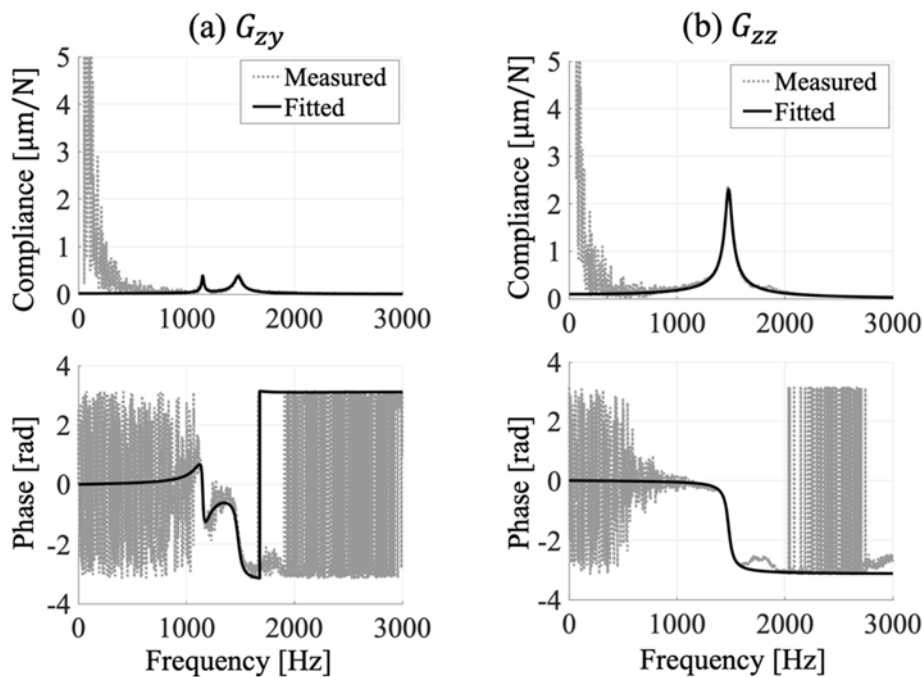


Fig. 2.10. Measured and fitted dynamic compliances: (a) cross dynamic compliance and (b) direct dynamic compliance.

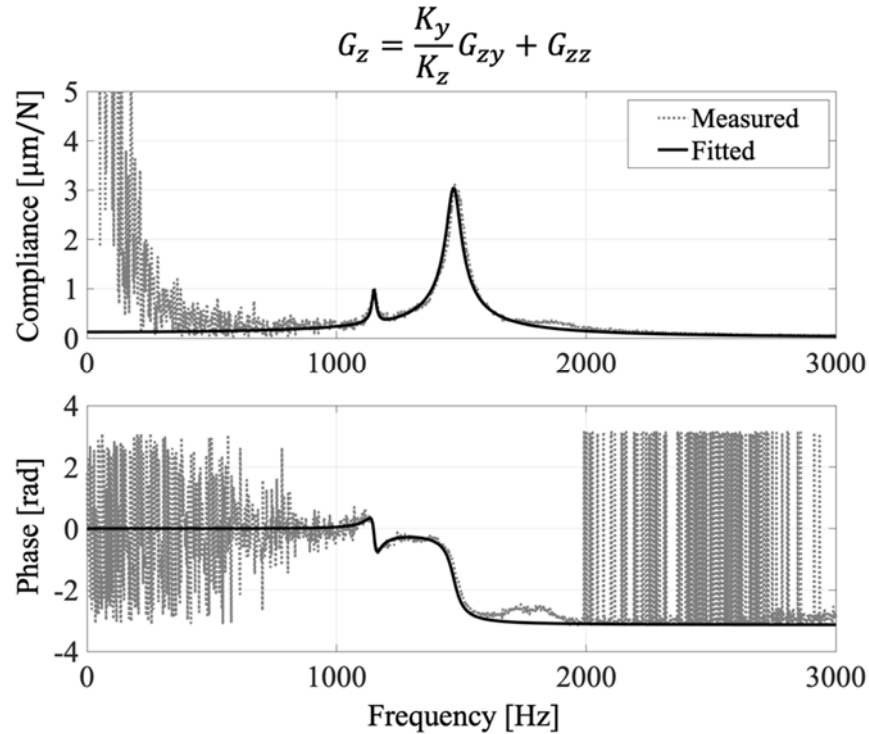


Fig. 2.11. Measured and fitted equivalent dynamic compliances.

2.4.3 Cutting experiments with CSS

Cutting experiments with CSS are conducted to confirm that the analytical stability limits agree well with the experimental results. The stability limits in CSS are also compared with those in SSV for investigating the degree of the stability improvement by utilizing SSV.

The spindle speed signal is obtained directly from the spindle motor encoder. An accelerometer is used to measure the tool vibration during cutting. The frequency components of vibration displacement are obtained by short-time Fourier transform, and the maximum component a_{max} in each result is investigated. The cutting conditions of CSS are shown in Table 2.3. Note that the measurement of the specific cutting forces in the principal (y) and thrust (z) directions are carried out in advance. Since SSV will be adopted in a wide range of the spindle speed, the specific cutting force in each direction is determined in multiple spindle speeds. At each spindle speed, the feed rate, i.e., static depth of cut, is varied, and the inclination of cutting force versus feed rate is identified as the specific cutting force, i.e., the edge force is excluded.

The specific cutting forces in the principal and thrust directions at all spindle speeds are averaged, and the averaged values, 1284 MPa and 711 MPa respectively as shown in Table 2.3, are utilized in the stability limit analysis. Note that the variations of specific cutting forces are as small as 2.5 % and 1.0 % in the principal and thrust directions, respectively, in a speed range from 1000 min⁻¹ to 3000 min⁻¹.

The feed rate or static depth of cut is fixed to 0.05 mm. The cutting width, i.e., the thickness of the pipe, is changed by means of pre-cutting, and the spindle speed is set variable.

Table 2.3. Experimental conditions for cutting with CSS.

Workpiece properties		
Material		Brass CuZn35
Diameter D	[mm]	70
Specific cutting force in principal direction K_y	[MPa]	1284
Specific cutting force in thrust direction K_z	[MPa]	711
Tool properties		
Width (feed dir.) × Height (cutting dir.)	[mm]	25×15
Projection length	[mm]	90
Cutting condition		
Feed rate (static depth of cut) h_0	[mm/rev]	0.05
Cutting width a	[mm]	0.4, 0.6, 0.8
Spindle speed n	[min ⁻¹]	1000 - 3000

The stability limit analysis in CSS is conducted with the measured equivalent dynamic compliance, and the stability limits are calculated by solving Eq. (2.4) [67]. The analytical and experimental results are shown in Fig. 2.12. Here, the dotted lines represent the results from the stability limit analysis, ○ represents the cutting result without chatter ($a_{max} < 1.5 \mu\text{m}_{0-p}$), and × represents the cutting result with chatter ($1.5 \mu\text{m}_{0-p} \leq a_{max}$). As can be observed in Fig. 2.12, the predicted stability limit and chatter frequency in each spindle speed agree well with the experimental results; e.g., in the case of a cutting width of 0.6 mm or more, chatter occurs under all spindle speed conditions. Therefore, it is confirmed that the measured equivalent dynamic

compliance and specific cutting forces utilized in the stability limit analysis are valid.

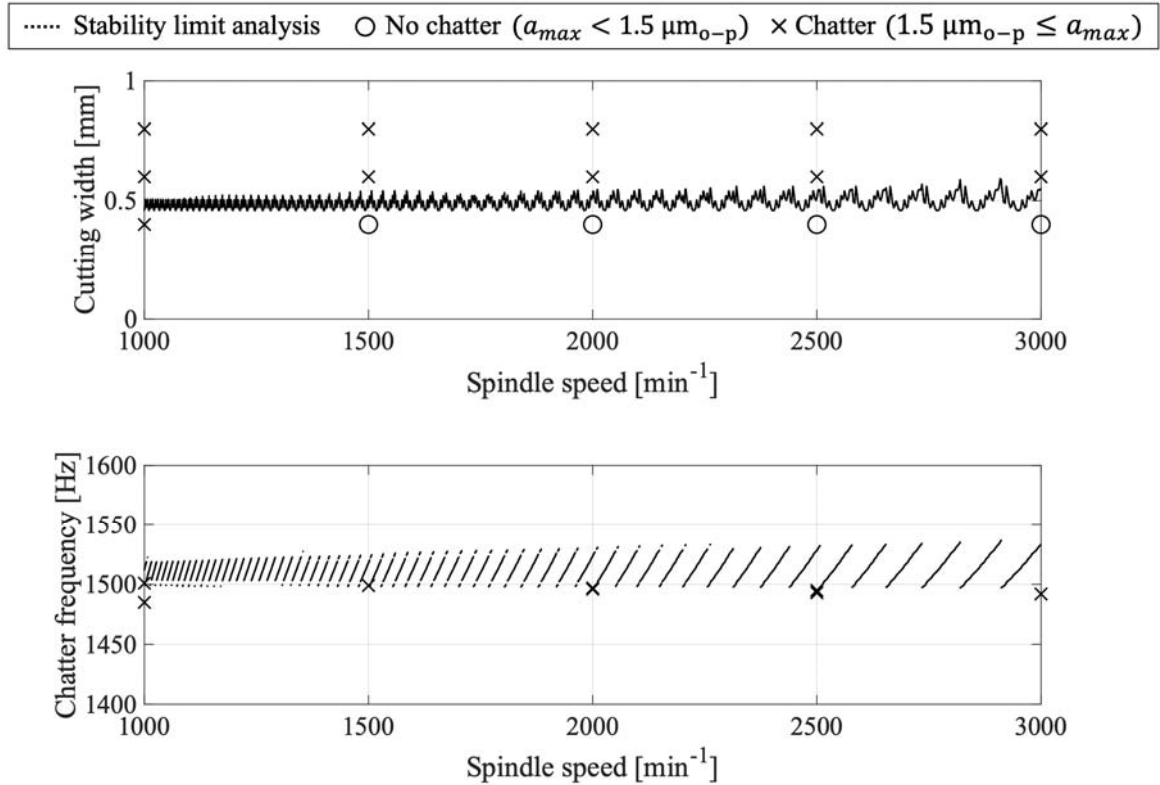


Fig. 2.11. Predicted stability limit and experimental results of CSS.

2.4.4 Cutting experiments with TSSV and comparison with simulations

Cutting experiments with TSSV are carried out by utilizing a commercially available function (Okuma Corp., Machining Navi L-g). Experimental conditions are shown in Table 2.4. Note that the values of the SSV parameters specified in Table 2.4 represent the set values, and the actual values are directly measured from the spindle speed signal. The value of r_a expressed in Eq. (2.9) is calculated by finding the moment of one revolution before from the integrated rotation angle and then calculating the proportion of the previous spindle speed to the present spindle speed. The value of the stability indices, i.e., $\overline{|r_a|}$ and N , are also calculated from the actual spindle speed. The cutting width is varied from 2.0 mm to 3.0 mm, which is about from 4 to 6 times the stability limit in CSS. The results of the cutting experiments

are compared with the results of the time-domain simulations. In the simulation, the actual spindle speed signal and modal parameters shown in Table 2.2 are utilized. Workpiece properties and cutting conditions in the simulation are the same with the experimental ones as shown in Tables 2.3 and 2.4.

Table 2.4. Experimental conditions for cutting with TSSV.

SSV parameters		
Nominal spindle speed n_0	[min ⁻¹]	1000, 1500, 2000
Variation period T	[sec]	0.5 - 3.5
Variation amplitude ratio RVA		0.1 - 0.5
Cutting conditions		
Feed rate (static depth of cut) h_0	[mm/rev]	0.05
Cutting width a	[mm]	2.0 - 3.0

The results of the cutting experiments and the time-domain simulations are shown in Fig. 2.13. Figures 2.13(a)-2.13(d) show the results in different cutting widths: (a) 2.0 mm, (b) 2.25 mm, (c) 2.5 mm, and (d) 3.0 mm. The horizontal and vertical axes represent $|\overline{r_a}|$ and N , respectively. Here, \circ represents the cutting result without chatter ($a_{max} < 1.5 \mu\text{m}_{0-p}$), Δ represents the cutting result with chatter ($1.5 \mu\text{m}_{0-p} \leq a_{max} < 6 \mu\text{m}_{0-p}$), and \times represents the cutting result with severe chatter ($6 \mu\text{m}_{0-p} \leq a_{max}$). In the simulation, the growing vibration in each period of SSV is considered as chatter. \square represents the simulation result without chatter, and $+$ represents the simulation result with chatter. The results of the experiments and the simulations show good correlation. From Fig. 2.13, the following characteristics concerned with the experiments are found.

First, when N is almost equal, the larger the $|\overline{r_a}|$, the larger the stability. Furthermore, when $|\overline{r_a}|$ is higher than about 8 %, the chatter can be suppressed even when the cutting width is set to 3.0 mm, i.e., about 6 times higher than the stability limit of CSS. Thus, it can be said that the stability increases with an increase of $|\overline{r_a}|$ regardless of the combination of SSV parameters shown in Table 2.4. Therefore, $|\overline{r_a}|$ is an effective index for

evaluating the stability of SSV, and hence the SSV parameters are desirable to be set so as to obtain a larger $\overline{|r_a|}$ for realizing a higher suppression effect of the chatter vibration throughout the cutting.

Second, when $\overline{|r_a|}$ is almost equal, the stability does not always increase as N increases in the experiment, e.g., A and B in Fig. 2.13(c). In addition, when $\overline{|r_a|}$ is smaller than 2 %, the chatter cannot be suppressed regardless of the value of N even at the smallest cutting width of 2.0 mm as shown in Fig. 2.13(a). From this, it can be considered that the influence of $\overline{|r_a|}$ on the chatter stability is more dominant than N , and these results are consistent with the simulation results shown in Fig. 2.7.

Note that some results disagree between the experiments and the simulations, e.g., A in Fig. 2.13(c). One reason for these disagreements can be thought to occur due to the criteria of chatter occurrence in the experiments which is judged from the magnitude of the dynamic displacement. More specifically, the smaller the N , the smaller the length of the unstable section. Hence, the chatter growth is also smaller, and this should result in a relatively smaller maximum amplitude of dynamic displacement. Therefore, when the stability of the cutting experiment is judged by the same criteria of a_{max} regardless of N , the results with a small N are likely to be more stable than the results with a large N .

Figure 2.14 shows an example of the experimental signals when chatter occurs which corresponds to C marked on Fig. 2.13(c). The cutting width is 2.5 mm, the nominal spindle speed n_0 is 1500 min⁻¹, the variation period T is 3.0 sec, and the variation amplitude ratio RVA is 0.5. The signal from the accelerometer is short-time Fourier transformed to confirm the chatter frequency and the displacement amplitude at each moment. During the cutting, the growth of chatter is observed in the transitions from the acceleration to the deceleration ($|r_a|$ is close to 0 %), and the chatter frequency changes in synchronization with the speed variation. More specifically, the chatter frequency decreases because of the negative acceleration rate. The chatter diminishes as $|r_a|$ increases, and the chatter does not grow in the transitions

from deceleration to acceleration because $|r_a|$ is large in the low speed. In order to verify the constant spatial frequency f_{sc} during chatter, the comparisons of f_{sc} at times t_a , t_b , and t_c marked on Fig. 2.14 are investigated by utilizing Eq. (2.6). The spindle speeds at times t_a , t_b , and t_c are 2195 min^{-1} , 2071 min^{-1} , and 1972 min^{-1} , respectively, and the chatter frequencies at times t_a , t_b , and t_c are 1540 Hz , 1465 Hz , and 1400 Hz , respectively. The calculated spatial frequencies at times t_a , t_b , and t_c are 6.70 , 6.76 , and 6.78 , respectively. From these results, it can be confirmed that the spatial frequencies at times t_a , t_b , and t_c are nearly the same. Therefore, the phenomena of the chatter frequency fluctuation in proportion to the spindle speed, i.e., the chatter grows up at a constant spatial frequency in SSV, is also validated experimentally.

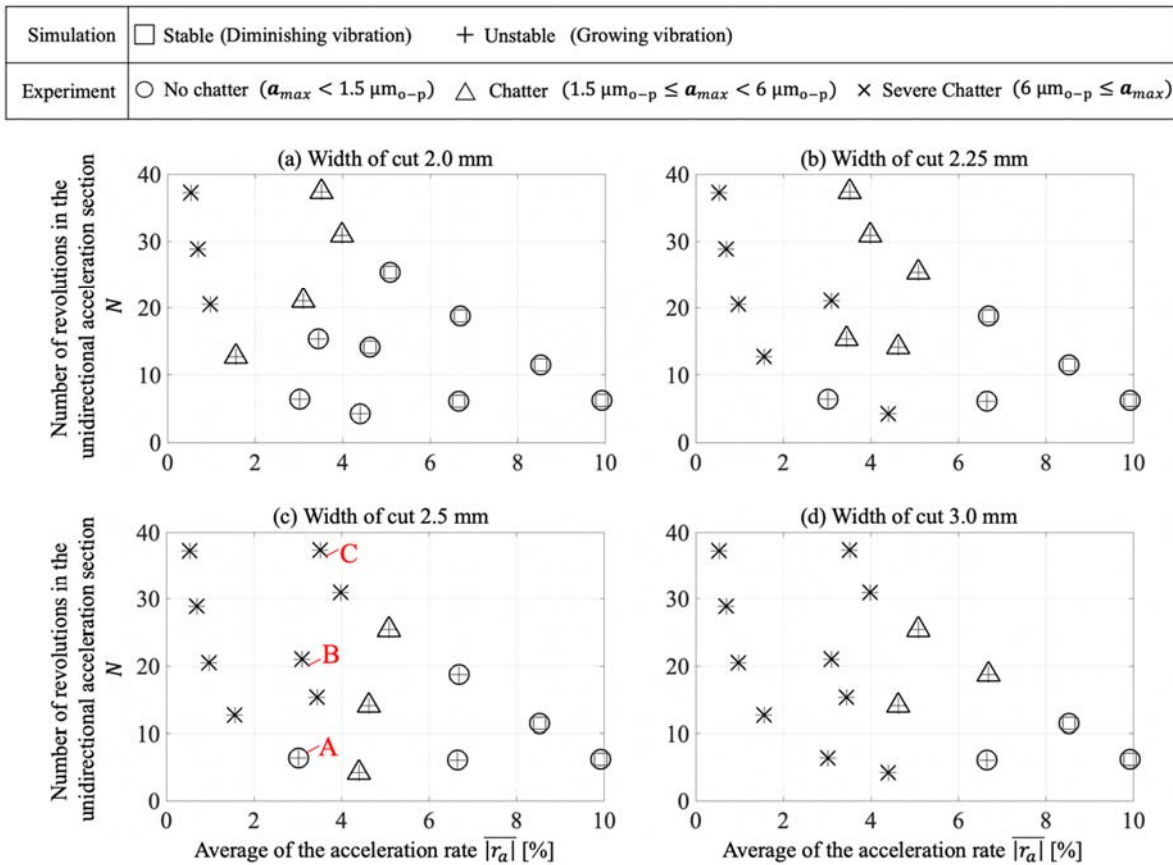


Fig. 2.13. Results of cutting experiments and time-domain simulations in TSSV against stability indices $\overline{|r_a|}$ and N under various cutting widths: (a) 2.0 mm, (b) 2.25 mm, (c) 2.5 mm, and (d) 3.0 mm.

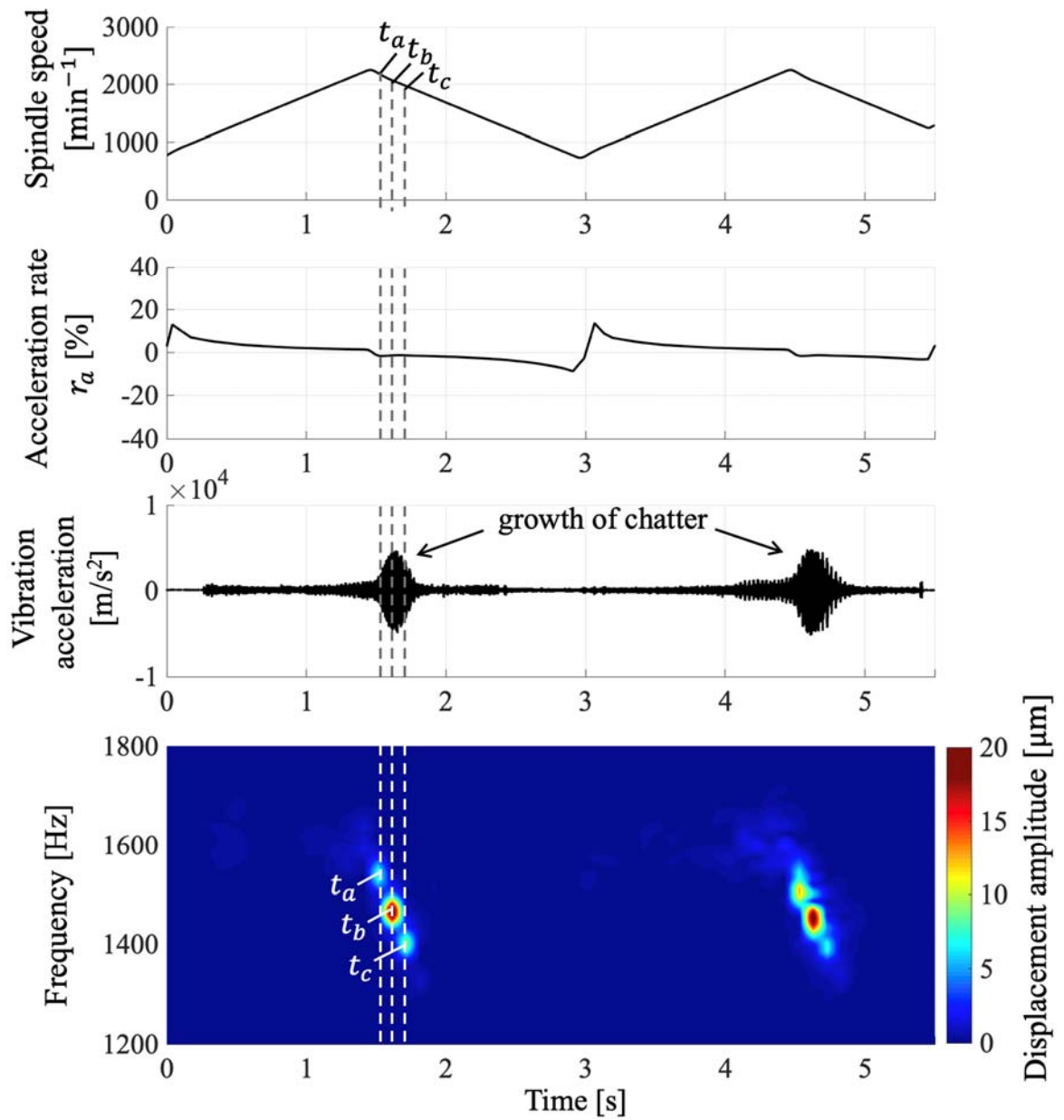


Fig. 2.14. Example of experimental signals of spindle speed and acceleration rate, corresponding vibration acceleration obtained from accelerometer, and short-time Fourier transform result of the vibration acceleration at unstable condition (C in Fig. 2.13) at $a=2.5$ mm, $n_0=1500$ min⁻¹, $T=3.0$ sec, and $RVA=0.5$ in TSSV.

2.5 Summary

The chatter growth characteristics in SSV were revealed, and the

suppression effect of SSV was newly explained focusing on the fluctuation of the time chatter frequency. Even when SSV is applied, the regenerative chatter can grow with a considerably flexible structure. It was found in this study that the regenerative chatter generally grows at a constant spatial frequency in SSV (the first chatter growth characteristic). Therefore, when chatter occurs, the time chatter frequency changes at the same ratio in which the spindle speed changes, meaning that the spatial frequency is kept constant, and it brings out change of the magnitude of the dynamic compliance. Due to the change of the magnitude, the chatter can be suppressed since the dynamic compliance usually reduces as the chatter frequency changes. It was found that the chatter is likely to grow during a period where r_a is small in SSV (the second chatter growth characteristic).

Based on the reduction of the compliance, the average of the absolute acceleration rate in one period of SSV $\overline{|r_a|}$ and the number of revolutions in a unidirectional acceleration section N were proposed as novel indices to evaluate the chatter stability in SSV, i.e. larger $\overline{|r_a|}$ and N result in a larger compliance reduction.

Through the analytical investigations with the time-domain simulation, it was proved that the revealed chatter growth characteristics are valid from the following facts:

- 1) The time chatter frequency changes in proportion to speed variation, and the spatial frequency is kept constant.
- 2) The chatter growth is confirmed during the period where r_a is small.

In addition, the relations between the stability and the proposed stability indices have been investigated, and the results are summarized as follows:

- 1) When N is equal, the higher the $\overline{|r_a|}$, the higher the stability regardless of the variation period T and the type of SSV. This denotes that $\overline{|r_a|}$ is an effective index for evaluating the stability in SSV.
- 2) When $\overline{|r_a|}$ is equal, the stability is the largest at a certain N , i.e., an optimal value of N exists. This is because a larger N causes a larger dynamic compliance reduction, but on the other hand it makes sections with small $|r_a|$

longer so that chatter grows there.

3) When the values of $\overline{|r_a|}$ and N are equal, the stability limits are almost identical regardless of the combination of SSV parameters, i.e., nominal spindle speed, variation period, and variation amplitude ratio. Hence, the stability limit can be estimated by utilizing the two proposed stability indices.

4) As a comparison of SSSV and TSSV, it was confirmed that the stability limit in SSSV is always smaller than TSSV when $\overline{|r_a|}$ and N are equal. This is because $|r_a|$ near the transitions from acceleration to deceleration becomes smaller in SSSV. Furthermore, a greater stability is always achieved in TSSV than SSSV under equal variation amplitude ratio RVA even though $\overline{|r_a|}$ and N in TSSV are lower than those in SSSV.

5) When RVA and T are equal, a greater stability can be achieved under lower nominal spindle speed since $\overline{|r_a|}$ increases. This indicates that the chatter suppression effect of TSSV and SSSV decreases in high-speed region, and thus remarkable improvement of machining efficiency cannot be realized unfortunately.

A series of experiments were carried out to verify the validity of the revealed chatter growth characteristics in SSV and to confirm the effectiveness of the proposed stability indices. The results of the cutting experiments with TSSV were compared with the time-domain simulations. The experimental results showed that when N is almost equal, the larger the $\overline{|r_a|}$, the larger the stability. Furthermore, when $\overline{|r_a|}$ is higher than about 8 %, the chatter can be suppressed in all the conditions of N even when the cutting width was set to 3.0 mm, i.e., about 6 times higher than the stability limit in CSS. These results indicate that $\overline{|r_a|}$ was experimentally verified as a valid stability index as it was verified in the analytical investigations, and it is important to set appropriate SSV parameters so that $\overline{|r_a|}$ is larger than the critical value which is required for the suppression of chatter throughout the cutting. On the other hand, when the values of $\overline{|r_a|}$ are almost equal, the stability does not always increase as N increases. In addition, when $\overline{|r_a|}$ was smaller than about 2%, the chatter

was not suppressed regardless of N even at the smallest cutting width. From these results, it was observed that the influence of $\overline{|r_a|}$ on the chatter stability is more dominant in comparison with N , and these results are consistent with the simulation results. The phenomena where the time chatter frequency changes at the same ratio in which the spindle speed changes, i.e., constant spatial frequency, was confirmed from the experimental signals. Finally, it was confirmed that the chatter grows during the periods where r_a is small. Hence, these denote that the revealed chatter growth characteristics are true.

Chapter 3

Proposal of Novel Spindle Speed Variation Profile with Constant Acceleration Rate for Improvement of Chatter Stability

3.1 Introduction

Extensive studies have been conducted to realize chatter suppression [3, 68]. Improving the design of the machine tool or cutting tool can expand the chatter-free zones [3]. For example, a specially designed cutting tool system to improve the damping capacity [26] and a special milling tool which can disrupt the regenerative effect with irregular pitch angle [60] or helix angle [33] were studied. Chatter can also be suppressed by adopting appropriate spindle speed [69] and rake/clearance angles [70] or utilizing actuators [71, 72].

As mentioned in Chapter 2, SSV is one of the effective and practical techniques for regenerative chatter suppression [62]. However, regenerative chatter can grow even if SSV is applied [46, 51, 52, 73] when the SSV parameters, i.e., nominal spindle speed, variation amplitude, and variation period, are set inappropriately. In Chapter 2, the chatter growth characteristics in the conventional SSV profiles, e.g., sinusoidal spindle speed variation (SSSV) and triangular spindle speed variation (TSSV), were clarified. When chatter occurs during cutting with SSV, it is found that the time chatter frequency changes at the same ratio as the spindle speed, meaning that the spatial frequency is kept constant (the first chatter growth characteristic) [73]. Here, the spatial chatter frequency denotes the number of waves which is left on the cut surface per radian due to the regenerative chatter. The change of the time chatter frequency causes the change of the magnitude of the dynamic compliance, and hence the chatter can be suppressed since the dynamic

compliance usually reduces as the chatter frequency changes. Note that a greater compliance reduction can be obtained by a higher rate of spindle speeds in two consecutive revolutions at the same angular position [73], i.e., acceleration rate, and thus the chatter grows where the acceleration rate is insufficient for suppressing the chatter (the second chatter growth characteristic).

Based on the magnitude of the compliance reduction, two novel indices to evaluate the chatter stability of SSV were proposed [73]. The first one is the average of the absolute acceleration rate in one period of SSV, and the second one is the number of revolutions in a unidirectional acceleration section. Their validity was verified through time-domain simulations and cutting experiments. On the other hand, it has been found that conventional SSV profiles has a limitation as follows: the acceleration rate always fluctuates in conventional SSV profiles, and hence suppressing chatter in all sections of SSV is difficult since the magnitude of chatter suppression effect changes during the speed variation. Especially, the acceleration rate decreases in a high-speed region, and thus remarkable improvement of machining efficiency cannot be realized.

In this research, a novel SSV which maintains a constant absolute acceleration rate, namely CAR-SSV, is proposed to overcome the limitation of the conventional SSV. Specifically, it is expected that the chatter stability can be improved in all speed regions by maintaining the absolute acceleration rate a constant which is higher than the critical value for suppressing chatter.

3.2 Proposal of CAR-SSV

3.2.1 Concept of CAR-SSV

When chatter grows in cutting with SSV, the time chatter frequency changes at the rate of spindle speeds in two consecutive revolutions at the same angular position, and hence the spatial frequency is constant in general [52, 73]. The time chatter frequency against time t , i.e., $f_c(t)$ [Hz], can be expressed as follows,

$$f_c(t) = \frac{n(t)}{n(t - \tau(t))} f_c(t - \tau(t)) \quad (3.1)$$

where $n(t)$ [min^{-1}], $\tau(t)$ [s], $n(t - \tau(t))$ [min^{-1}], and $f_c(t - \tau(t))$ [Hz] are the spindle speed against time t , spindle rotational period which varies depending on the spindle speed profile, the spindle speed at one revolution before, and the chatter frequency at one revolution before, respectively.

Since regenerative chatter tends to occur near the resonance, the change of the time chatter frequency causes a reduction of the magnitude of the dynamic compliance of the vibratory structure. A larger compliance reduction can be obtained with a larger change of time chatter frequency. Since the acceleration rate r_a [%] is equivalent to the rate of the change of the time chatter frequency, it was proposed as a key parameter to evaluate the chatter suppression effect by speed variation [52, 73]. For SSV, the average of the absolute acceleration rate in one period of SSV $\overline{|r_a|}$ was proposed as one of the indices to evaluate the chatter stability [73]. As introduced in the previous chapter, r_a [%] and $\overline{|r_a|}$ [%] were defined as follows.

$$r_a(t) = \left(\frac{n(t)}{n(t - \tau(t))} - 1 \right) \times 100 \quad (3.2)$$

$$\overline{|r_a|} = \frac{1}{T} \int_0^T |r_a(t)| dt \quad (3.3)$$

In general, the variation amplitude is set high to suppress regenerative chatter when utilizing SSV. This increases the number of revolutions in a unidirectional acceleration section N , which is the second stability index of SSV. However, it has been found that the acceleration rate inevitably fluctuates with this increase, and it becomes small in the high-speed region. Thus, the chatter suppression effect decreases. This is the limitation of the conventional SSV, and a remarkable improvement of the machining efficiency cannot be realized when utilizing them.

To overcome the limitation of the conventional SSV, CAR-SSV, where the absolute acceleration rate is maintained a constant which is higher than the critical value for suppressing chatter, is proposed. It is expected that the

chatter stability can be improved in all speed regions.

Examples of the spindle speed and the acceleration rate in CAR-SSV and TSSV are shown in Fig. 3.1. The red solid and blue dashed lines represent the profiles of CAR-SSV and TSSV, respectively. n_{min} , n_{max} , $n_{0,T}$, and $n_{0,C}$ in the spindle speed profile are the minimum spindle speed, the maximum spindle speed, nominal spindle speed in TSSV, and reference spindle speed in CAR-SSV, respectively. Note that $n_{0,C}$ is defined as the spindle speed at half the time period of a unidirectional acceleration, e.g., spindle speed at $T/4$. To maintain $|r_a|$ constant in the acceleration section in CAR-SSV, the speed change in each revolution becomes larger according to the increase of the spindle speed. In other words, a larger acceleration is necessary for higher spindle speeds, and thus the time period for changing a certain amount of spindle speed will be smaller in the higher spindle speeds compared to the lower spindle speeds. From this reason, the average spindle speeds in TSSV and CAR-SSV denote different values.

In order to make the spindle speed profiles in the acceleration and deceleration sections symmetrical against the spindle speed axis, $|r_a|$ in those sections are maintained unequal as $r_{s,acc}$ and $r_{s,dec}$ shown in the acceleration rate profile of CAR-SSV in Fig. 3.1. Specifically, assuming that n_h is a high spindle speed and n_l is a low spindle speed, $r_{s,acc}$ and $r_{s,dec}$ can be expressed as $r_{s,acc} = (n_h/n_l - 1) \times 100$ and $r_{s,dec} = (n_l/n_h - 1) \times 100$, respectively. The absolute values of those are unequal. However, the discrepancy between $r_{s,acc}$ and $r_{s,dec}$ is not large since they are usually small values. For instance, when $r_{s,acc}$ is set to 5%, $r_{s,dec}$ is about 4.8%. For the generation of the spindle speed profile, $r_{s,acc}$ is defined first, and then $r_{s,dec}$ is determined subordinately. Therefore, $r_{s,acc}$ will be utilized as set (aimed) acceleration rate r_s [%] in this research. Note that $r_{s,dec}$ can be set equal to $r_{s,acc}$, but the time period for the acceleration and deceleration sections will differ in that case. In the sections where the acceleration direction switches, i.e., switching from acceleration to deceleration ($= t_{1,C}$) or from deceleration to

acceleration ($= t_{2,c}$), $|r_a|$ is close to zero.

As for TSSV, it can be confirmed that r_a in TSSV fluctuates largely throughout the speed variation region. $\pm r_{max,T}$ and $\pm r_{min,T}$ represent the maximum and minimum acceleration rates of TSSV in all sections, respectively, except for the sections where the acceleration direction switches. t_h represents the time length where $|r_a|$ in CAR-SSV is greater than that in TSSV, and t_l represents the time length where $|r_a|$ in CAR-SSV is less than that in TSSV.

Chatter suppression effect throughout the cutting is expected in CAR-SSV since $|r_a|$ is maintained constant regardless of the speed variation except for the sections where the acceleration direction switches. Furthermore, when the critical $|r_a|$ necessary for suppressing the chatter is larger than $|r_{min,T}|$ but smaller than $|r_s|$, chatter can be effectively suppressed throughout the cutting when CAR-SSV is utilized. On the other hand, chatter grows during t_h when TSSV is utilized.

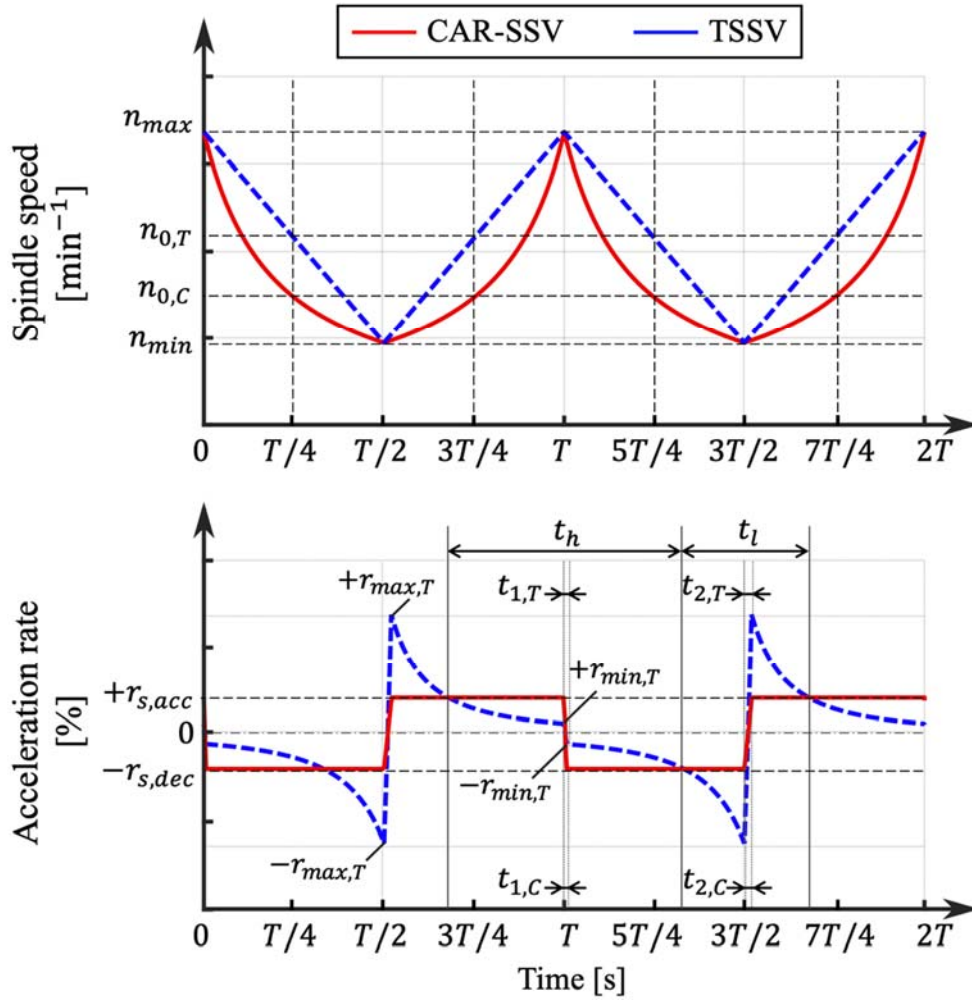


Fig. 3.1. Profiles of spindle speed and acceleration rate in CAR-SSV and TSSV.

3.2.2 Formulation of CAR-SSV profile

This section introduces the formulation of the CAR-SSV profile in order to utilize it in the time-domain simulation. The formulations of TSSV and SSSV have been introduced in the previous works [46, 73]. For CAR-SSV, the acceleration rate should be kept in acceleration/deceleration section. That means, the spindle speed should be increased/decreased as same as the acceleration rate during 1 revolution. Therefore, the following relations should be satisfied:

$$\begin{cases} n_{acc,C}(\theta) = \left(1 + \frac{r_{s,acc}}{100}\right) n_{acc,C}(\theta - 2\pi) \\ n_{dec,C}(\theta) = \left(1 + \frac{r_{s,dec}}{100}\right) n_{dec,C}(\theta - 2\pi) \end{cases} \quad (3.4)$$

Where $n_{acc,C}$ [min^{-1}] and $n_{dec,C}$ [min^{-1}] are the spindle speed of CAR-SSV in

the acceleration section and the deceleration section, respectively. From those relations, $n_{acc,C}$ [min^{-1}] and $n_{dec,C}$ [min^{-1}] can be formulated as follows:

$$\begin{cases} n_{acc,C}(\theta) = n_{ini} \left(1 + \frac{r_{s,acc}}{100}\right)^{\frac{\theta}{2\pi}} \\ n_{dec,C}(\theta) = n_{ini} \left(1 + \frac{r_{s,dec}}{100}\right)^{\frac{\theta}{2\pi}} \end{cases} \quad (3.5)$$

where n_{ini} [min^{-1}] is the initial spindle speed in that section. The following differential equation in the acceleration section can be obtained:

$$\frac{d\theta}{dt} = \frac{2\pi n_{acc,C}(\theta)}{60} = \frac{2\pi n_{ini} \left(1 + \frac{r_{s,acc}}{100}\right)^{\frac{\theta}{2\pi}}}{60} \quad (3.6)$$

This equation can be transformed as follows:

$$\frac{dt}{d\theta} = \frac{60}{2\pi n_{ini} \left(1 + \frac{r_{s,acc}}{100}\right)^{\frac{\theta}{2\pi}}} = \frac{60}{2\pi n_{ini}} e^{-\frac{\theta}{2\pi} \ln\left(1 + \frac{r_{s,acc}}{100}\right)} \quad (3.7)$$

Next, Eq. (3.8) can be obtained from the integration of Eq. (3.7):

$$\begin{aligned} t &= \int \frac{dt}{d\theta} d\theta = \frac{60}{2\pi n_{ini}} \int e^{-\frac{\theta}{2\pi} \ln\left(1 + \frac{r_{s,acc}}{100}\right)} d\theta \\ &= -\frac{60}{n_{ini} \ln\left(1 + \frac{r_{s,acc}}{100}\right)} e^{-\frac{\theta}{2\pi} \ln\left(1 + \frac{r_{s,acc}}{100}\right)} + C \end{aligned} \quad (3.8)$$

where C is an integral constant, and C can be determined by utilizing the initial condition ($t(0) = 0$) as follows:

$$C = \frac{60}{n_{ini} \ln\left(1 + \frac{r_{s,acc}}{100}\right)} \quad (3.9)$$

From Eqs. (3.8) and (3.9), $\theta(t)$ can be calculated as:

$$\theta(t) = -\frac{2\pi}{\ln\left(1 + \frac{r_{s,acc}}{100}\right)} \ln\left\{1 - \left(\frac{n_{ini}}{60} \ln\left(1 + \frac{r_{s,acc}}{100}\right)\right) t\right\} \quad (3.10)$$

The following differential equation is obtained:

$$\frac{d\theta(t)}{dt} = \frac{2\pi n_{ini}}{60 - \left\{n_{ini} \ln\left(1 + \frac{r_{s,acc}}{100}\right)\right\} t} \quad (3.11)$$

By using Eqs. (3.6) and (3.11), $n_{acc,C}(t)$ can be derived as follows:

$$n_{acc,c}(t) = \frac{n_{ini}}{1 - \left\{ \frac{n_{ini}}{60} \ln \left(1 + \frac{r_{s,acc}}{100} \right) \right\} t} \quad (3.12)$$

In the same manner with Eqs. (3.6)-(3.11), the formulation of $n_{dec,c}(t)$ can be derived as:

$$n_{dec,c}(t) = \frac{n_{ini}}{1 - \left\{ \frac{n_{ini}}{60} \ln \left(1 + \frac{r_{s,dec}}{100} \right) \right\} t} \quad (3.13)$$

In this research, $r_{s,acc}$ is defined as the set acceleration rate r_s [%].

$|r_a|$ is close to zero at the sections where the acceleration direction switches. Since the angle of these sections is one revolution, i.e., 2π rad, the time lengths t_1 and t_2 satisfy the following equations.

$$\int_{\frac{kT}{2}}^{\frac{kT}{2}+t_1} \frac{n(t)}{60} dt = 1 \quad (k = 2, 4, 6, 8 \dots) \quad (3.14)$$

$$\int_{\frac{k'T}{2}}^{\frac{k'T}{2}+t_2} \frac{n(t)}{60} dt = 1 \quad (k' = 1, 3, 5, 7 \dots) \quad (3.15)$$

3.3 Analytical investigations of CAR-SSV

3.3.1 Time-domain simulation model

Time-domain simulations are carried out to investigate the influence of the parameters of CAR-SSV on the chatter stability and to verify the validity of CAR-SSV through comparison with SSSV and TSSV. Figure 3.2 shows a schematic illustration of the dynamic model in a SDOF vibratory system. It is assumed that the cutting tool is flexible in the thrust (z) direction, and the regeneration occurs only in the z direction. The dynamic uncut chip thickness $h(t)$ [m] and dynamic cutting force in the thrust direction $F_z(t)$ [N] can be expressed as follows:

$$h(t) = h_0 + \mu z(t - \tau(t)) - z(t) = h_0 + \mu z(\theta(t) - 2\pi) - z(t) \quad (3.16)$$

$$F_z(t) = K_z a h(t) \quad (3.17)$$

where h_0 [m] is the static depth of cut, μ is the overlapping factor ($\mu = 1$ in orthogonal cutting process such as pipe-plunging), $\tau(t)$ [s] is the time-varying

spindle rotational period, $z(t)$ [m] is the dynamic displacement, $\theta(t)$ [rad] is the spindle rotational angle, $z(\theta(t) - 2\pi)$ is the dynamic displacement of one revolution before at the spindle rotational angle $\theta(t)$, K_z [Pa] is the specific cutting force in the thrust direction, and a [m] is the cutting width.

The equation of motion of the tool can be expressed as follows:

$$m\ddot{z}(t) + c\dot{z}(t) + kz(t) = K_z a (h_0 + \mu z(\theta(t) - 2\pi) - z(t)) \quad (3.18)$$

where m [kg], c [N/(m·s)], and k [N/m] are the modal mass, damping coefficient, and stiffness of the tool, respectively. The time-varying spindle rotational period $\tau(t)$ can be calculated by the following equation.

$$\int_{t-\tau(t)}^t \frac{n(t)}{60} dt = 1 \quad (3.19)$$

In the time-domain simulation, $z(t)$ is calculated by solving Eq. (3.18) directly, and the solution is approximated by the 4th order Runge-Kutta method. In order to calculate $\theta(t)$, $z(\theta(t) - 2\pi)$, and $r_a(t)$, the values of $z(t)$ and $n(t)$ at each calculation step of the time-domain simulation are memorized. For instance, $\theta(t)$ can be calculated by integrating the spindle speed by Eq. (3.20), and the time difference between the present and previous revolutions at the same angular position $\tau(t)$ is determined by finding the minimum value of K satisfying the following modulo function: $\text{mod}(\theta(t) - \theta(t - K \times t_{res}), 2\pi) \cong 0$, i.e., $\tau(t) = \min(K) \times t_{res}$, where t_{res} is the time resolution of the simulation.

$$\theta(t) = 2\pi \int_0^t \frac{n(t)}{60} dt \quad (3.20)$$

The static depth of cut gradually increases at the beginning of the simulation, and this is the only source of chatter applied in it. Note that the tool disengagement from the workpiece due to the chatter growth, i.e., $h(t) = 0$, and the multiple regenerative effect [74] from this phenomenon are considered in the simulation.

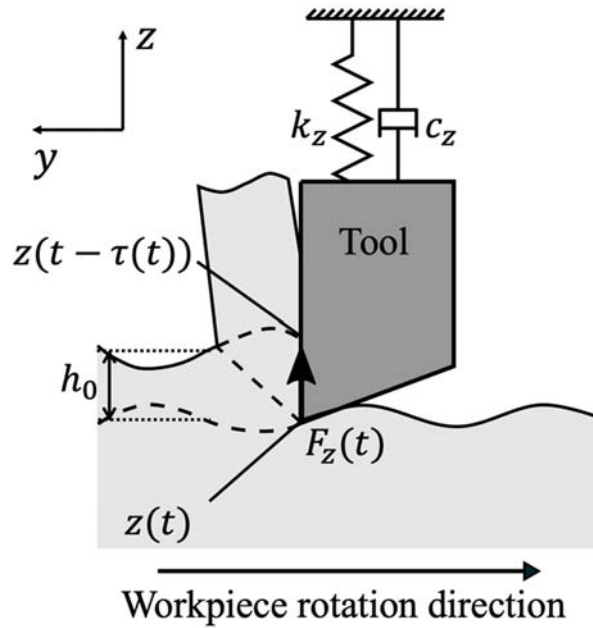


Fig. 3.2. Schematic illustration of dynamic cutting model with SDOF vibratory system.

3.3.2 Comparison with conventional SSV based on stability indices

In order to verify the effectiveness of CAR-SSV, a comparison of the stability of CAR-SSV and conventional SSV is carried out based on the stability indices [73], i.e., $|\overline{r_a}|$ and N . The parameters utilized in the time-domain simulation are shown in Table 3.1. The cutting width is increased by 0.1 mm increment, and the cutting width where chatter occurs is searched. Note that the growing vibration in each period of SSV is considered as chatter. By subtracting one increment from that width, the stability limit a_{lim} [mm] is determined.

Table 3.1. Parameters used in time-domain simulation.

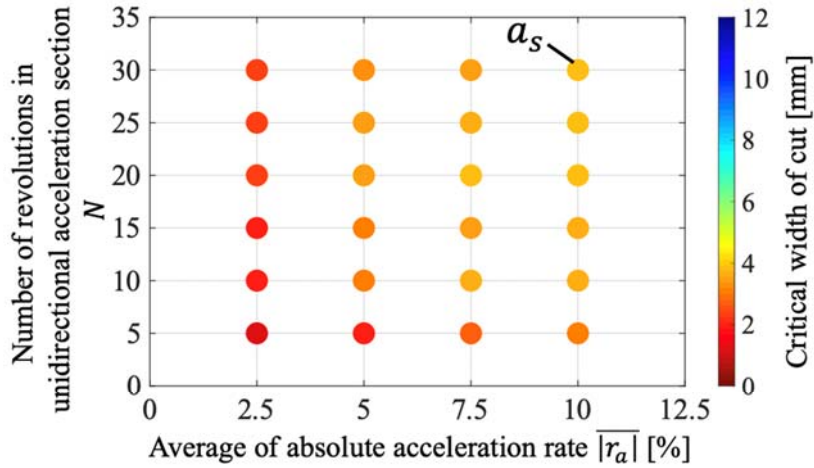
Workpiece properties			
Diameter D		[mm]	70
Specific cutting force in thrust direction K_z		[MPa]	711
Modal parameters			
Mass m		[kg]	0.2266
Damping coefficient c		[N/(m·s)]	44.19
Stiffness k		[N/m]	1.118×10^7
Parameters of CAR-SSV			

Reference spindle speed $n_{0,C}$	[min ⁻¹]	600-3500
Variation period T	[s]	1.0
Set acceleration rate r_s	[%]	2.5-10.2
Cutting conditions		
Feed rate (static depth of cut) h_0	[mm/rev]	0.05
Cutting width a	[mm]	0.1 – 12.0

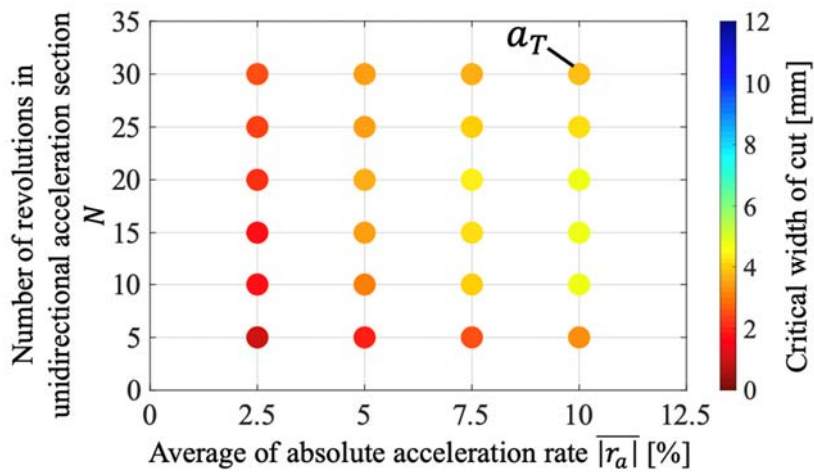
Figure 3.3 shows the stability limits against the stability indices $\overline{|r_a|}$ and N in (a) SSSV [73], (b) TSSV [73], and (c) CAR-SSV at $T = 1.0$ s. In the case of SSSV and TSSV, $n_{0,S}$ and $n_{0,T}$ is proportional to N at a constant T [73]. Meanwhile, since the average spindle speed in CAR-SSV is different from $n_{0,C}$, the values of $n_{0,C}$ and r_s in CAR-SSV at each condition in Fig. 3.3(c) that satisfy the defined values of $\overline{|r_a|}$ and N are searched. The magnitude of the stability limit (critical cutting width) is represented by utilizing a color map. From Fig. 3.3, the following remarks are found.

- 1) When $\overline{|r_a|}$ and N are the same, the stability limit of CAR-SSV is always equal to or higher than those of SSSV and TSSV. The increase of the stability limit of CAR-SSV to those of SSSV and TSSV at each condition is calculated. From the result, it is confirmed that the larger the $\overline{|r_a|}$ and N , the larger the increase. Especially, the stability limit at $\overline{|r_a|} = 10$ % and $N = 30$ in CAR-SSV (a_C in Fig. 3.3(c)) is about 2.70 times those of SSSV (a_S in Fig. 3.3(a)) and TSSV (a_T in Fig. 3.3(b)).
- 2) When N is the same, the stability limit increases with an increase of $\overline{|r_a|}$ regardless of the type of SSV.
- 3) When $\overline{|r_a|}$ is the same, the stability limits of SSSV and TSSV are the largest at a certain N , e.g., 20 in the case of $\overline{|r_a|} = 10$, but the stability limit of CAR-SSV increases with an increase of N under all $\overline{|r_a|}$. The reason for this can be considered as follows. In the cases of SSSV and TSSV, the fluctuation amplitude of $|r_a|$ becomes large with an increase of N [73], and hence the chatter can grow when $|r_a|$ is insufficient to suppress the chatter. In contrast, when utilizing CAR-SSV, $|r_a|$ is

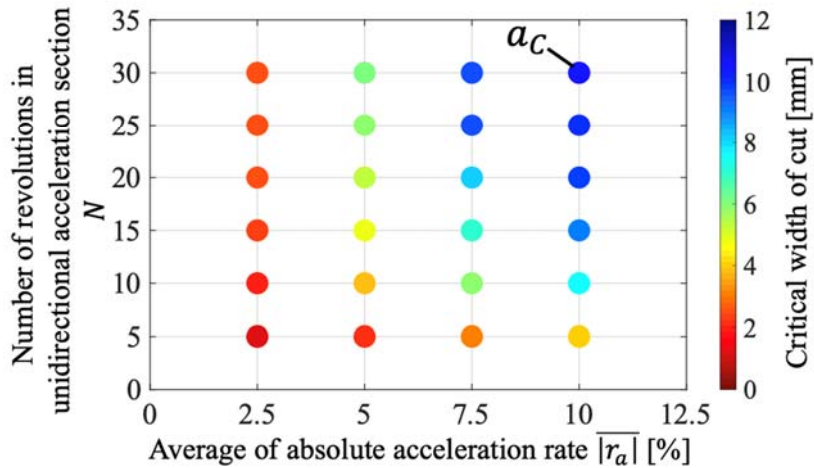
sufficient in almost all sections since $|r_a|$ is kept constant except for the sections where the acceleration direction switches. Therefore, a larger change of chatter frequency can be obtained with a larger N , and it increases the stability limit.



(a) SSSV, $T = 1.0$ s



(b) TSSV, $T = 1.0$ s



(c) CAR-SSV, $T = 1.0$ s

Fig. 3.3. Stability limits against stability indices $\overline{|r_a|}$ and N in (a) SSSV, (b) TSSV, and (c) CAR-SSV at $T = 1.0$ s.

3.3.3 Clarification of effects of CAR-SSV parameters on stability

Next, the relations between the CAR-SSV parameters and the stability are investigated to propose the strategies for setting appropriate parameters. The parameters of CAR-SSV utilized in investigation are shown in Table 3.2. Figure 3.4 shows the simulation results at multiple variation periods: (a) $T = 0.5$ s, (b) $T = 1.0$ s, (c) $T = 2.0$ s, and (d) $T = 4.0$ s. Each graph represents the stability limit against the acceleration rate. The black dotted line with crosses represents the results at $n_{0,C} = 1000$ min⁻¹, the blue dashed line with triangles represents the results at $n_{0,C} = 1500$ min⁻¹, and the red solid line with circles represents the results at $n_{0,C} = 2000$ min⁻¹. Figures 3.5 (a), (b), and (c) show the profiles of the spindle speed $n(t)$, the acceleration rate $r_a(t)$, and the spindle rotational angle $\theta(t)$ which correspond to A, B, and C marked on Fig. 3.4, respectively. Here, the set acceleration rate r_s in the three profiles are the same, i.e., 3 %, but $n_{0,C}$ and T are different: (a) $n_{0,C} = 1000$ min⁻¹, $T = 0.5$ s, (b) $n_{0,C} = 2000$ min⁻¹, $T = 0.5$ s, and (c) $n_{0,C} = 1000$ min⁻¹, $T = 4.0$ s. Note that even if $n_{0,C}$ and r_s are the same, the larger the T , the higher the maximum spindle speed and the lower the minimum spindle speed as shown in Figs. 3.5 (a) and 3.5 (c). From the results, the following remarks are found.

Table 3.2. Parameters of CAR-SSV used in time-domain simulation.

Parameters of CAR-SSV		
Reference spindle speed $n_{0,C}$	[min ⁻¹]	1000, 1500, 2000
Variation period T	[s]	0.5, 1.0, 2.0, 4.0
Set acceleration rate r_s	[%]	1, 2, 3, 4, 5, 6

- 1) The stability limit increases with a higher r_s under most $n_{0,C}$ and T , except for when r_s increases from 5 % to 6 % at $T = 4.0$ s shown in

Fig. 3.4(d). Hence, in order to increase the chatter stability, it is desirable to set a larger r_s as long as the limit of the spindle motor load is not exceeded.

- 2) When r_s is the same, the stability limit mostly increases with an increase of $n_{0,C}$ and T . To investigate this reason, $\overline{|r_a|}$ [%] and N of the profiles shown in Fig. 3.5 are evaluated. Note that N is calculated as follows:

$$N = \frac{\int_{T/2}^T \theta(t) dt}{2\pi} = \frac{\int_T^{3T/2} \theta(t) dt}{2\pi} \quad (3.21)$$

t_1 is the time period of the section where the acceleration directions switches from deceleration to acceleration, t_2 is the time period of the section where the acceleration direction switches from acceleration to deceleration, t_3 is the time period of the acceleration section, and t_4 is the time period of the deceleration section. The calculated values of $(\overline{|r_a|}, N)$ at the conditions of A, B, and C are (2.68 %, 4.18), (2.86 %, 8.35), and (2.99 %, 36.1), respectively. From these, it is confirmed that the larger the $n_{0,C}$ and T , the larger the $\overline{|r_a|}$ and N even though the set value r_s is the same. Thus, the stability increases because the chatter frequency can be greatly changed, and the dynamic compliance can be greatly reduced. Assuming the initial chatter frequency f_0 , the change of chatter frequency can be expressed as $f_0 \times (1 + r_s/100)^N$. The value of $(1 + r_s/100)^N$ at A, B, and C are 1.12, 1.27, and 2.90, respectively. The dominant reason for the reduction of the compliance is the increase of N because $\overline{|r_a|}$ in all conditions show a similar value. One more reason can be the increase of $\overline{|r_a|}$ from the decrease of t_1 and t_2 , which means that the length of the section where $|r_a|$ is insufficient decreases as shown in Fig. 3.5. For reference, the ratio of the sum of the time periods where the acceleration direction changes ($t_1 + t_2$) to the sum of the time periods where r_a is maintained a constant ($t_3 + t_4$) is calculated. The calculated $(t_1 + t_2)/(t_3 + t_4)$ at the conditions of A, B, and C are 0.3256, 0.1358, and 0.0312, respectively. From these two

reasons, by setting a large $n_{0,c}$ and T , a remarkable improvement of the machining efficiency can be realized by utilizing CAR-SSV since a large cutting width, i.e., large stability limit, can be adopted. Hence, CAR-SSV can be an effective solution to overcome the limitation of conventional SSV.

- 3) The tendency of the increase of the stability with a higher $n_{0,c}$ is not confirmed at $T = 4.0$ s. This is thought to happen because the chatter frequency changes excessively due to an extremely large N at a large T . More specifically, when the chatter frequency excessively changes from the resonance, the reduction effect of the dynamic compliance reaches a certain asymptotic value since the compliance is nearly constant far away from the resonance. Therefore, the increase of the stability against the increase of N becomes smaller.

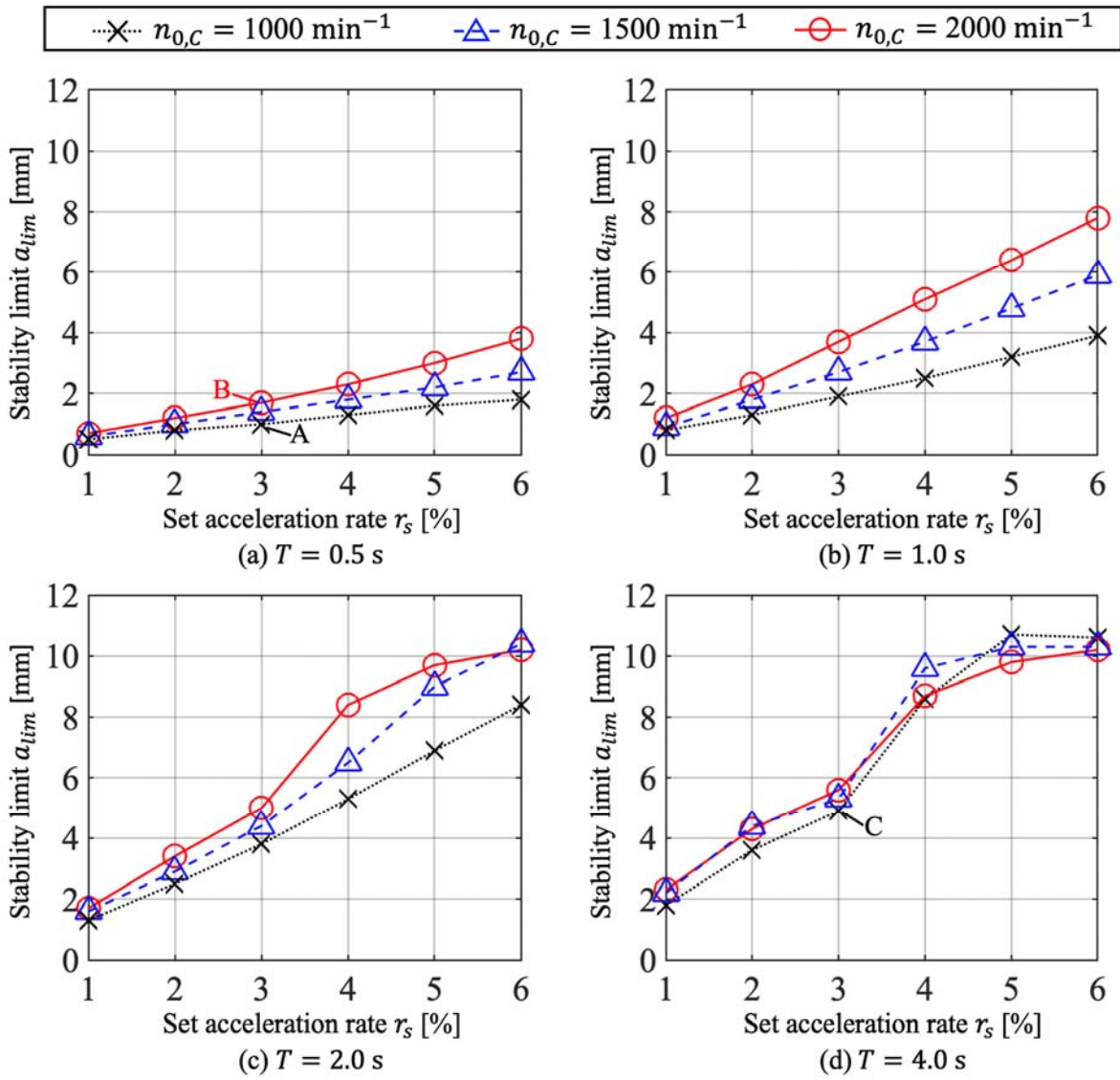


Fig. 3.4. Stability limits against acceleration rate under varied $n_{0,c}$ and T .

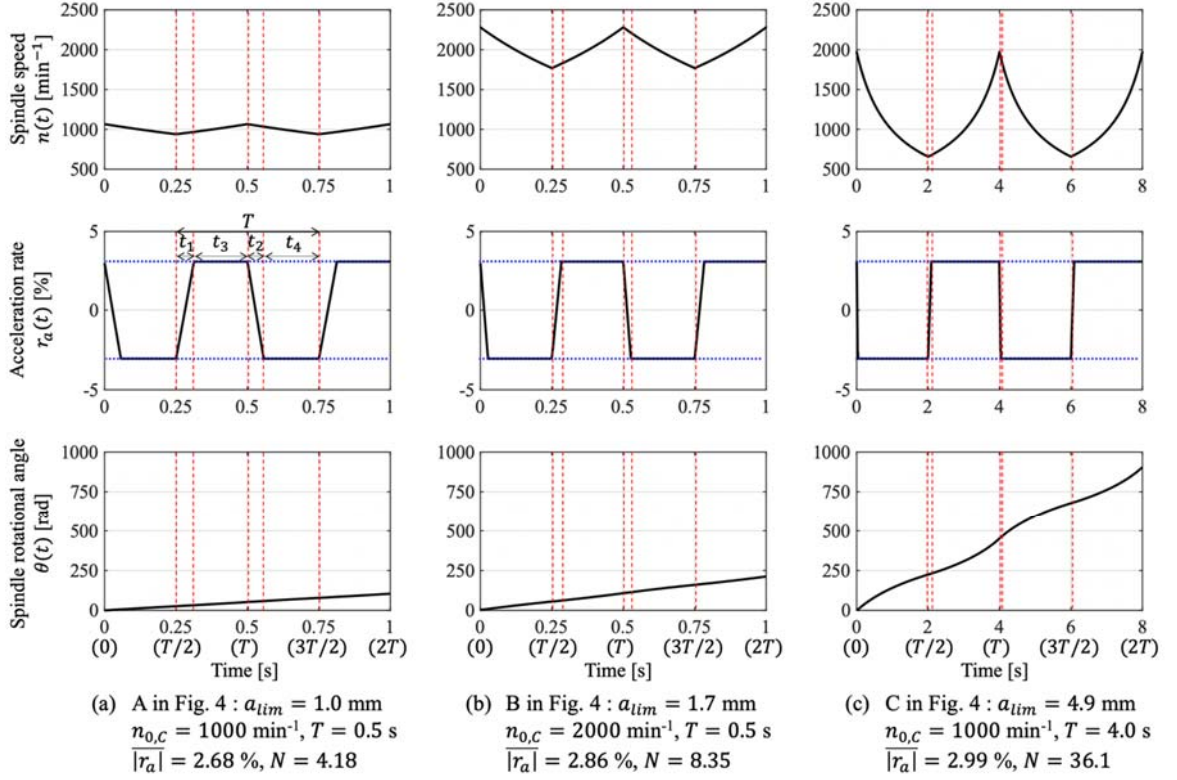


Fig. 3.5. Profiles of spindle speed, acceleration rate, and spindle rotational angle.

3.3.4 Comparison with conventional SSV focusing on its applicability

To verify the effectiveness of CAR-SSV focusing on its applicability to the actual industry, the machining efficiency against the thermal load of the spindle motor in CAR-SSV, TSSV, and SSSV are compared.

The spindle speeds of TSSV $n_T(t)$ [min $^{-1}$] and SSSV $n_S(t)$ [min $^{-1}$] can be described as follows.

$$n_T(t) = \begin{cases} n_{0,T} + n_{A,T} - \frac{4n_{A,T}}{T} \text{mod}(t, T) & \text{if } 0 \leq \text{mod}(t, T) < T/2 \\ n_{0,T} - 3n_{A,T} + \frac{4n_{A,T}}{T} \text{mod}(t, T) & \text{if } T/2 \leq \text{mod}(t, T) < T \end{cases} \quad (3.22)$$

$$n_S(t) = n_{0,S} + n_{A,S} \sin\left(\frac{2\pi}{T}t + \frac{\pi}{2}\right) \quad (3.23)$$

Here, $n_{0,T}$ [min $^{-1}$] and $n_{0,S}$ [min $^{-1}$] are the nominal spindle speeds in TSSV and SSSV, respectively, and $n_{A,T}$ [min $^{-1}$] and $n_{A,S}$ [min $^{-1}$] are the variation amplitudes in TSSV and SSSV, respectively. The profiles of CAR-SSV are created at first, and then the profiles of TSSV and SSSV are created with identical thermal load and identical average spindle speed as those of CAR-

SSV so that the three profiles can be compared from a practical viewpoint. As a first step, the average spindle speed of CAR-SSV n_{ave} [min⁻¹] is calculated by Eq. (3.24), and $n_{0,T}$ and $n_{0,S}$ are set equal to n_{ave} .

$$n_{ave} = \frac{2}{T} \int_{T/2}^T n_{acc,c}(t) dt \quad (3.24)$$

The thermal load of the spindle motor is basically proportional to the square of the current. Since the current increases proportionally to the spindle acceleration, the thermal load of the spindle motor increases proportionally to the square of the acceleration. Hence, the average of the square of the spindle acceleration \bar{H} [rev²/s⁴] is equivalent to the average thermal load increase of the spindle motor. The average of the square of the spindle acceleration in SSV \bar{H} [rev²/s⁴] can be calculated as follows.

$$\bar{H} = \frac{2}{T} \int_{T/2}^T \left(\frac{dn(t)}{dt} \frac{1}{60} \right)^2 dt \quad (3.25)$$

\bar{H} in CAR-SSV is calculated, and then $n_{A,T}$ and $n_{A,S}$ are determined to satisfy the following relations in order to set the same thermal load from Eqs. (3.22)-(3.25).

$$n_{A,T} = 15T\sqrt{\bar{H}} \quad (3.26)$$

$$n_{A,S} = \frac{30T\sqrt{2\bar{H}}}{\pi} \quad (3.27)$$

The utilized parameters of CAR-SSV are shown in Table 3.2 and the parameters of TSSV and SSSV are determined by Eqs. (3.25)-(3.27). The machining efficiency P [mm³/min] is defined with material removal rate (MRR) as follows:

$$P = a_{lim}\pi D h_0 n_{ave} \quad (3.28)$$

As shown in Table 3.1, D and h_0 are fixed values which are set the same as those in the experimental conditions. Figure 3.6 shows the obtained P against \bar{H} in the three types of SSV under varied T : (a) $T = 0.5$ s, (b) $T = 1.0$ s, (c) $T = 2.0$ s, and (d) $T = 4.0$ s. Red circles represent the results of CAR-SSV, blue triangles represent the results of TSSV, and green crosses represent the results of SSSV. Note that the variation amplitudes of TSSV and SSSV should

be set smaller than their average spindle speeds because the spindle speed cannot be lower than 0 min^{-1} . Therefore, the conditions which do not satisfy this constraint are neglected, and those are not plotted in Fig. 3.6.

Figure 3.7 shows the profiles of the spindle speed and the acceleration rate in CAR-SSV, TSSV, and SSSV which correspond to A, B, and C marked on Fig. 3.6: (A) $T = 0.5 \text{ s}$, $n_{0,C} = 1000 \text{ min}^{-1}$, and $r_s = 3 \%$, (B) $T = 0.5 \text{ s}$, $n_{0,C} = 2000 \text{ min}^{-1}$, and $r_s = 6 \%$, and (C) $T = 2.0 \text{ s}$, $n_{0,C} = 1000 \text{ min}^{-1}$, and $r_s = 3 \%$. From Figs. 3.6 and 3.7, the following remarks are found.

- 1) When \bar{H} is the same, P of CAR-SSV is almost equal to or higher than those of TSSV and SSSV. It is verified that CAR-SSV is more effective to suppress chatter, and the applicability to the actual industry is superior to that of the conventional SSV profiles.
- 2) From Fig. 3.6, it is confirmed that the increase of the machining efficiency in CAR-SSV compared to those of TSSV and SSSV becomes larger with a larger \bar{H} and T . The reason for this can be explained as follows. As shown in Fig. 3.7, the larger the \bar{H} and T , the larger the fluctuation amplitude of r_a in TSSV and SSSV. Consequently, the sections where $|r_a|$ in TSSV and SSSV is smaller than $|r_a|$ in CAR-SSV (near the transitions from acceleration to deceleration) becomes longer. Hence, the change of chatter frequency becomes smaller in those sections in TSSV and SSSV, and the stabilization effect decreases since a sufficient compliance reduction cannot be obtained. In contrast, in the case of CAR-SSV, the time periods t_1 and t_2 of the sections where $|r_a|$ decreases, i.e., the transitions of the acceleration direction, become shorter with a larger \bar{H} and T , and thus CAR-SSV can overcome the limitation of TSSV and SSSV.

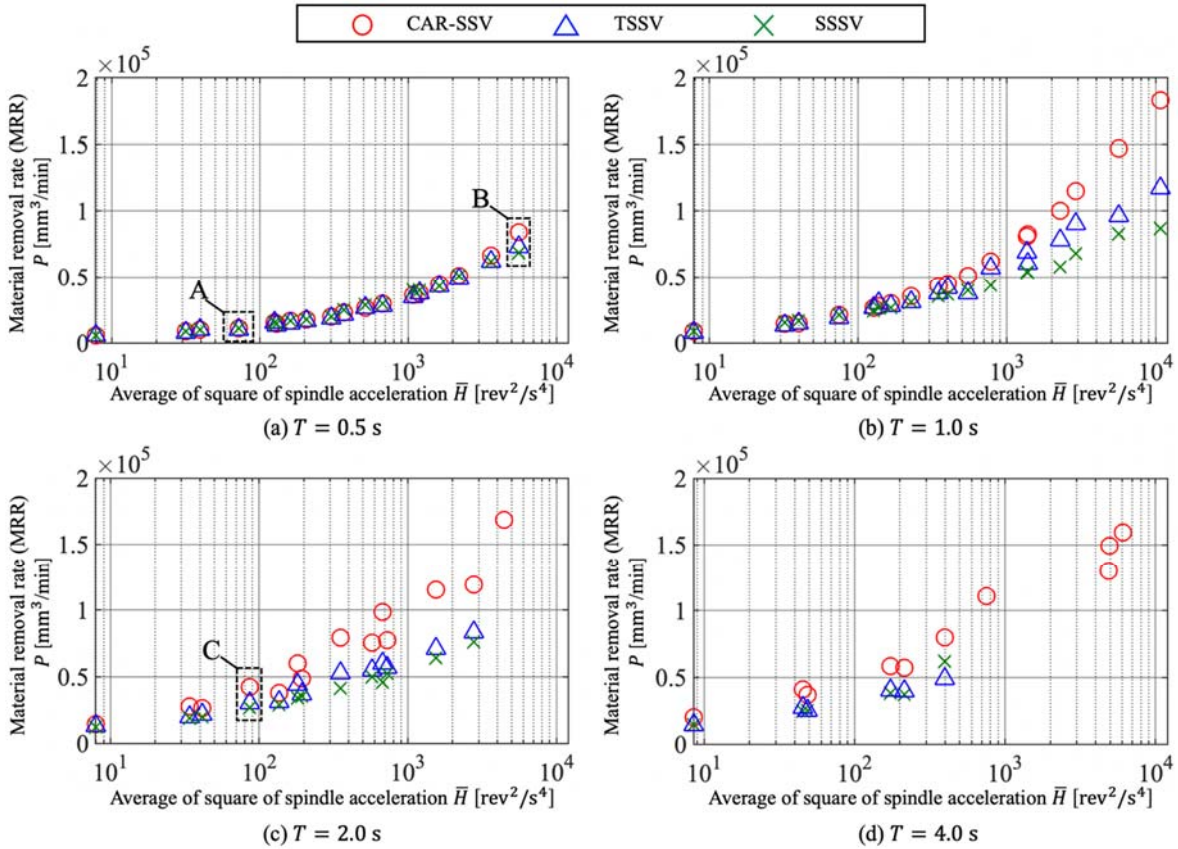


Fig. 3.6. Simulation results of material removal rate (MRR) P against average of square of spindle acceleration \bar{H} under varied T .

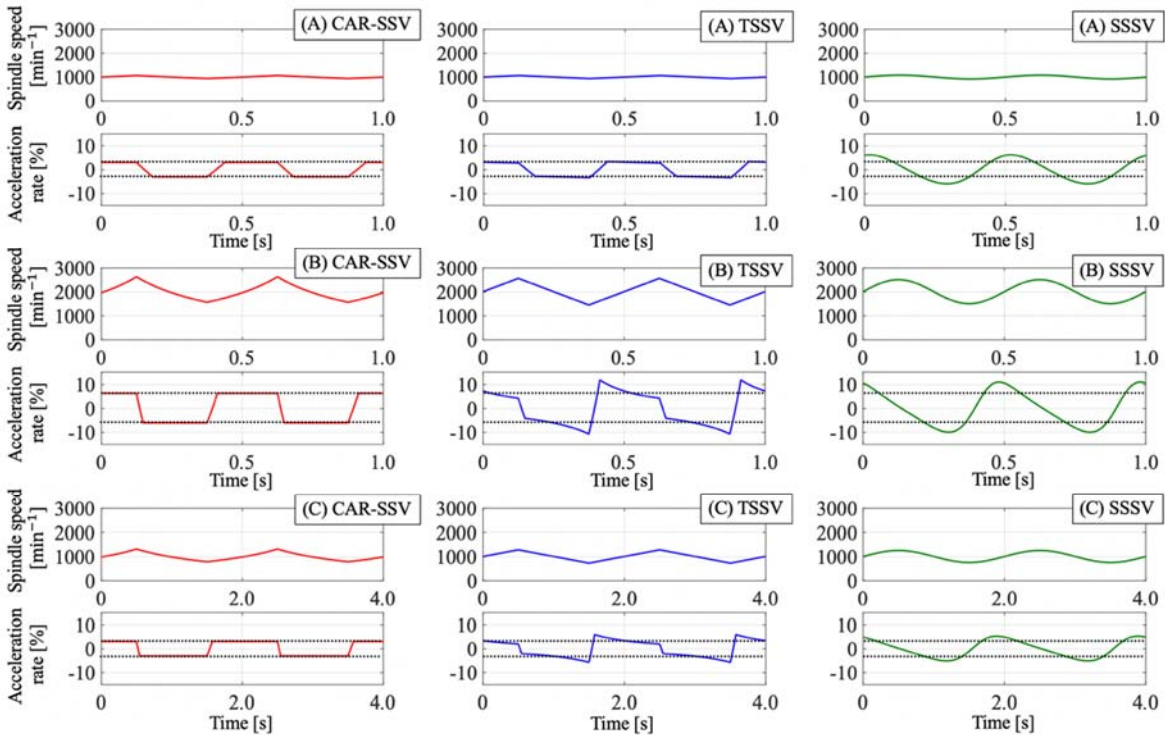


Fig. 3.7. Profiles of spindle speed and acceleration rate corresponding to A, B, and C.

C marked in Fig. 3.6.

3.4 Experimental investigations into CAR-SSV

3.4.1 Experimental setup

Two series of experiments are carried out to verify the effectiveness of CAR-SSV. Figure 3.8 shows a photograph of the experimental setup for the pipe-end plunging. A 2-turret CNC lathe (Okuma Corp., SIMUL TURN LU3000EX) is utilized, and a tool insert (Mitsubishi Material Corp., TCMW16T308 HTi10) mounted on a tool shank (steel, ISO C45) with a rectangular cross-section is used to cut a pipe-shaped workpiece (brass, ISO CuZn35). The rake and clearance angles of the tool are 0 and 7 deg, respectively. The spindle speed and vibration acceleration signals are obtained from the spindle motor encoder and a 3-axis accelerometer mounted on the tool shank, respectively.

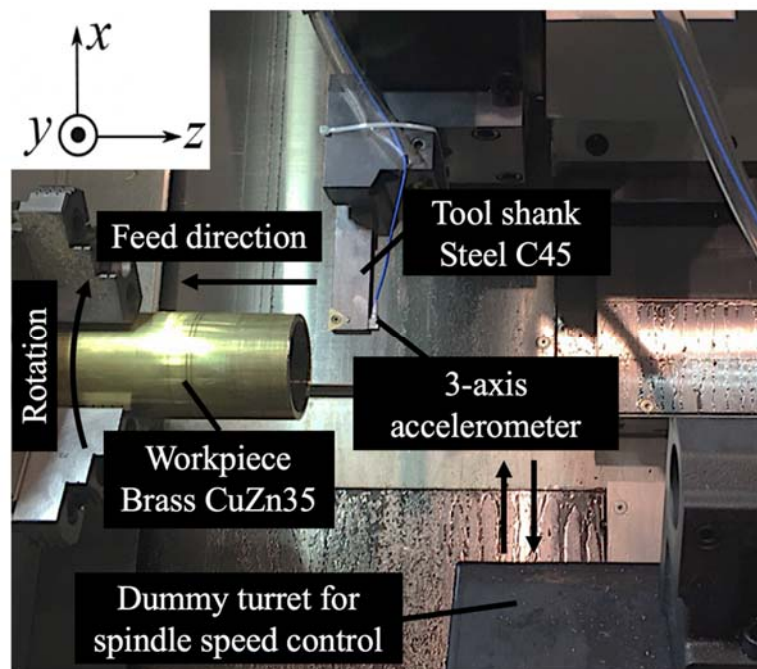


Fig. 3.8. Experimental setup for pipe-end plunging.

3.4.2 Measurement of dynamic compliance of tool shank

The dynamic compliance of the tool shank is measured with an impact

hammer (PCB Electronics Inc., 086E80), an accelerometer (PCB Electronics Inc., 356A01), and a dummy tool insert with flat perpendicular faces. These faces are perpendicular to the principal and thrust directions, and they are utilized for accurate force input. The width and the height of the utilized tool is 25 mm and 15 mm, respectively. The projection of the tool shank is set as long as 80 mm, and the workpiece is rigid in the z direction. The impact for each direction is repeated 10 times, and their average is utilized for higher reliability of the measurement. After the measurement of the dynamic compliances, their modal parameters are identified in order to utilize them in the time-domain simulations and compare the results with those of the cutting experiments. The details of the identification of the modal parameters are described in the previous work [73]. The identified modal parameters are shown in Table 3.3.

The measured and fitted dynamic compliances are shown in Fig. 3.9, where (a) shows the cross dynamic compliance G_{zy} and (b) shows the direct dynamic compliance G_{zz} . The equivalent dynamic compliance [73] in the thrust direction $G_z(s)$ is calculated by utilizing Eq. (3.29) as introduced in the previous chapter, and the measured and fitted equivalent dynamic compliances are shown in Fig. 3.10. Here, K_y and K_z in Eq. (3.29) are the specific cutting forces in the principal (y) and thrust (z) directions, respectively, and they are measured in advance. The dashed blue lines and the solid red lines in Figs. 3.9 and 3.10 represent the measured and fitted dynamic compliances, respectively.

$$G_z(s) = \{G_{zy} \ G_{zz}\} \begin{Bmatrix} K_y/K_z \\ 1 \end{Bmatrix} = K_y/K_z \times G_{zy} + G_{zz} \quad (3.29)$$

Table 3.3. Numerically identified modal parameters.

Modal mass		
m_{yy}	[kg]	0.0658
m_{yz}	[kg]	0.0221
m_{zy}	[kg]	-0.0107
m_{zz}	[kg]	0.1807
Modal damping coefficient		
c_{yy}	[N/(m·s)]	32.73

c_{yz}	[N/(m·s)]	-42.28
c_{zy}	[N/(m·s)]	13.61
c_{zz}	[N/(m·s)]	84.99
Modal stiffness		
k_{yy}	[N/m]	8.203×10^6
k_{yz}	[N/m]	2.624×10^6
k_{zy}	[N/m]	-5.478×10^5
k_{zz}	[N/m]	2.076×10^7

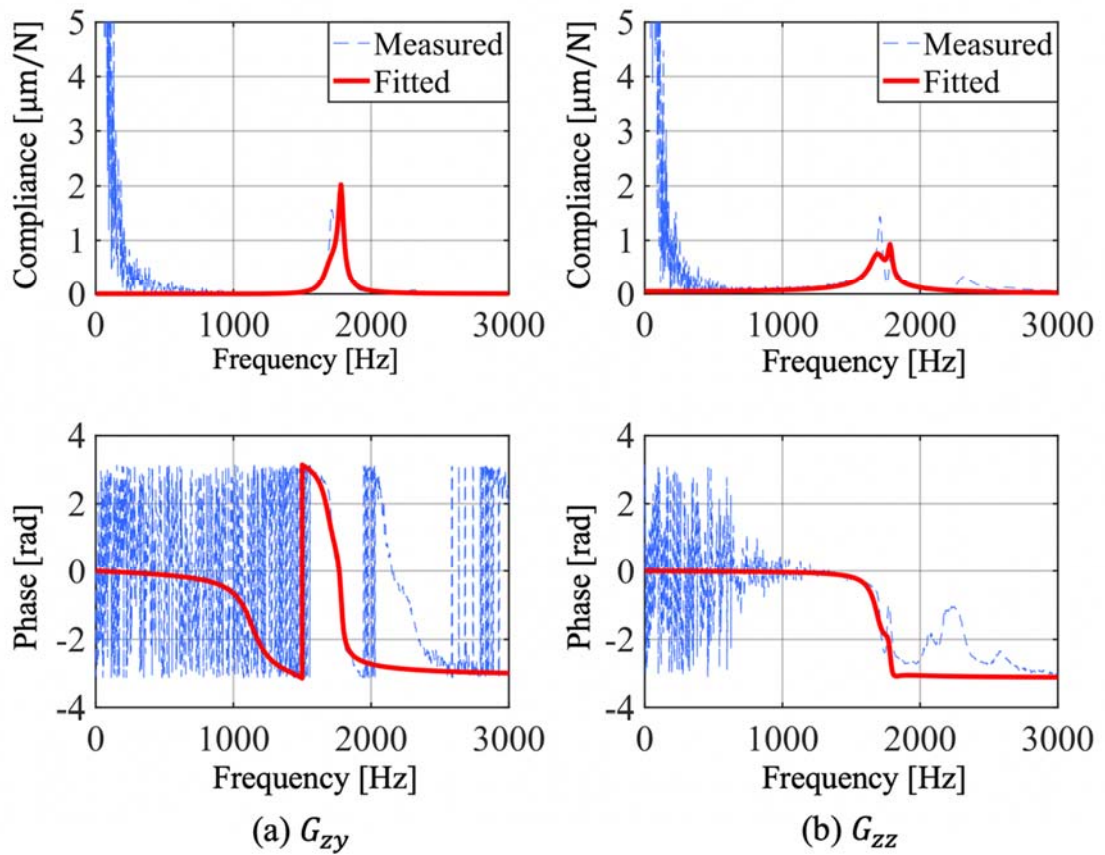


Fig. 3.9. Measured and fitted dynamic compliances: (a) cross dynamic compliance and (b) direct dynamic compliance.

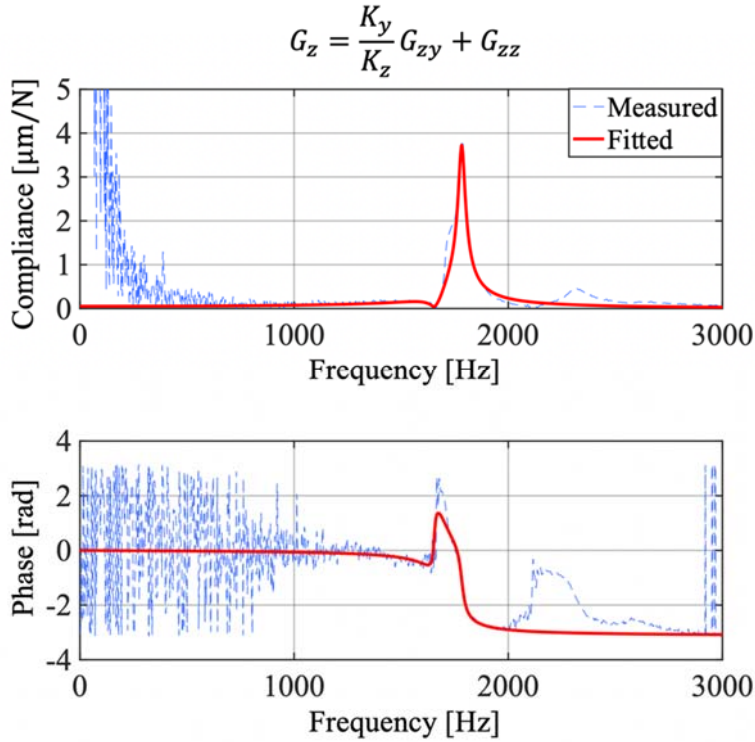


Fig. 3.10. Measured and fitted equivalent dynamic compliances.

3.4.3 Cutting experiments with constant spindle speed

Cutting experiments with constant spindle speed (CSS) are conducted to confirm the validity of the dynamic compliance by means of comparing the predicted and experimental stability limits. In addition, the degree of the stability improvement by utilizing CAR-SSV and TSSV compared to CSS can be investigated by comparing the stability limits.

Experimental conditions for cutting with CSS are shown in Table 3.4. The feed rate, i.e., static depth of cut in pipe-end plunging, is fixed to 0.05 mm, the cutting width, i.e., the thickness of the pipe, is changed by means of pre-cutting, and the spindle speeds are set variable from 1000 to 3000 [min⁻¹]. The stability limits are calculated by utilizing the measured and fitted equivalent dynamic compliances. The predicted stability limits and experimental results are shown in Fig. 3.11. The blue and red solid lines represent the predicted stability limit with the measured and fitted compliances, respectively. As for the experimental results, the measured vibration acceleration is short-time Fourier transformed to confirm the chatter frequency and the maximum vibration amplitude a_{max} . The circles and the crosses in Fig. 3.11 represent the cutting

results without chatter ($a_{max} < 1.0 \mu\text{m}_{0-p}$) and with chatter ($1.0 \mu\text{m}_{0-p} \leq a_{max}$), respectively. As can be observed in Fig. 3.11, chatter occurs regardless of the spindle speeds when the cutting width is 1.4 mm, and the experimental results represent higher stability than the predicted stability limit especially in the high-speed region (2500 min^{-1} and 3000 min^{-1}). This may come from the change of the specific cutting force in the wide cutting speed range, i.e., the specific cutting force generally decreases with the increase of the cutting speed. Meanwhile, it can be confirmed that the predicted stability limits with measured and fitted compliances are almost equal, and the predicted and measured chatter frequencies are all in good agreement; hence, the modal parameters can be used in the time-domain simulation with SSV.

Table 3.4. Experimental conditions for cutting with CSS.

Workpiece properties		
Material		Brass CuZn35
Diameter D	[mm]	70
Specific cutting force in principal direction K_y	[MPa]	1284
Specific cutting force in thrust direction K_z	[MPa]	711
Tool properties		
Width (feed dir.) × Height (cutting dir.)	[mm]	25×15
Projection length	[mm]	80
Cutting condition		
Feed rate (static depth of cut) h_0	[mm/rev]	0.05
Cutting width a	[mm]	0.8, 1.0, 1.2, 1.4
Spindle speed n	[min^{-1}]	1000 - 3000

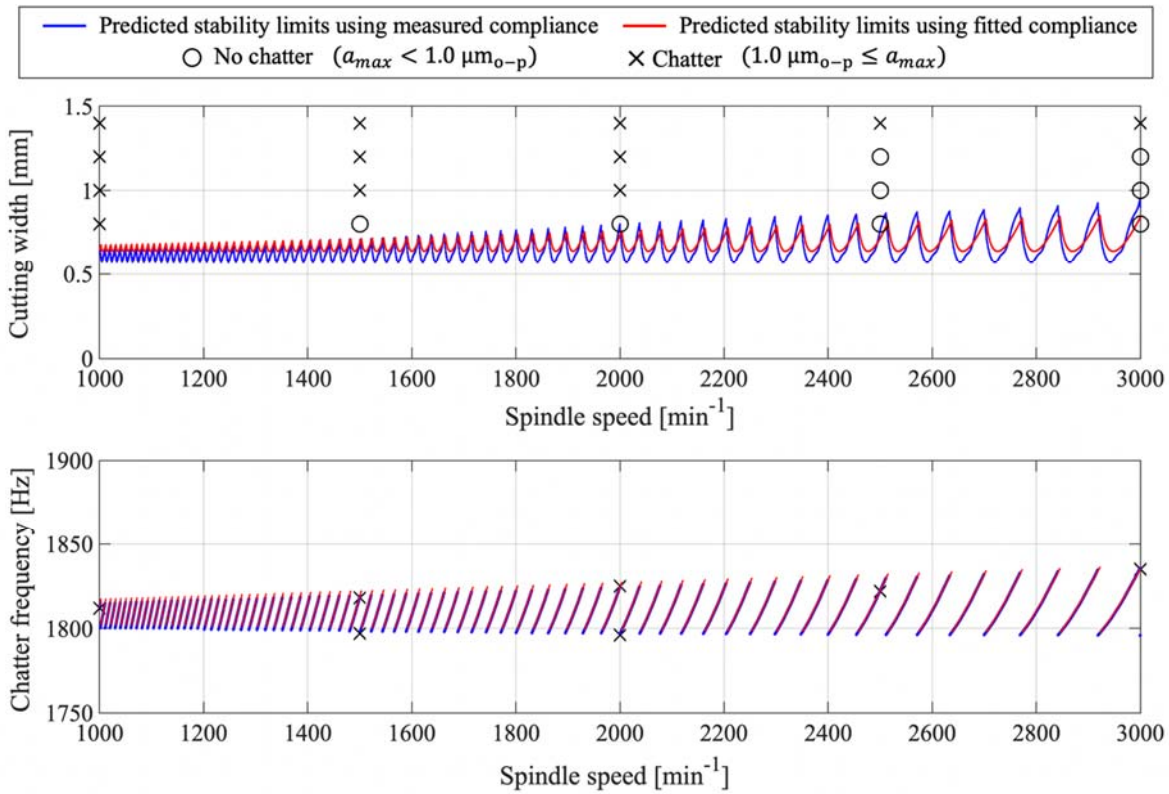


Fig. 3.11. Predicted stability limits and experimental results of CSS.

3.4.4 Method for generating CAR-SSV profile and experimental conditions

Cutting experiments with CAR-SSV and TSSV are carried out to verify the effectiveness of CAR-SSV as well as to confirm the relations between the parameters of CAR-SSV and the stability. The experimental conditions are shown in Table 3.5. Experiments with TSSV are carried out by utilizing a commercially available function (Okuma Corp., Machining Navi L-g). Note that the variation amplitude ratio RVA , which is defined as the ratio of the speed variation amplitude to the average spindle speed $n_{A,T}/n_{ave}$, is limited to 0.5 or lower. The values of the parameters of CAR-SSV and TSSV specified in Table 3.5 represent the set values, and the actual values are directly measured from the obtained spindle speed signals.

Table 3.5. Experimental conditions for cutting with CAR-SSV and TSSV.

Parameters of CAR-SSV

Reference spindle speed $n_{0,C}$	[min ⁻¹]	1000, 1500, 2000
Variation period T	[s]	0.5, 1.0, 2.0, 4.0
Set acceleration rate r_s	[%]	1.0 – 6.0
Parameters of TSSV		
Nominal spindle speed $n_{0,T}$	[min ⁻¹]	1000, 2000
Variation period T	[s]	1.0, 2.0, 4.0
Variation amplitude ratio RVA		0.1 - 0.5
Cutting conditions		
Feed rate (static depth of cut) h_0	[mm/rev]	0.05
Cutting width a	[mm]	1.0 - 5.0

Since CAR-SSV, which maintains a constant absolute acceleration rate, cannot be realized by existing NC commands, specially designed cutting experiments are conducted. The dummy turret of the CNC lathe shown in Fig. 3.8 is utilized to control the spindle speed. The spindle speed is controlled by the constant peripheral speed control function in which the spindle speed changes according to the x -axis position of the dummy turret. Here, the dummy turret is moved in accordance with previously prepared commands so that $\overline{|r_a|}$ is kept constant in the acceleration/deceleration section. For example, the spindle speed at the k -th revolution at a certain spindle rotational angle n_k [min⁻¹] can be expressed by Eq. (3.30) using the set constant peripheral speed V [m/min] and the distance from the center of the workpiece to the dummy turret at the k -th revolution R_k [mm] for the acceleration/deceleration section. In order to maintain $\overline{|r_a|}$ as r_s , the spindle speeds in two successive revolutions, i.e., n_k and n_{k-1} , should satisfy Eq. (3.3). From Eqs. (3.30) and (3.31), R_k can be calculated by Eq. (3.32).

$$n_k = \frac{1000V}{2\pi R_k} \quad (3.30)$$

$$n_k = \left(1 + \frac{r_s}{100}\right) n_{k-1} \quad (3.31)$$

$$R_k = \frac{R_{k-1}}{\left(1 + \frac{r_s}{100}\right)} \quad (3.32)$$

The dummy turret position in each revolution are calculated by utilizing Eq. (3.32), and they are interpolated with constant time steps.

An example of the experimental signals of the spindle speed, the acceleration rate, the spindle acceleration, the dummy turret position (x axis), the tool position (z axis), and the feed rate of the tool (z axis) at $n_{0,C} = 1000 \text{ min}^{-1}$, $T = 4.0 \text{ s}$, and $r_s = 2.0 \%$ are shown in Fig. 3.12. In order to calculate r_a , the spindle rotational angle is memorized in every moment, and then the moment of one revolution before as well as the spindle speed at that moment are determined. From the r_a profile, $\overline{|r_a|}$ is stably maintained as r_s in almost all sections except for the small overshoots near the sections where the acceleration direction switches. In addition, the feed rate of the tool is kept almost constant, and this denotes a constant static depth of cut. Every profile under each experimental condition is confirmed beforehand, and the conditions in which r_s can be stably maintained constant are selected for the cutting experiments. Since the original thickness of the pipe, i.e., the maximum cutting width, is 5.0 mm, the cutting width is varied from 1.0 mm to 5.0 mm with increments of 0.5 mm.

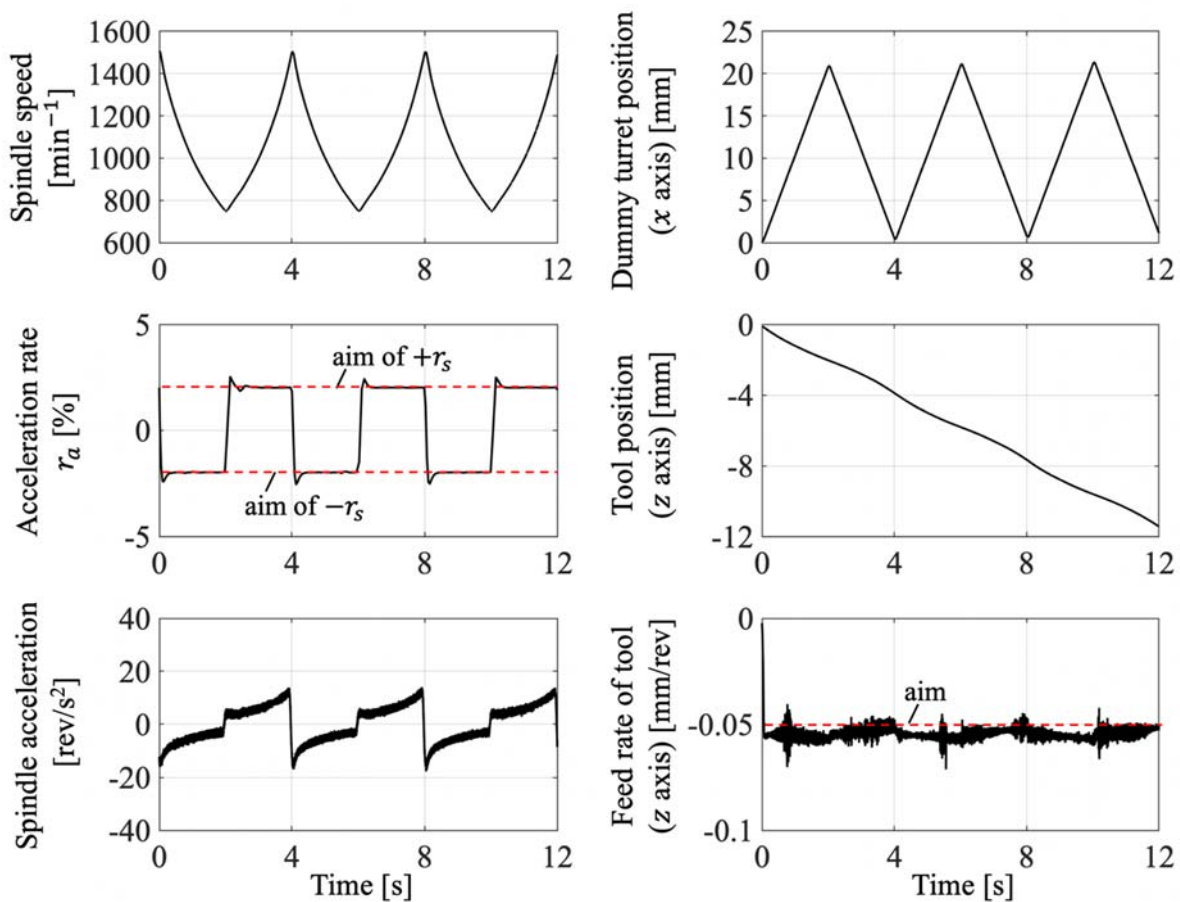


Fig. 3.12. Example of experimental signals of CAR-SSV at $n_{0,C} = 1000 \text{ min}^{-1}$, $T = 4.0 \text{ s}$, and $r_s = 2.0 \%$.

3.4.5 Experimental results and discussions

Cutting experiments are carried out to confirm the validity of the analytical investigations with the time-domain simulation, and the experimental results are described with the same order in Chapter 3. Firstly, the stability of CAR-SSV is evaluated based on the stability indices $\overline{|r_a|}$ and N , and the results are shown in Fig.3.13 under varied cutting widths: (a) 2.0 mm, (b) 3.0 mm, (c) 4.0 mm, and (d) 5.0 mm. The blue circles represent the cutting results without chatter ($a_{max} < 1.0 \mu\text{m}_{0-p}$), and the red crosses represents the cutting results with chatter ($1.0 \mu\text{m}_{0-p} \leq a_{max}$). Since the maximum cutting width is 5 mm because of the original thickness of the pipe, the stable experimental results at 5 mm mean that the actual stability limit is over 5 mm. $\overline{|r_a|}$ and N are directly calculated from the measured spindle speed signals. From Fig. 3.13, the following remarks which have been found from the simulation are confirmed as follows:

- 1) When N is almost the same, the stability increases with an increase of $\overline{|r_a|}$. Especially, when $\overline{|r_a|}$ is near 4 %, chatter is stably suppressed under all N even if the cutting width is set to 5.0 mm, which is 4 times the asymptotic stability limit of CSS. Therefore, it can be said that $\overline{|r_a|}$ is an effective stability index in CAR-SSV.
- 2) When $\overline{|r_a|}$ is almost the same, the stability increases with an increase of N . For example, when $\overline{|r_a|}$ is almost equal to or higher than 2 % and N is higher than 10, chatter is stably suppressed even if the cutting width is set to 5.0 mm. Hence, it can be said that N is also an effective stability index in CAR-SSV.

Consequently, it is desirable to set higher $\overline{|r_a|}$ and N to achieve higher stability.

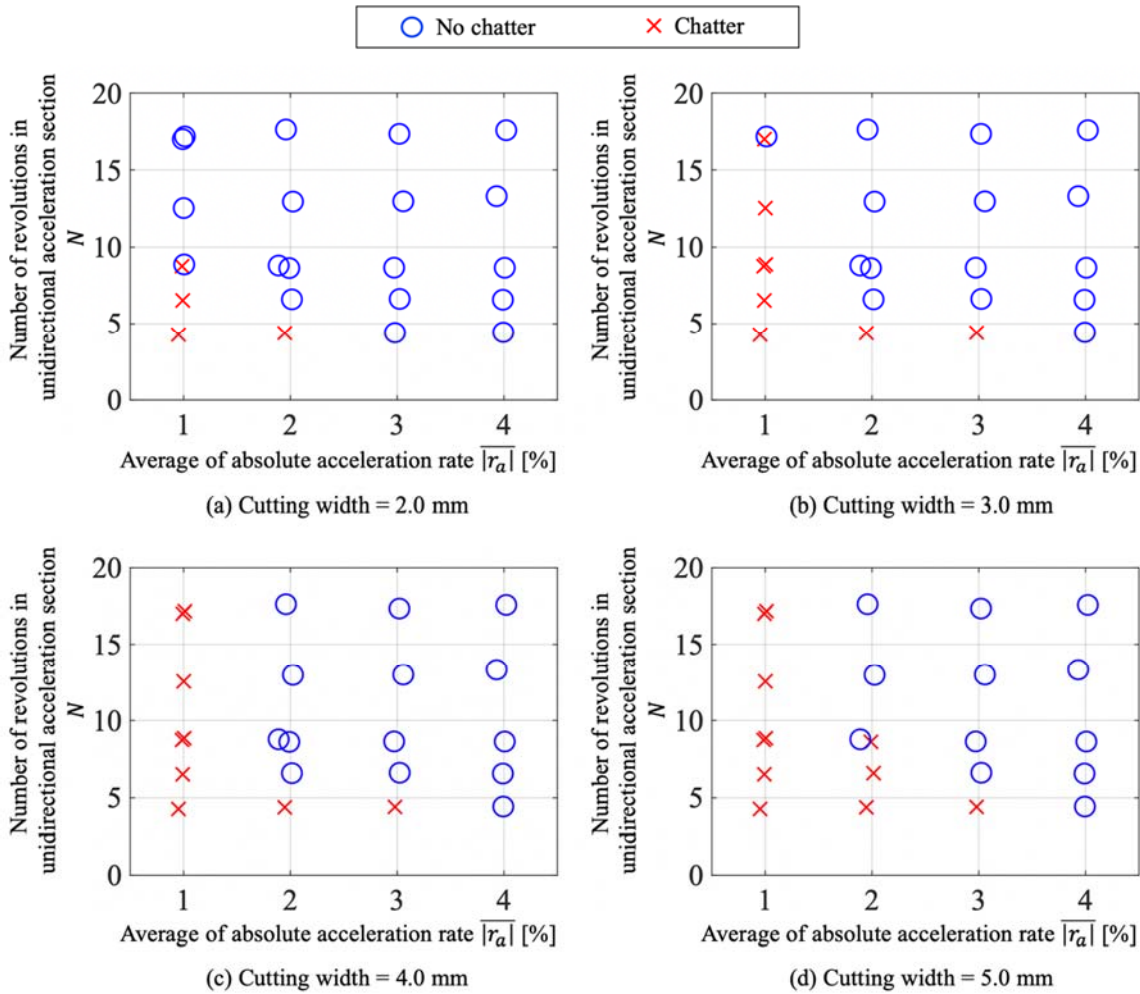


Fig. 3.13. Results of cutting experiments in CAR-SSV against stability indices $\overline{|r_a|}$ and N under varied cutting width.

Secondly, the relations between the parameters of CAR-SSV and the stability are investigated. The results of the cutting experiments and the time-domain simulations are shown in Fig. 3.14. Figures 3.14(a)-3.14(f) show the results under varied conditions of $n_{0,C}$ and T : (a) $n_{0,C} = 1000 \text{ min}^{-1}$, $T = 0.5 \text{ s}$, (b) $n_{0,C} = 1000 \text{ min}^{-1}$, $T = 1.0 \text{ s}$, (c) $n_{0,C} = 1000 \text{ min}^{-1}$, $T = 2.0 \text{ s}$, (d) $n_{0,C} = 1500 \text{ min}^{-1}$, $T = 0.5 \text{ s}$, (e) $n_{0,C} = 1500 \text{ min}^{-1}$, $T = 1.0 \text{ s}$, and (f) $n_{0,C} = 1500 \text{ min}^{-1}$, $T = 2.0 \text{ s}$. Note that the measured spindle speed signals and the identified modal parameters shown in Table 3.3 are utilized in the time-domain simulations. The horizontal and vertical axes represent the set acceleration rate r_s and the cutting width, respectively. The blue dotted line with squares represents the predicted stability limit. For the predicted stability

limit, the cutting width where chatter occurs is searched at first, and then by subtracting one increment from that width, the stability limit a_{lim} [mm] is determined.

Since the acceleration rate cannot be maintained nearly constant at $n_{0,C} = 1500 \text{ min}^{-1}$, $T = 2.0 \text{ s}$, and $r_s = 4 \%$, this condition is excluded. As shown in Fig. 3.14, it can be confirmed that the experimental results show higher stability than the predicted ones. This is consistent with the results of CSS shown in Fig. 3.11. In addition, the tendency of the stability within the experiments and within the simulations are consistent. The following remarks which have been found from the simulation are confirmed as follows:

- 1) The higher r_s , the higher the stability under the conditions with the same $n_{0,C}$ and T . Especially, when r_s is 4.0 %, the whole thickness of the pipe, i.e., 5 mm, which is about 3.5 times the maximum stability limit in CSS, is cut without chatter regardless of $n_{0,C}$ and T . Hence, it is desirable to set a larger r_s , without exceeding the limit of the spindle motor load, to obtain higher stability.
- 2) When r_s and $n_{0,C}$ are the same, the higher T , the higher the stability (see Figs. 3.14(a)-3.14(c) and 3.14(d)-3.14(f)). In the same manner, when r_s and T are the same, the higher $n_{0,C}$, the higher the stability (see Figs. 3.14(a) and 3.14(d), 3.14(b) and 3.14(e), and 3.14(c) and 3.14(f)). As described in the analytical investigations, the reasons for these tendencies can be explained as follows. The larger T and $n_{0,C}$ under the same r_s , the larger $\overline{|r_a|}$ and N , and hence the stability becomes higher. It is experimentally verified that CAR-SSV is an effective solution to overcome the limitation of conventional SSV.
- 3) The increase of the stability against the increase of T becomes small at $n_{0,C} = 1500 \text{ min}^{-1}$ (see Figs. 3.14(e) and 3.14(f)). The reduction effect of the dynamic compliance reaches a certain asymptotic value since the compliance is nearly constant far away from the resonance. Therefore, there is a limitation in the stabilizing effect from the increase

of T .

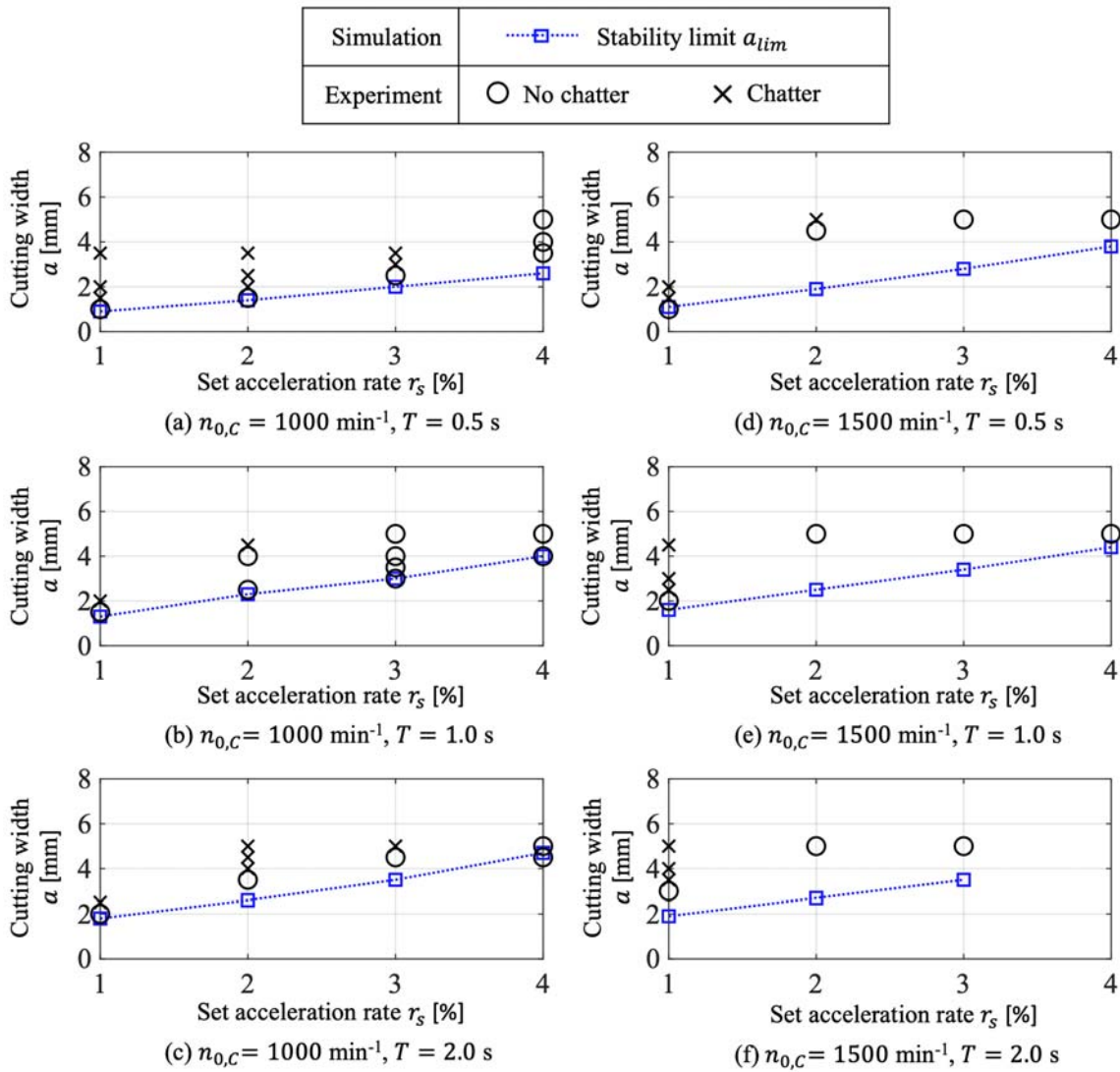


Fig. 3.14. Results of cutting experiments and time-domain simulation in CAR-SSV against set acceleration rate r_s under varied $n_{0,C}$ and T .

Finally, in order to verify the effectiveness of CAR-SSV focusing on its applicability to the actual industry, a comparison between CAR-SSV and TSSV is conducted considering the thermal load of the spindle. As shown in Section 3.2, the machining efficiency against the thermal load of the spindle motor is compared between the two profiles. The average of the square of the spindle acceleration \bar{H} [rev^2/s^4] is utilized as a proportional value to the average thermal load of the spindle motor. \bar{H} is calculated from the measured spindle speed signal. The average spindle speed of CAR-SSV $n_{ave,C}$ and TSSV

$n_{ave,T}$ are also calculated from the measured spindle speed signal, and they are utilized for the calculation of the machining efficiency, i.e., material removal rate (MRR), P [mm^3/min] expressed in Eq. (3.28). Figure 3.15 shows the results of P against \bar{H} under varied T 's: (a) $T = 1.0$ s, (b) $T = 2.0$ s, and (c) $T = 4.0$ s. The red circles and blue triangles represent the results of CAR-SSV and TSSV, respectively. The stability limit is determined from the results shown in Fig. 3.14, and it is utilized for the calculation of P . As in the other experiment, the condition where the maximum thickness of the pipe (5.0 mm) is stably cut is excluded. In addition, the conditions where the profile of TSSV cannot be generated due to the limitation of RVA are excluded. In Fig. 3.15, an increase of \bar{H} means an increase of the acceleration, and hence RVA of TSSV and r_s of CAR-SSV take higher values with higher \bar{H} . Figure 3.16 shows examples of the experimental signals of the spindle speed, the acceleration rate, the vibration acceleration obtained from accelerometer, and the short-time Fourier transform results of the vibration acceleration for the profiles marked as A and B on Fig. 3.15: (a) CAR-SSV ($a = 3.5$ mm, $\bar{H} = 39.51$ rev^2/s^4 , $n_{ave,C} = 1014$ min^{-1} , $T = 2.0$ s, and $r_s = 2.0$ %) and (b) TSSV ($a = 2.5$ mm, $\bar{H} = 38.70$ rev^2/s^4 , $n_{ave,T} = 1002$ min^{-1} , $T = 2.0$ s, and $RVA = 0.2$). From Figs. 3.15 and 3.16, the following remarks which have been found in the simulation are confirmed as follows.

- 1) When \bar{H} is almost the same, the machining efficiency is increased by utilizing CAR-SSV under all conditions. Therefore, it is experimentally verified that the effectiveness of CAR-SSV is superior to that of TSSV considering the motor load.
- 2) As shown in Fig. 3.16, although the cutting width of CAR-SSV (A of Fig. 3.15) is 40% larger than that of TSSV (B of Fig. 3.15), the vibration amplitude in CAR-SSV is extremely small except for the vibration at the beginning of the cutting caused by the initial cutting force input. On the other hand, in the case of TSSV, the growth of the vibration with a decrease of $|r_a|$ can be observed where the acceleration direction

switches. From these results, it can be concluded that the superior chatter suppression effect of CAR-SSV is verified experimentally.

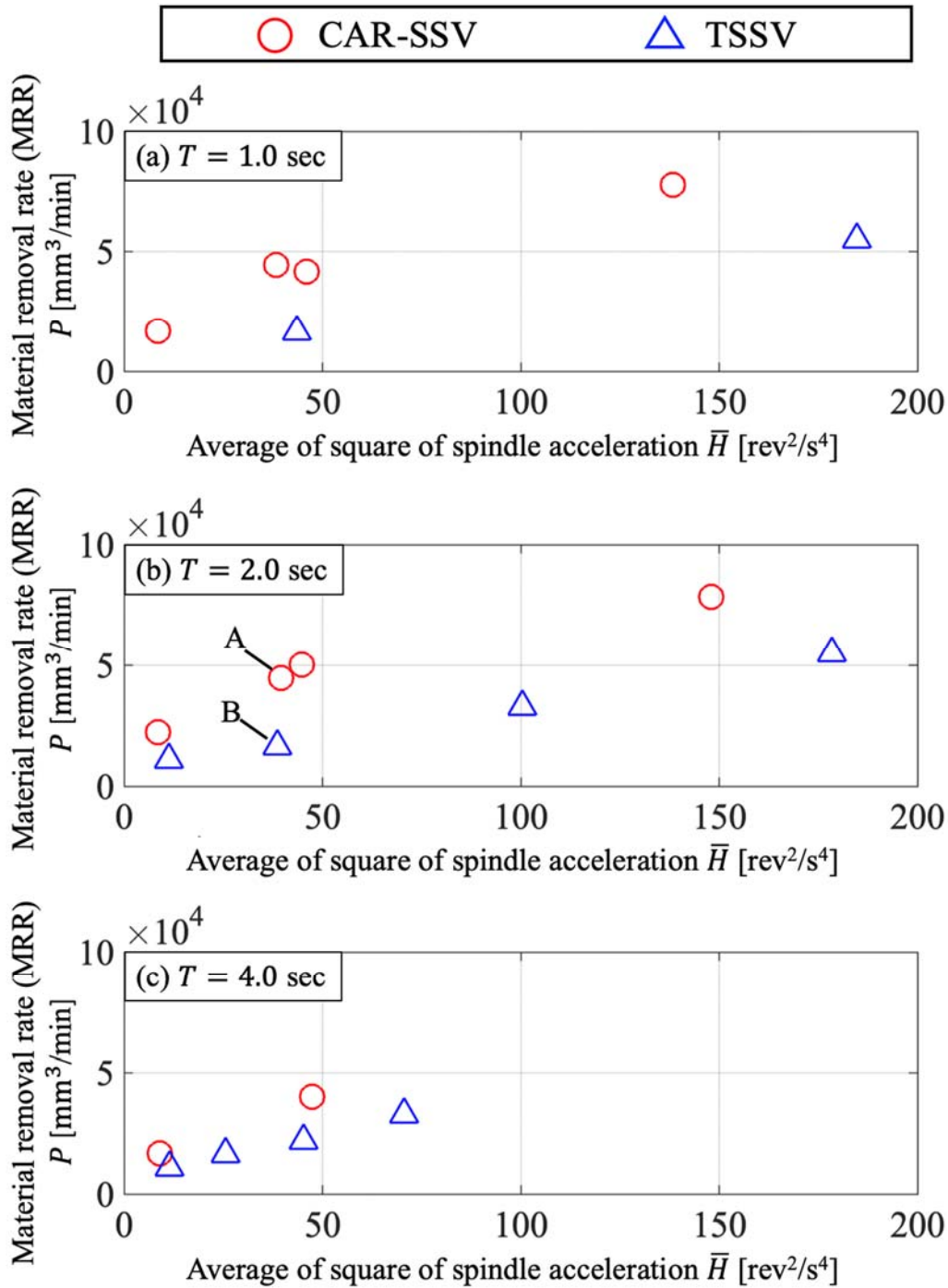


Fig. 3.15. Experimental results of material removal rate (MRR) P [mm³/min] against average of square of spindle acceleration \bar{H} [rev²/s⁴] under varied T : (a) $T = 1.0$ s, (b) $T = 2.0$ s, and (c) $T = 4.0$ s.

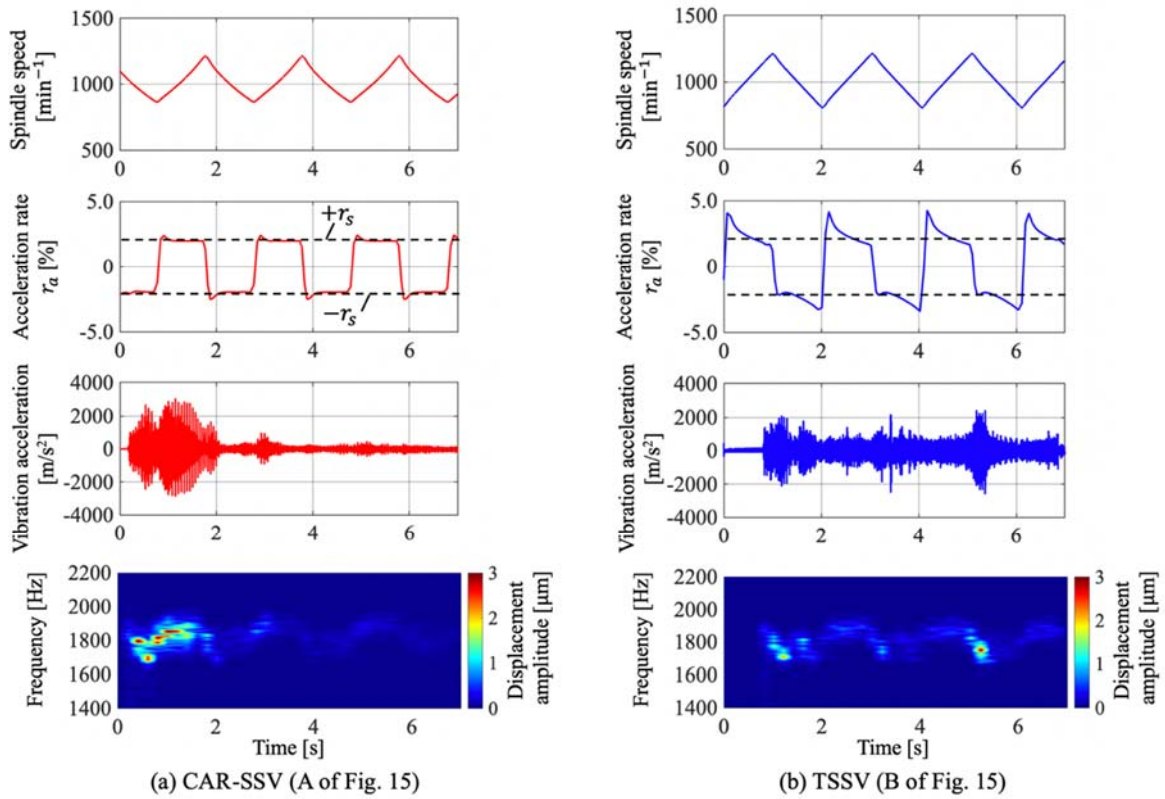


Fig. 3.16. Example of experimental signals of spindle speed and acceleration rate, corresponding vibration acceleration obtained from accelerometer, and short-time Fourier transform result of vibration acceleration under cutting conditions marked as A and B on Fig. 3.15: (a) CAR-SSV ($a = 3.5$ mm, $\bar{H} = 39.51$ rev²/s⁴, $n_{ave,C} = 1014$ min⁻¹, $T = 2.0$ s, and $r_s = 2.0\%$) and (b) TSSV ($a = 2.5$ mm, $\bar{H} = 38.70$ rev²/s⁴, $n_{ave,T} = 1002$ min⁻¹, $T = 2.0$ s, and $RVA = 0.2$).

3.5 Summary

A new SSV profile, which was named CAR-SSV (SSV with constant acceleration rate), was proposed to overcome the limitation of the chatter stability improvement in conventional SSV. Since the absolute acceleration rate is maintained a constant, chatter suppression throughout the cutting can be achieved.

Analytical investigation was conducted to reveal the potential of the proposed profile. Firstly, the relations between the stability limit and the proposed stability indices in SSSV, TSSV, and CAR-SSV were investigated, and the results of CAR-SSV were compared with those of SSSV and TSSV. From the investigation, the following remarks were found.

- 1) When $\overline{|r_a|}$ and N are the same, the stability limit of CAR-SSV is always equal to or higher than those of SSSV and TSSV. The larger the $\overline{|r_a|}$ and N , the larger the increase of the stability limit.
- 2) When N is the same, the stability limit increases with an increase of $\overline{|r_a|}$.
- 3) When $\overline{|r_a|}$ is the same, the stability limit of CAR-SSV increases with an increase of N under all $\overline{|r_a|}$.

Secondly, the following relations between the parameters of CAR-SSV and the chatter stability were revealed:

- 1) The stability increases with a higher r_s , and hence it is desirable to set a larger r_s under the imposed limitation of the spindle motor load.
- 2) When r_s is the same, the stability limit increases with larger $n_{0,C}$ and T in most cases. This is because the larger T and $n_{0,C}$, the larger $\overline{|r_a|}$ and N . This denotes that CAR-SSV can be an effective solution since the machining efficiency increases with higher T and $n_{0,C}$, i.e., higher stability limit (cutting width).
- 3) The increase of the stability with higher $n_{0,C}$ is small under a long T . Because the reduction effect of the dynamic compliance reaches a certain asymptotic value since the compliance is nearly constant far away from the resonance. Consequently, there is a limitation for the improvement of the stability with an increase of $n_{0,C}$ and T .

Thirdly, to verify the effectiveness of CAR-SSV considering its applicability to the actual industry, the machining efficiency P , i.e., material removal rate (MRR), against the thermal load of the spindle motor \overline{H} was compared with the conventional SSV profiles. The results were summarized as follows:

- 1) When \overline{H} is the same, P of CAR-SSV is equal to or higher than that of conventional SSV in most conditions.

- 2) The increase of P by utilizing CAR-SSV becomes larger with larger \bar{H} and T . The larger the \bar{H} and T , the larger the fluctuation amplitude of r_a in TSSV and SSSV, and the sections become longer where $|r_a|$ in TSSV and SSSV is smaller than $|r_a|$ in CAR-SSV. Hence, the stabilization effect decreases in TSSV and SSSV since a sufficient compliance reduction cannot be obtained.

A series of experiments were carried out to confirm the relations between the parameters of CAR-SSV and the stability as well as to verify the effectiveness of CAR-SSV. Since CAR-SSV cannot be realized by existing NC commands, specially designed cutting experiments were conducted.

The stability of CAR-SSV was evaluated based on the stability indices $\overline{|r_a|}$ and N . When N is almost the same, the stability increases with an increase of $\overline{|r_a|}$. Next, when $\overline{|r_a|}$ is almost the same, the stability increases with an increase of N . Hence, it can be said that $\overline{|r_a|}$ and N are effective stability index.

The experimental results showed that a higher stability can be obtained by setting a higher r_s , and this is consistent with the results of the simulation. Especially, when r_s is 4.0 %, the whole thickness of the pipe, which is 3.5 times larger than the maximum stability limit in CSS, was stably cut. Next, when r_s and $n_{0,C}$ are the same, a higher stability was obtained with a higher T . In addition, when r_s and T are the same, a higher stability was obtained with a higher $n_{0,C}$. These results were exactly the same with the analytical results. From these results, it was verified that a remarkable improvement of the machining efficiency can be realized by utilizing CAR-SSV, and CAR-SSV is an effective solution to overcome the limitation of conventional SSV.

From the comparison between CAR-SSV and TSSV focusing on their practicality, higher machining efficiency was obtained by utilizing CAR-SSV under all conditions. These results indicate that the superior effectiveness of CAR-SSV when considering the motor thermal load was experimentally verified. Furthermore, although the cutting width in CAR-SSV was set 40 %

larger than TSSV, the vibration amplitude diminished when utilizing CAR-SSV, and the amplitude near the end of cutting was extremely smaller than that in TSSV. On the other hand, in the case of TSSV, the growth of the vibration with a decrease of $|r_a|$ was observed at the transitions from acceleration to deceleration. Therefore, it was verified that CAR-SSV can effectively suppress chatter throughout the cutting when r_s is set larger than the critical value. From these results, it can be concluded that CAR-SSV is a valid solution to overcome the limitation of conventional SSV.

Chapter 4

Proposal of 'accelerative cutting' for Suppression of Regenerative Chatter

4.1 Introduction

There are numerous industrial needs for short-duration plunge cutting, e.g. finishing of sealing, seating, and bearing surfaces. For example, the finishing of the sealing of a hydraulic part is shown in [Fig. 4.1](#). Although the cutting time is like a few tenths of a second in these particular cutting processes, a large cutting width is necessary which often causes chatter. Especially, chatter caused by the regeneration of the previously cut surface, i.e. regenerative chatter, occurs in practical cutting methods, e.g. turning and milling, and it is the dominant factor among all chatter phenomena.

A variety of researches have been carried out to tackle the regenerative chatter problem. A simple method to increase the efficiency is the selection of the spindle speed and cutting width where regenerative chatter is most unlikely to occur [\[75\]](#). This method can be applied effectively in the low number lobes, i.e. high spindle speed or cutting speed. Other methods are such as the use of variable pitch/helix cutters [\[58, 76\]](#) and the optimization of those [\[33, 60\]](#) (for milling), use of vibration absorbers or dampers [\[77\]](#), etc.

As described in [Chapter 2 and 3](#), another method for the suppression of chatter is the spindle speed variation (SSV), and many works have been dedicated to reveal its suppression mechanism and to validate its effect both experimentally and analytically. The numerous simulation methods in time domain and frequency domain have been proposed, including the semi-discrete time-domain simulation [\[78\]](#), frequency-domain simulations focusing on the eigenvalue [\[79\]](#), etc. [\[80,81\]](#).

However, it is known that SSV has an effect to some level but does not have a significant effect depending on the SSV conditions and vibratory structure [80]. Even worse, it sometimes destabilizes effective conditions in constant speed machining [44]. Therefore, it can be observed that there is a limit to the effect of SSV, and correct parameters need to be adapted to realize the suppression effect.

Although conventional methods, for example variable pitch cutters, can be used for the targeted short-duration plunge cutting processes, there is a need of knowing the chatter frequency and other parameters beforehand. In addition, these processes have a short duration, so SSV may cause unstable cutting depending on the SSV parameters because of the aforementioned nature of SSV in Chapter 2 and 3. Specifically, the change of chatter frequency decreases at the transient sections from acceleration to deceleration or from deceleration to acceleration since the change of spindle speed decreases in those sections. Even CAR-SSV is utilized, those sections exist because it is also cyclical and continuous profile having the transient sections as shown in Fig. 3. 16. The time length of the transient section changes with the set SSV parameters, and thus the chatter can grow when the time length of this section is large.

In order to increase the stability in short duration cutting by resolving the instability in the transient sections, a novel suppressive cutting method for regenerative chatter, namely 'accelerative cutting', is proposed. In this method, the spindle speed is accelerated/decelerated in a unidirectional manner so that the speeds in the present and previous revolutions change at every moment causing suppression throughout the cutting.

In this research, the limit of SSV is explained first, and accelerative cutting is described focusing on the acceleration rate. Second, a time-domain simulation is conducted to reveal its effect against regenerative chatter. Third, since the proposed method cannot be realized by conventional NC functions, specially designed cutting experiments are carried out to validate its effectiveness, and the results are discussed clearly. Last, conclusions follow.

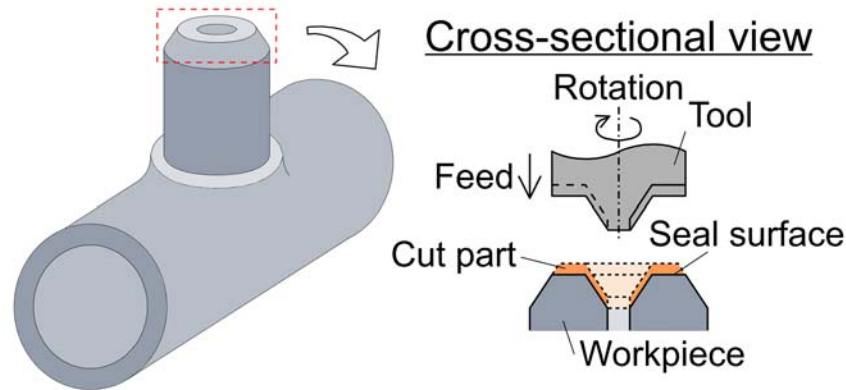


Fig. 4.1. Schematic of finishing process of sealing of a hydraulic part.

4.2 Accelerative cutting and its advantage

4.2.1 Limit of SSV

In SSV, there are moments where the spindle speeds, or cutting speeds, of the present and previous revolutions do not change, hence causing chatter. To confirm this problem, cutting with its experimental setup shown in Fig. 4.2(a) is conducted with SSV on a turning center (Okuma Corp., Spaceturn LB3000EX). In addition to the spindle speed profile obtained from the spindle motor encoder and vibration acceleration signal obtained from an accelerometer, the acceleration rate r_a , i.e. $r_a = (n_{pres}/n_{prev}) - 1$, of the profile is shown in Fig. 4.2(b) where n_{pres} and n_{prev} are the speeds in the present and previous revolutions, respectively. n_{prev} is obtained by determining the spindle speed at the position 2π rad, or 1 rotation, before. As observed in the figure, there are moments where r_a is near 0% when the accelerative direction of the spindle changes, which means ordinary constant speed machining is performed, i.e. there is no suppression effect. If r_a is insufficient for suppression and it continues, chatter can grow. In this experiment, the tool is flexible, and plunge cutting of a brass pipe is conducted. It can be observed that chatter grows at moments where r_a is near 0%. In other parts, r_a is sufficient, and thus the chatter diminishes.

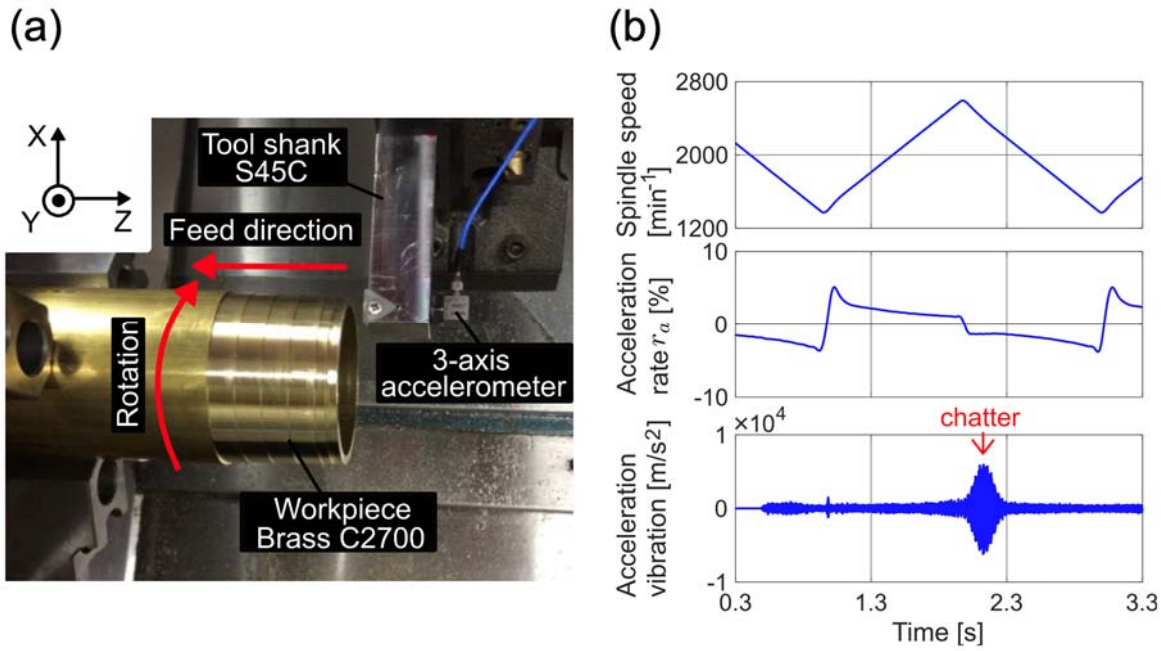


Fig. 4.2. (a) Experimental setup for SSV experiment and (b) spindle speed profile, acceleration rate r_a , and vibration acceleration signal.

4.2.2 Proposal of accelerative cutting and its advantage

From the above results, it is observed that sections where the accelerative direction changes limit conventional SSV. Therefore, a novel method named 'accelerative cutting' is proposed where there are no such sections. In this method, the spindle speed is continuously accelerated/decelerated in a unidirectional manner resulting in sufficient speed difference between the present and previous revolutions. In addition, the spindle speed is controlled to keep r_a constant, and hence chatter is suppressed in the whole cutting process. Since short-duration plunge cutting, e.g. cutting time of few tenths of a second, is targeted, only a small number of revolutions are needed. Hence, the speed range is within a few ten percent of the beginning speed. Therefore, the spindle is able to keep its speed within its limitation, and also built-up edges in low speeds and tool wear in high speeds will not be a problem.

Accelerative cutting cannot be realized by conventional NC functions since the cutting has to end while the spindle is still accelerating. Figure 4.3 shows the ideal machine tool motion for accelerative cutting. The spindle

speed is accelerated so that r_a is constant, i.e. +2% in this case, and the cutting ends, meaning that the feed ends, when the spindle is still accelerating. By doing so, chatter cannot grow throughout the cutting as long as r_a is sufficient. Note that the acceleration/deceleration profile does not always have to be commanded to keep r_a constant, but the minimum rate throughout the cutting has to be larger than the critical rate for the suppression of chatter.

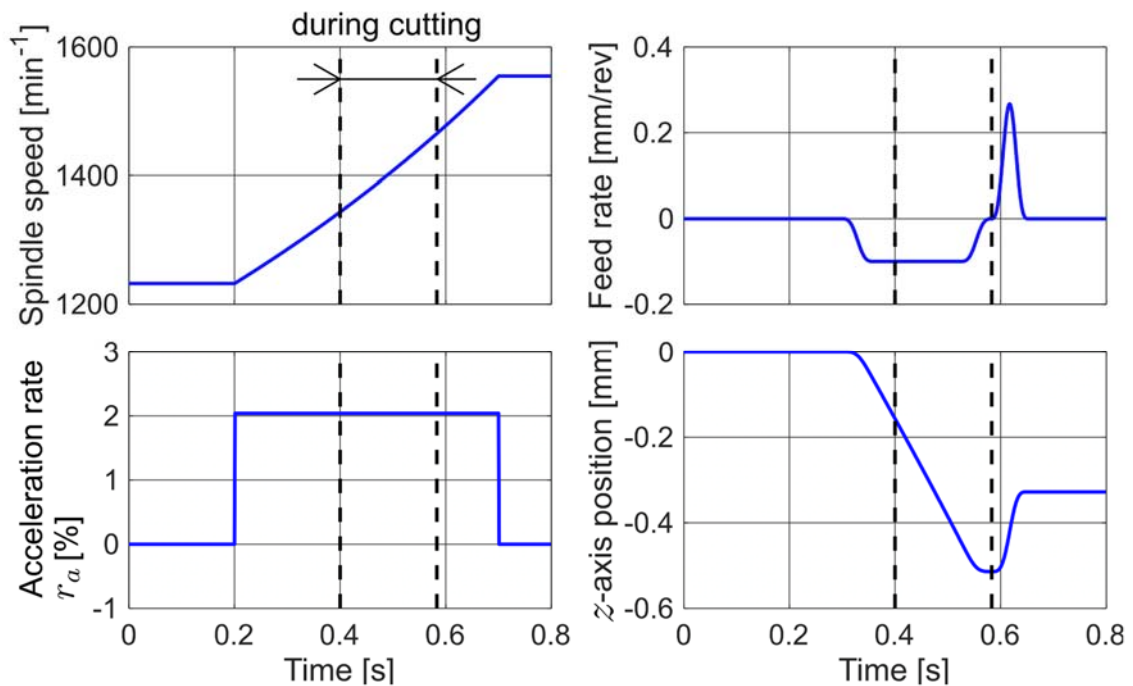


Fig. 4.3. Ideal machine tool motion for accelerative cutting.

4.3 Time-domain simulation of accelerate cutting

4.3.1 Time-domain simulation model

To verify the effectiveness of accelerative cutting and show evidence of the critical rate, time-domain simulations are conducted. A single-degree-of-freedom (SDOF) vibratory system is assumed, which is a simplified form of the actual system in Fig. 4.1, but here the tool is flexible instead of the workpiece. The schematic illustration of the SDOF model is shown in Fig. 4.4. It is well known that the vibration in the previous revolution affects the present cutting. Hence, the uncut chip thickness $h(t)$ can be formulated as follows.

$$h(t) = h_0 + z(\theta(t) - 2\pi) - z(t) \quad (4.1)$$

Here, h_0 is the static depth of cut, $\theta(t)$ is the angular position, and z is the displacement in the depth of cut direction. In order to obtain $\theta(t)$, the spindle speed is first expressed as a function of θ : $n(\theta) = n_0(1 + r_a)^{\theta/(2\pi)}$, where r_a is constant as in Fig. 4.3 and n_0 is the initial speed. As $d\theta/dt = 2\pi n/60$, the differential equation $d\theta/dt = 2\pi n_0(1 + r_a)^{\theta/(2\pi)}/60$ is obtained and solved as follows: $\theta(t) = -2\pi \ln(1 - n_0 t \ln(1 + r_a)/60) / \ln(1 + r_a)$, and $n(t) = n_0 / (1 - n_0 t \ln(1 + r_a)/60)$.

The cutting force $F_z(t)$ fluctuates according to the uncut chip thickness as follows.

$$F_z(t) = K_t b h(t) \quad (4.2)$$

where K_t is the specific cutting force in the thrust, i.e. depth of cut, direction, and b is the total cutting width. The tool's equation of motion is expressed by using modal parameters, and the governing equation of the SDOF system can be expressed as follows.

$$m\ddot{z}(t) + c\dot{z}(t) + kz(t) = K_t b \{h_0 + z(\theta(t) - 2\pi) - z(t)\} \quad (4.3)$$

Here, m , c , and k are the modal mass, damping coefficient, and stiffness, respectively. In the simulation, the initial increase in the depth of cut is the only inputted source of displacement which can grow to chatter. Note that this depth of cut increases gradually in the beginning of cutting due to the nature of the turning process. The solution is approximated by the 4th order Runge-Kutta method. $\theta(t)$ and $z(t)$ are memorized at each calculation step, and they are utilized afterwards as the previous displacement $z(\theta(t) - 2\pi)$. The utilized parameters are shown in Table 4.1.

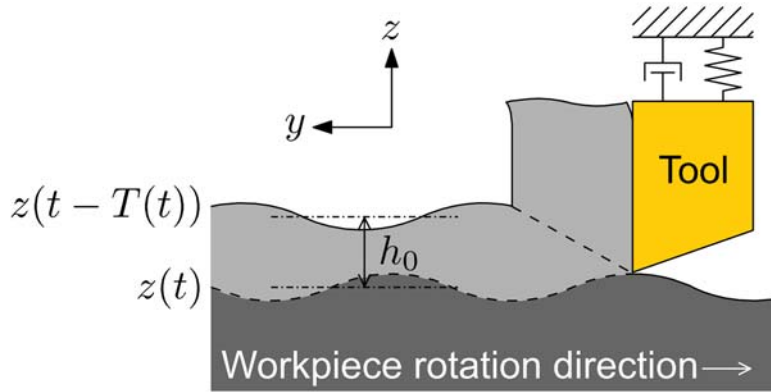


Fig. 4.4. Schematic of SDOF model.

Table 4.1. Parameters used in time-domain simulation.

Material properties		
Specific cutting force in thrust direction	[MPa]	711
Modal parameters		
Mass	[kg]	0.2266
Damping coefficient	[N/(m · s)]	44.19
Stiffness	[N/m]	1.118×10^6
Cutting conditions		
Static depth of cut (feed rate)	[mm]	0.050

4.3.2 Simulation results

First, a simple simulation is conducted to prove that there is a critical acceleration rate. In the simulation, the spindle speed is accelerated so that r_a decreases gradually, and the cutting width is 3.5mm. The simulation result is shown in Fig. 4.5.

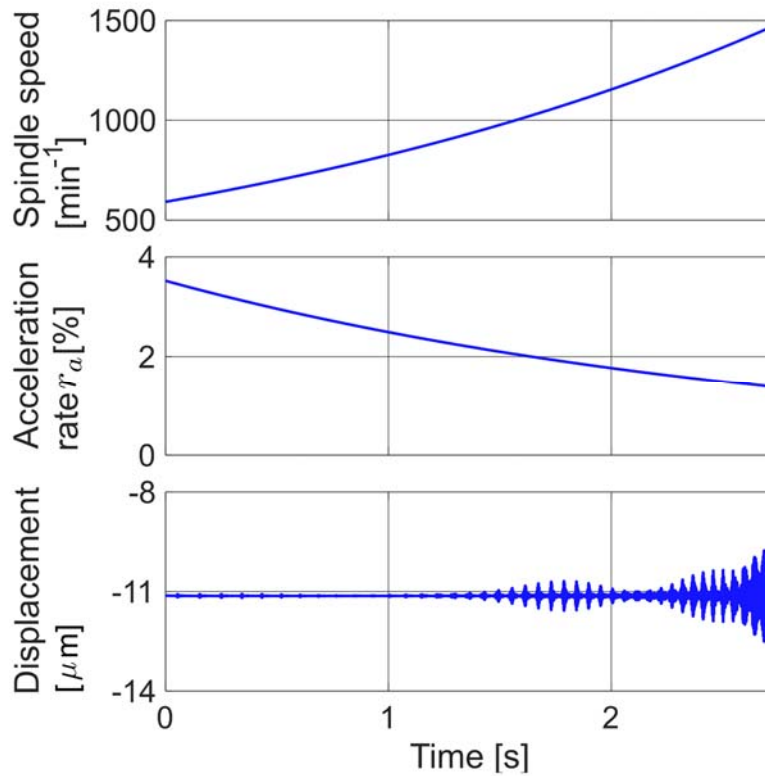


Fig. 4.5. Simulated spindle speed profile, acceleration rate r_a , and vibration displacement signal when r_a changes gradually.

From the displacement signal, it is observed that as r_a gets near 2%, chatter starts to grow. In this research, the growing vibration profile until the cutting ends will be considered as unstable, and the diminishing profile is considered as stable. As observed in the figure, chatter is suppressed due to accelerative cutting before r_a is near 2%; r_a is sufficient for suppression. This can be explained as follows. As vibration occurs during cutting, the tool cuts the workpiece with the vibration with a frequency of ω_{prev} left from the previous revolution. Since the spindle speed changes in speed variation methods, the time frequency of the present cutting changes, i.e. $\omega_{pres} = (n_{pres}/n_{prev}) \times \omega_{prev}$. The change of the time frequency causes the change of the amplitude of the present vibration due to the compliance of the vibratory structure which affects the dynamic chip thickness. Therefore, the larger the speed difference, the larger the stability since the compliance is smaller in higher frequencies considering a single dominant mode.

Next, another simulation is conducted to verify the effect of accelerative cutting. The spindle is accelerated so that the acceleration rate is constant. The width of cut versus r_a with the critical stability is shown in Fig. 4.6, and the results for r_a of 1% and 3.1% at the width of cut of 3mm are shown in Fig. 4.7. The simulation is conducted with 0.1mm increments of the width of cut.

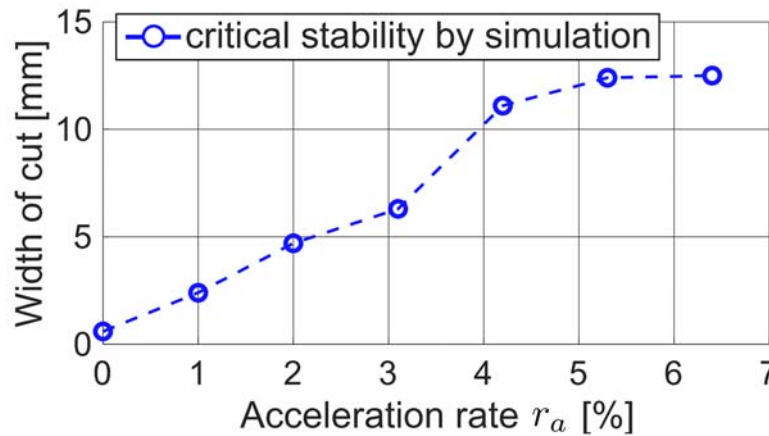


Fig. 4.6. Critical stability of accelerative cutting.

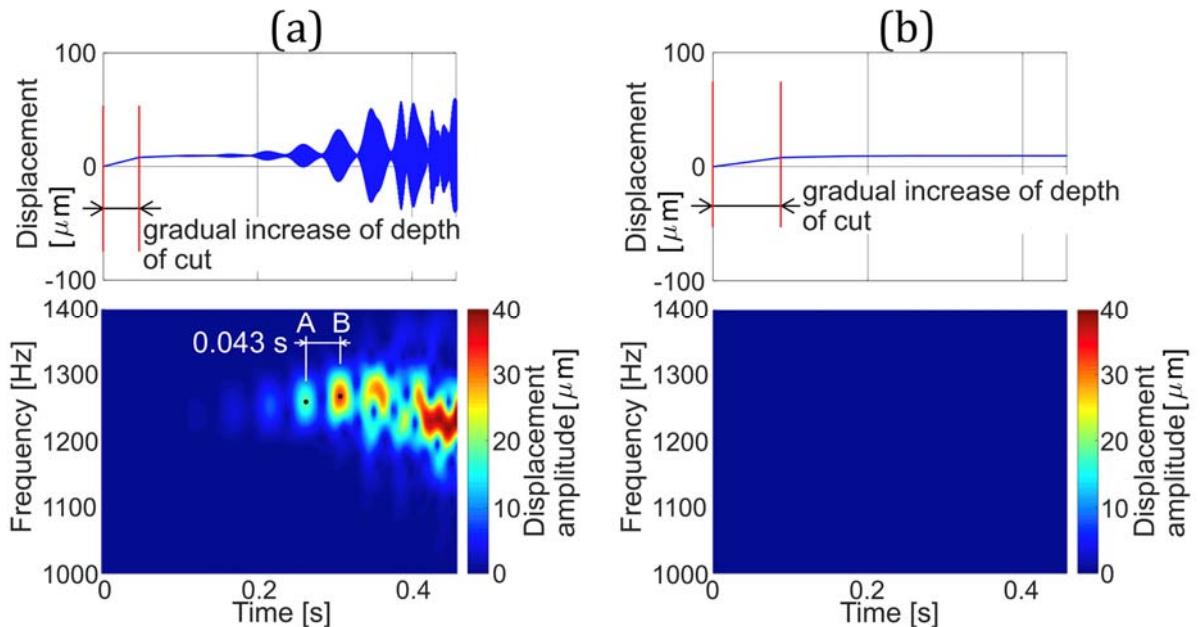


Fig. 4.7. Displacement signals and short time Fourier transforms of them when acceleration rate is (a) 1 % and (b) 3.1 %

As shown in Fig.4.6, the stability greatly increases as the acceleration rate increases. Contrary to the stable example shown in Fig. 4.7(b), chatter

occurs in the example of [Fig. 4.7\(a\)](#) and shows that the time frequency of chatter changes as the spindle speed changes. For example, the time frequency at moment A is 1257Hz, but in the next revolution, i.e. after 0.043s which is roughly equal to the revolution period at that moment, the frequency changes to 1268Hz $\approx (1 + r_a) \times 1257\text{Hz}$, or 1268Hz $\approx (1370\text{rpm}/1357\text{rpm}) \times 1257\text{Hz}$, at moment B. Since there are small forced vibration marks in various frequencies left by the initial increase of depth of cut, the vibration marks regenerate time to time due to the acceleration, and accordingly it virtually appears like it is chattering at a single frequency. Note that the period of the periodic chatter vibration is nonlinear to time since the revolution period is different at each timing, and the vibration grows against time from the initial vibration in various low frequencies.

4.4 Experimental results and discussions

4.4.1 Experimental setup and conditions

Specially designed cutting experiments are conducted to verify the effectiveness of accelerative cutting. Since it cannot be realized by existing NC functions, a 2-turret turning center (Nakamura Tome Precision Industry Co., Ltd., WY-100) is utilized. The experimental setup is shown in [Fig. 4.8](#). A dummy tool is used for a dummy face turning, and the spindle speed is controlled by the constant peripheral speed control according to the x position of it. By adequately commanding the x position of the dummy tool, the spindle speed can be accelerated arbitrarily. Then, a cutting tool is used for plunge turning of the pipe material which realizes accelerative cutting.

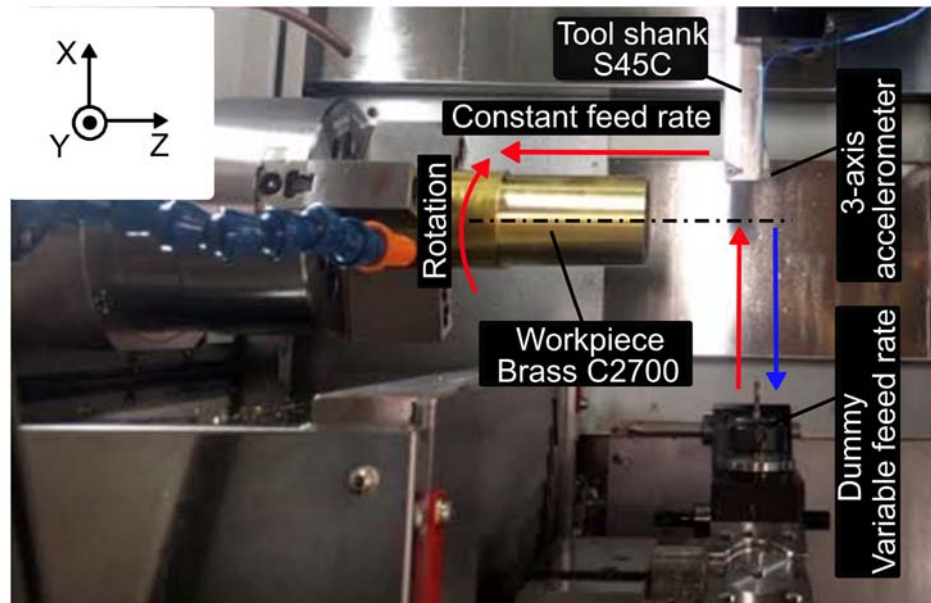


Fig. 4.8. Photograph of experimental setup

An example of the spindle speed signal for r_a of 2% indirectly commanded by the dummy tool and the position trajectory of the cutting tool are shown in Fig. 4.9. The spindle speed signal is obtained directly from the spindle motor encoder, and the z -axis position is obtained by a CMOS laser displacement sensor (Keyence Corp., IL-100). As can be observed, cutting ends while the spindle is still accelerating, and a nearly constant acceleration rate is sustained during cutting. Note that several tens of revolutions are cut in this example to validate the effect of accelerative cutting, but only several revolutions are usually needed in practical finishing, i.e. the speed range will be much smaller.

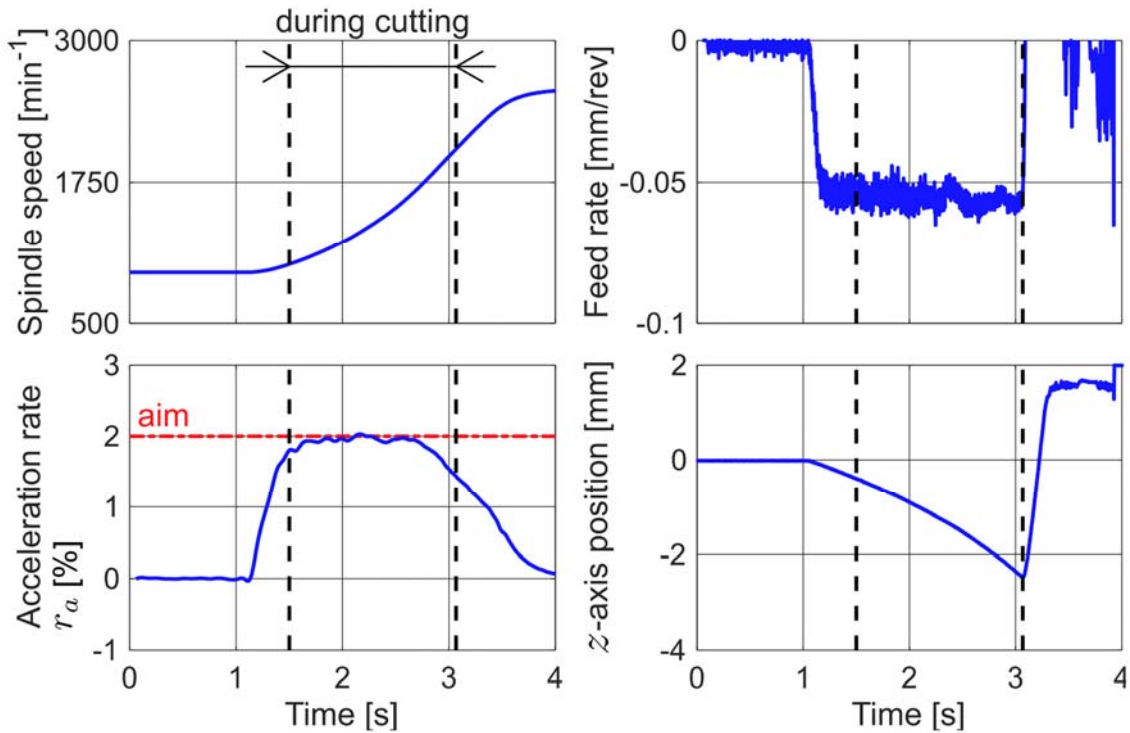


Fig. 4.9. Example of spindle speed signal and position trajectory.

The cutting tool is flexible in this experiment, and the vibration acceleration of it during cutting is measured by an accelerometer (PCB Inc., 356A01). The measured compliance of the cutting tool by a hammering test is shown in Fig. 4.10. Since the cross compliance due to the principal force (force in y direction) affects the stability [66], the equivalent compliance is measured and utilized for the simulation. The modal parameters are fit to the equivalent compliance, and they are the same as those shown in Table 4.1. The experimental conditions are shown in Table 4.2.

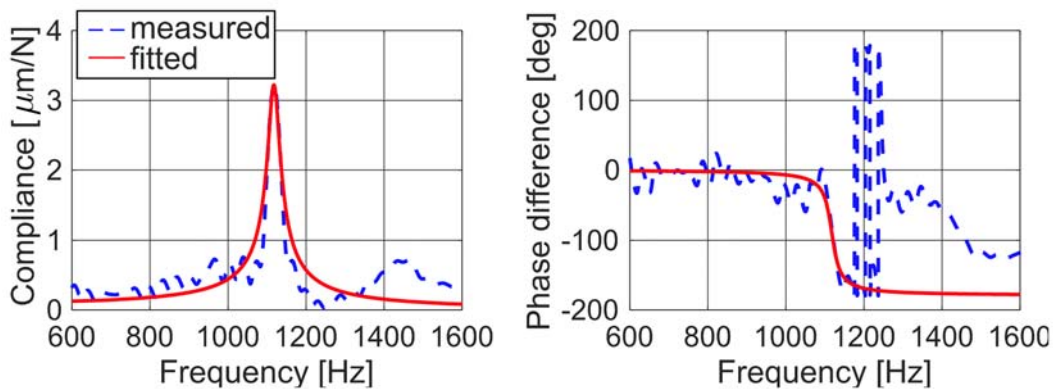


Fig. 4.10. Measured and fitted equivalent compliance.

Table 4.2. Experimental conditions for cutting experiment.

Material properties		
Material type		Brass C2700
Diameter	[mm]	70
Specific cutting force in principal direction	[MPa]	1284
Specific cutting force in thrust direction	[MPa]	711
Tool parameters		
Width (feed dir.) × Height (cutting dir.)	[mm]	25×15
Projection length	[mm]	90
Cutting conditions		
Static depth of cut (feed rate)	[mm/rev]	0.050

4.4.2 Results and discussions

The results are shown in Fig. 4.11. 'o' and 'x' represent stable and unstable machining in the experiment, respectively, and the line represents the critical stability obtained by the time-domain simulation with 0.1mm increments of the cutting width. Note that the actual spindle speed profile with the same start/end of cutting is used in the simulation. Concrete examples of the measured vibration acceleration signals are shown in Fig. 4.12 for acceleration rates of 1% and 3.1% at cutting width of 3mm. Note that the experimental asymptotic critical stability of constant speed cutting, i.e. $r_a = 0\%$, is 0.6mm and agrees well with the simulation. As observed in Fig. 4.11, accelerative cutting can increase the stability greatly. For example, a cutting width of about 7 times that of constant speed can be realized when the acceleration rate is 3.1%. In addition, the simulation and experimental results agree well, therefore confirming the effectiveness of accelerative cutting in both manners. As observed in Fig. 4.12(a), chatter grows as the cutting proceeds, which means that r_a of 1% is insufficient. On the other hand, the increase of r_a to 3.1% stabilizes the cutting process as shown in Fig. 4.12(b). Note that the vibration at the beginning of cutting is forced vibration caused by the initial increase of depth of cut, and it diminishes after a while. From these results, it can be concluded that accelerative cutting is an effective method for suppression of regenerative chatter in short-duration plunge cutting, and the acceleration rate

should be kept constant to achieve its complete effect.

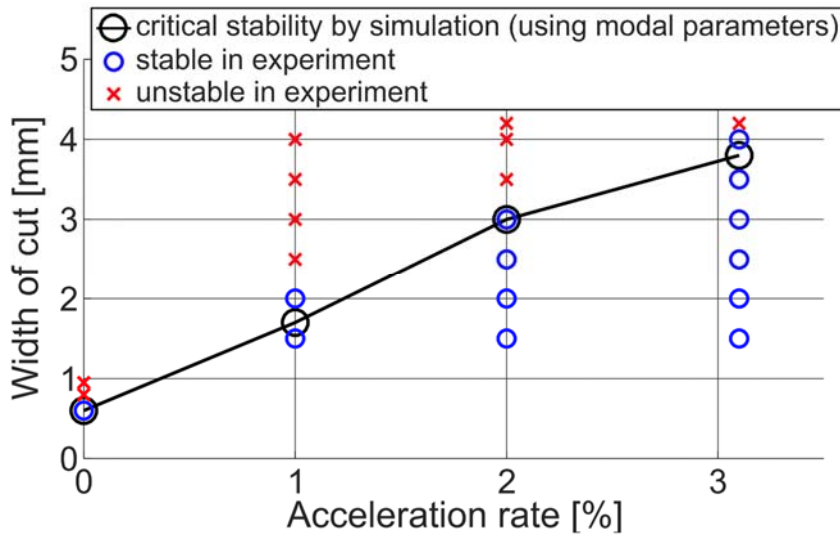


Fig. 4.11. Simulation and experimental results for accelerative cutting.

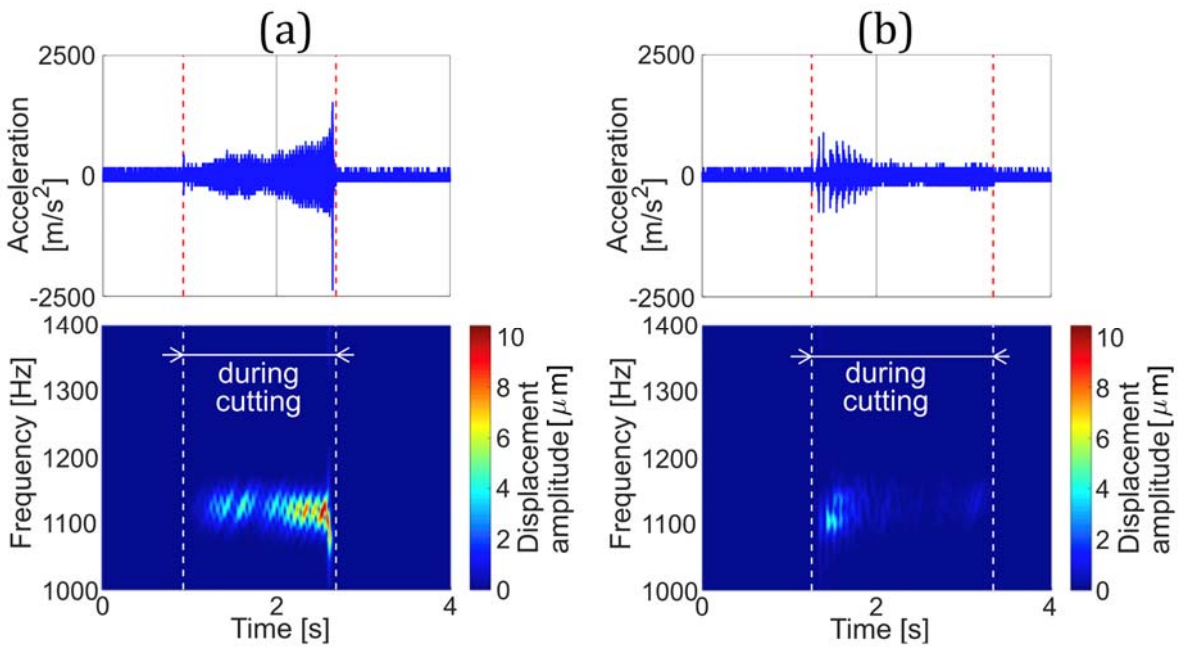


Fig. 4.12. Acceleration signals and short time Fourier transforms of them at cutting width of 3 mm where acceleration rate is (a) 1.0 % and (b) 3.1 %.

4.5 Summary

Accelerative cutting has been proposed, and its effectiveness has been validated through analyses and experiments. The spindle is

accelerated/decelerated in a unidirectional manner; the direction of acceleration does not change. Thus, there is always a sufficient speed difference between the present and previous revolutions. The spindle is accelerated so that the acceleration rate r_a is kept above the critical rate, therefore suppressing regenerative chatter. A time-domain simulation has been conducted, and it has proved that the stability increases drastically by the accelerative cutting. Specifically, r_a is kept constant, and the increase of it causes a great increase of the critical stability. Since accelerative cutting cannot be realized by conventional NC functions, specially designed experiments have been carried out. It has been validated that stable cutting can be carried out at large widths of cut, e.g. 7 times larger than that of constant speed cutting. Therefore, it is expected that accelerative cutting can be utilized for short-duration plunge cutting and increase the stability drastically in practice.

Chapter 5

Real-World Data Circulation in High-Efficiency Cutting

Here, the contributions of the thesis to Real-World Data Circulation (RWDC) are described. RWDC is a new academic field, and it means the procedures of data acquisition, analysis, and implementation to the real-world. Creating new values through the interactive integration of the three procedures is an essential objective of RWDC. In this chapter, the author's researches are introduced and interpreted in terms of the RWDC. Particularly, the kinds of data utilized, detailed description of data circulation, social value of data circulation, and imagined future RWDC of researches in the thesis are mainly described.

5.1 Real-World Data and its measurement in High-Efficiency Cutting

Extensive data exist in the real-world, and it is a critical issue to acquire data being needed from them with a proper measurement method. With advances in the availability and affordability of sensors and data acquisition systems in manufacturing sites, effective and appropriate data selection/acquisition according to the purpose is important. In the thesis, many kinds of data measurements were carried out to figure out the chatter growth phenomena in cutting with SSV and suppress it. Data acquisition was conducted before/during/after the cutting experiments for different purposes. Then, the acquired data were analyzed by various methods such as Fast Fourier transform, numerical calculations, and introduction to the simulator. Through these processes, it was possible to verify the reason for the chatter

problem of SSV and propose new speed variation techniques for the improvement of machining efficiency. The detailed description of the data sources in the thesis are as follows:

- **Vibration**

Several types of machine tool vibrations occur during the cutting process such as forced vibration and self-excited vibrations from the interaction of the cutting forces and structural dynamics of the machine tool. Since these vibrations cause poor cut surface quality, damage to the cutting tools, and loss of productivity, it is a critical issue to suppress the vibrations during the cutting process. The growth mechanisms for each type of vibration are different from each other, and hence the suppression techniques are also various [2-3]. Both a comprehensive understanding of the cutting process and structural dynamics of the machines and appropriate methods for data acquisition of the cutting process and machine tools are necessary.

The author's thesis focused on the most commonly occurring self-excited vibration, i.e., regenerative chatter vibration, in the cutting process. As shown in Fig. 2.2, the dynamic compliance, which is the transfer function between the dynamic displacement of the cutting tool and the dynamic force was measured through the hammering test should be measured for conducting the chatter stability analysis. In addition, the chatter vibration during the cutting process with SSV was measured by an accelerometer to investigate the behavior of vibration as shown in Fig. 2.13. Through the short-time Fourier transform of measured vibration signals, the change of time-chatter frequency during chatter in cutting with SSV was revealed. As a result, the chatter growth characteristics of SSV were clarified, and the countermeasures for suppressing chatter vibration and improving the machining efficiency could be proposed. More specifically, the change of time chatter frequency induces the reduction of the magnitude of dynamic compliance, and it makes the vibratory system stable. Therefore, it is possible to increase the chatter stability by largely changing the chatter frequency [52, 73].

- **Spindle speed and thermal load of spindle motor**

Spindle speed variation techniques varies the spindle speed cyclically around a nominal speed, i.e., average speed. In order to change the spindle speed, it is necessary to change the spindle acceleration by changing the torque of the spindle motor. Each spindle motor has a certain limit on the acceleration that can be output, and if excessive acceleration is continuously outputted, a heat generation problem occurs in the electric spindle motor [82, 83]. It is an important issue that minimizing the heat of the electric spindle motor and extending the life of it.

In author's thesis, the new SSV profile is proposed to resolve the limitations of conventional SSV and improve the machining efficiency in Chapter 3. Considering the practicality and applicability at the manufacturing site, it is expected to obtain high machining efficiency under the same thermal load condition. In order to verify the effectiveness of the proposed SSV profile, the comparison with conventional SSV profiles was carried out in this criterion in Chapter 3. For comparing the machining efficiency, the material removal rate was calculated by utilizing the average spindle speed information from the directly measured signals of the spindle motor. Next, from the relation that the average of the square of the spindle acceleration is proportional to the average thermal load of the spindle motor, the thermal load of the spindle motor is calculated from the measured spindle speed. From the comparison, it was confirmed that the proposed SSV profile can achieve a higher machining efficiency, i.e., material removal rate (MRR), than the conventional SSV profiles under the same motor thermal load condition as shown in Fig. 3.15. Hence, the effectiveness of the proposed SSV profile was revealed out through the comparison from the measurement of spindle speed and thermal load of the spindle motor. Furthermore, the measured spindle speed was utilized for calculating the acceleration rate, which is the key parameter for suppressing chatter vibration with SSV. Specifically, the chatter frequency changes in proportion to acceleration rate, the compliance reduction effect increase with

a larger acceleration rate, and hence the greater chatter suppression effect can be obtained. In order to calculate the acceleration rate, the measured spindle speed was utilized to find the spindle speed before one revolution having the same spindle angle, and the ratio of present spindle speed to found previous spindle speed was calculated throughout the cutting process as shown in Fig. 3.16.

- **Cutting force**

The cutting force is essential to evaluate the cutting process because not only the cutting conditions but also the cutting tool and tool properties directly result in the cutting force fluctuations. In particular, the real-time monitoring techniques of the cutting force are very usefully utilized to figure out the stability of the cutting process and the progress of tool wear. The measurement of the cutting forces can be conducted by the dynamometer consisted of piezoelectric sensors that are clamped between two plates [84]. However, it is not desirable to be utilized in general manufacturing sites since the dynamometers are too expensive and there is often no space near the cutting point for their installation. In order to overcome the limitations, several studies have been conducted on indirect cutting force measurement [85-93]. For instance, the signals from the components of the machine tools such as the spindle drive system [86-88] and the feed drive system [89-91] have been utilized for estimating the cutting forces. In addition, those techniques were applied for monitoring the cutting process such as detection of the tool breakage [91] and the chatter vibration [92, 93].

In the author's thesis, the cutting force measurements were carried to identify the specific cutting force and cutting force ratio, which utilized for chatter stability analysis and time-domain simulations [52, 73]. Specifically, the specific cutting force denotes the generating cutting force per unit cutting area and the cutting force ratio denotes the ratio of principal directional cutting force and thrust directional cutting force. As shown in Fig. 2.2, both factors affect chatter stability, their information is essential for stability limit analysis and

time-domain simulations. Accurate cutting forces measurement determines the accuracy of the stability limit analysis and the time-domain simulations. As shown in [Fig. 2.11](#) and [Fig. 4.11](#), the results from the stability limit analysis and time-domain simulations were agreed well with the experimental results, and it denotes the accurate cutting forces measurement in the thesis.

- **Tool positions**

The error between the command value and the actual tool position during the cutting process affects the quality of the machined surface and fluctuations in the cutting force. For example, in plunge cutting, the feed rate of the tool determines the magnitude of the static cutting force, and hence accurate tracking is necessary. In particular, in the cutting process where the depth of cut is very small, the specific cutting force increases at a smaller depth of cut, which is called the 'size effect', and therefore accurate tool trajectory is more important.

In the author's thesis, in order to investigate the effectiveness of the proposed techniques, i.e., new SSV profile and accelerative cutting method, the command value of the tool position according to the time was calculated in advance using a developed simulator, and then the experiments were performed by implementing it on a machine tool. After that, internal information was acquired from the machine tool and the actual tool position and the command position were compared to verify the followability. In case the error occurs in the actual tool position, there may be a difference between the predicted chatter stabilizing effect of the proposed techniques and the actual effect. Therefore, conditions with good followability were selected to determine the experimental conditions. Particularly, in the cutting process with the accelerative cutting method, it is important to keep the acceleration rate until the tool is separated from the workpiece after the cutting for suppressing chatter vibration, and hence the accurate spindle speed and the tool position is more critical. As shown in [Fig. 3.12](#) and [Fig. 4.9](#), accurate tool positions and feed rates during the experiments were confirmed.

5.2 Real-World Data Circulation in High-Efficiency Cutting

In [Chapter 2](#), to clarify the reason for the temporal chatter growth in cutting with SSV and to propose the novel chatter stability indices of SSV, a series of experiments were conducted. At first, the cutting experiments were conducted to investigate the chatter growth characteristics of SSV. The measured acceleration vibration signals from the accelerometer during the cutting process were analyzed by short-time Fourier transform. From the results, it was clarified that the time chatter frequency changes, which means the spatial frequency is kept constant during the chatter in SSV. It was understood that the change of time chatter frequency causes the change of the magnitude of dynamic compliance, and the chatter can grow when the compliance reduction is not sufficient to suppress the chatter vibration. In addition, the fact that the time chatter frequency changes in proportion to the change of spindle speed was clarified. Since the larger change of spindle speed results in the larger change of time chatter frequency, the greater compliance reduction can be obtained, and hence the greater chatter suppression effect can be obtained. Based on the understanding, the chatter stability indices of SSV were proposed. In order to verify the validity of the proposed stability indices, the time-domain simulator was developed. In the simulator, the measured and calculated dynamic compliance, specific cutting force, and cutting force ratio from the experiments were utilized. Next, the relations between the SSV parameters and the chatter stability were investigated by utilizing the simulator, and the results were explained based on the proposed stability indices. Finally, the appropriate strategies for setting the SSV parameters for improving the chatter stability were explained. The cutting experiments were carried out again in order for confirming the validity of the proposed stability indices and the proposed strategies for setting the SSV parameters. Experimental results were coincided well with the results from the simulator. As a result, it was concluded that the author's

understanding of the temporal chatter growth in the cutting with SSV were proper, and the proposed chatter stability indices were effective, and hence the appropriate strategies for setting the SSV parameters were proposed. The illustration of RWDC in Chapter 2 is shown in Fig. 6.1.

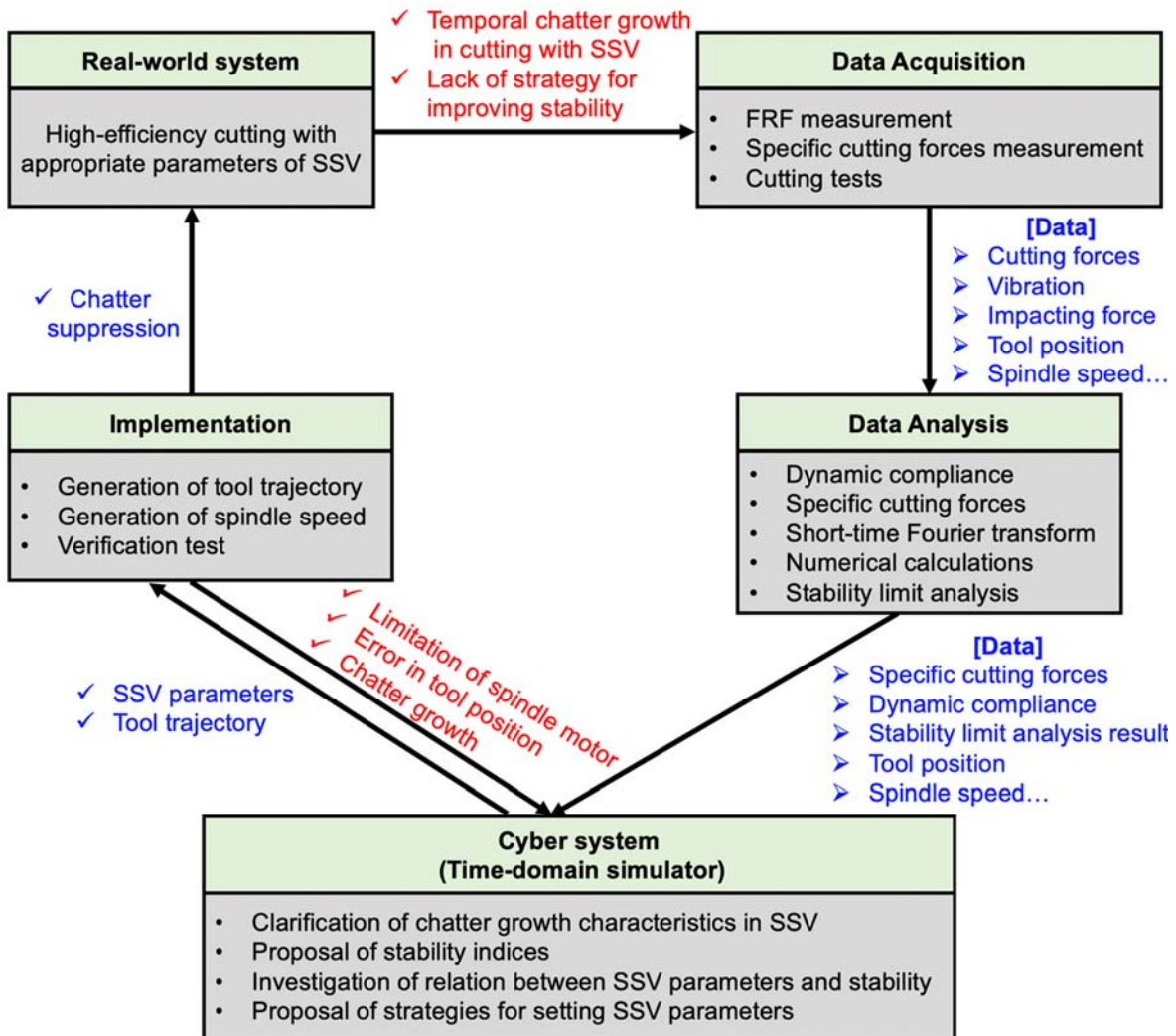


Fig. 6.1. Illustration of RWDC in Chapter 2.

In Chapter 3, the new SSV profile was proposed for improvement of chatter stability compared to conventional SSV. It has been found that conventional SSV profiles a limitation as follows: the acceleration rate always fluctuates in conventional SSV profile, and hence suppressing chatter in all sections of SSV is difficult since the magnitude of chatter suppression effect changes during the speed variation. Especially, the acceleration rate decreases in a high-speed region, and thus remarkable improvement of

machining efficiency cannot be realized. A novel SSV which maintains a constant absolute acceleration rate was proposed to overcome those limitation. Analytical investigation was conducted to reveal the potential of the proposed profile by utilizing the developed time-domain simulator. The higher stability was confirmed in the proposed SSV profiled under the same conditions of the stability indices. Moreover, the higher machining efficiency against the thermal load of the spindle motor in the proposed SSV profile could be achieved. For realizing the greater chatter suppression effect, the relations between the parameters of the proposed SSV profile and the chatter stability were investigated. A series of experiments were carried out to confirm the relations between the parameters of CAR-SSV and the stability as well as to verify the effectiveness of CAR-SSV. The experimental results were consistent with the results of the simulation. As a result, it was concluded that the proposed SSV profile is an effective solution to overcome the limitation of conventional SSV and it can realize higher applicability to the industry. The illustration of RWDC in [Chapter 3](#) is shown in [Fig. 6.2](#).

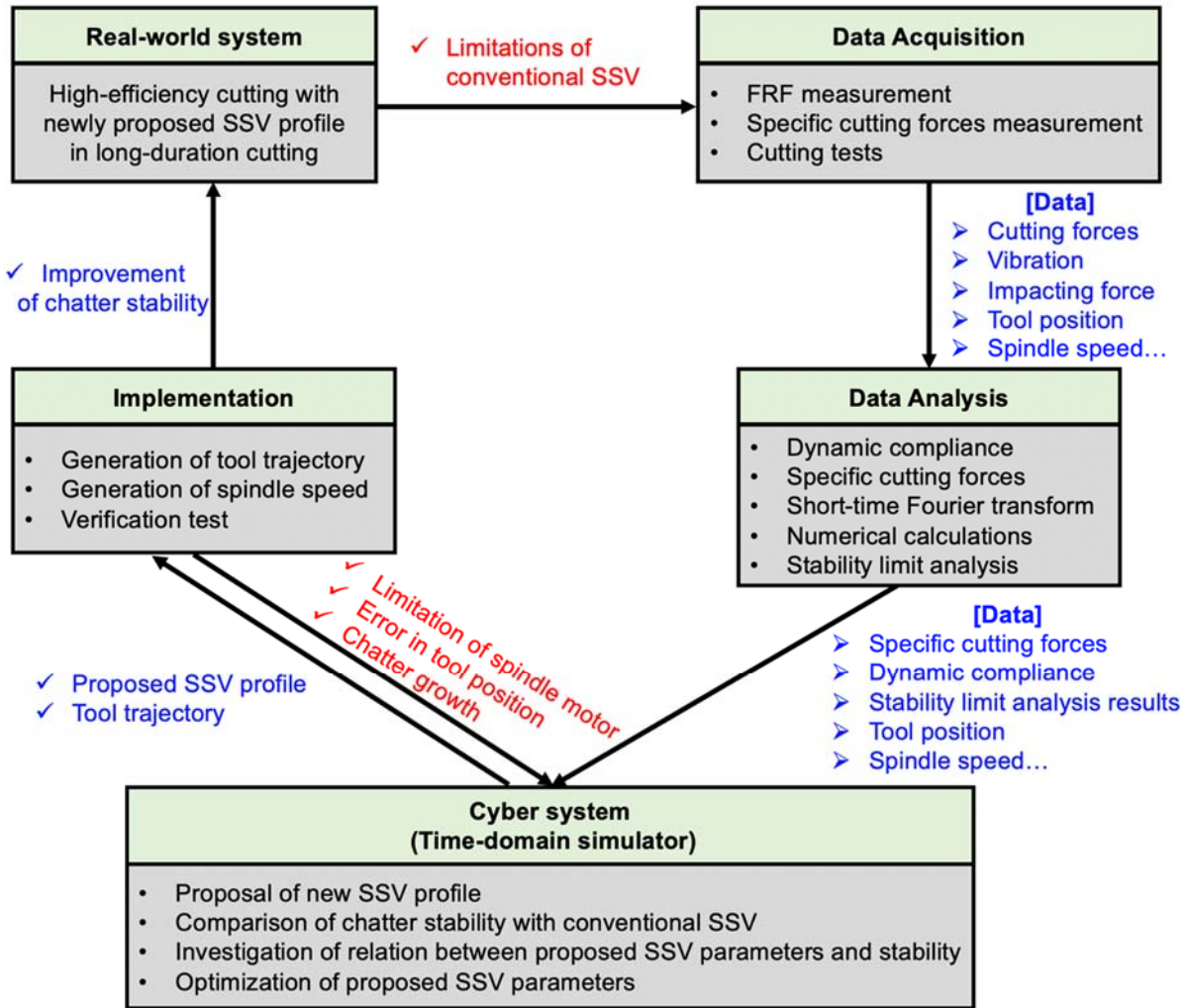


Fig. 6.2. Illustration of RWDC in Chapter 3.

In Chapter 4, a novel suppressive cutting method for regenerative chatter, namely ‘accelerative cutting’, was proposed. When SSV is used for long-duration cutting, the difference in spindle speed between the moments of present and one revolution before decreases in the sections of acceleration direction switches, in which the chatter suppression effect decreases in those sections. In the proposed accelerative cutting, the spindle speed is accelerated/decelerated in a unidirectional manner with a constant acceleration rate so that the speeds in the present and previous revolutions change at every moment causing suppression throughout the cutting. Since the limitation of spindle speed exists, the accelerative cutting can be utilized in short-duration cutting. However, there are numerous industrial needs for short-duration cutting, e.g., finishing of sealing, seating, and bearing surfaces, it can

be said that the scope of application of this technology is still wide. The limitation of SSV was investigated by utilizing time-domain simulations. The effectiveness of the accelerative cutting was verified through the same analytical and experimental verification methods introduced in Chapters 2 and 3. From the results, the increase of set acceleration rate causes a great increase of the stability limit. Specifically, it has been validated that stable cutting could be carried out at large widths of cut, e.g., 7 times larger than that of constant speed cutting. As a result, it was concluded that the proposed accelerative cutting method can be utilized for short-duration cutting and increase the stability drastically in practice. The illustration of RWDC in Chapter 4 is shown in Fig. 6.3.

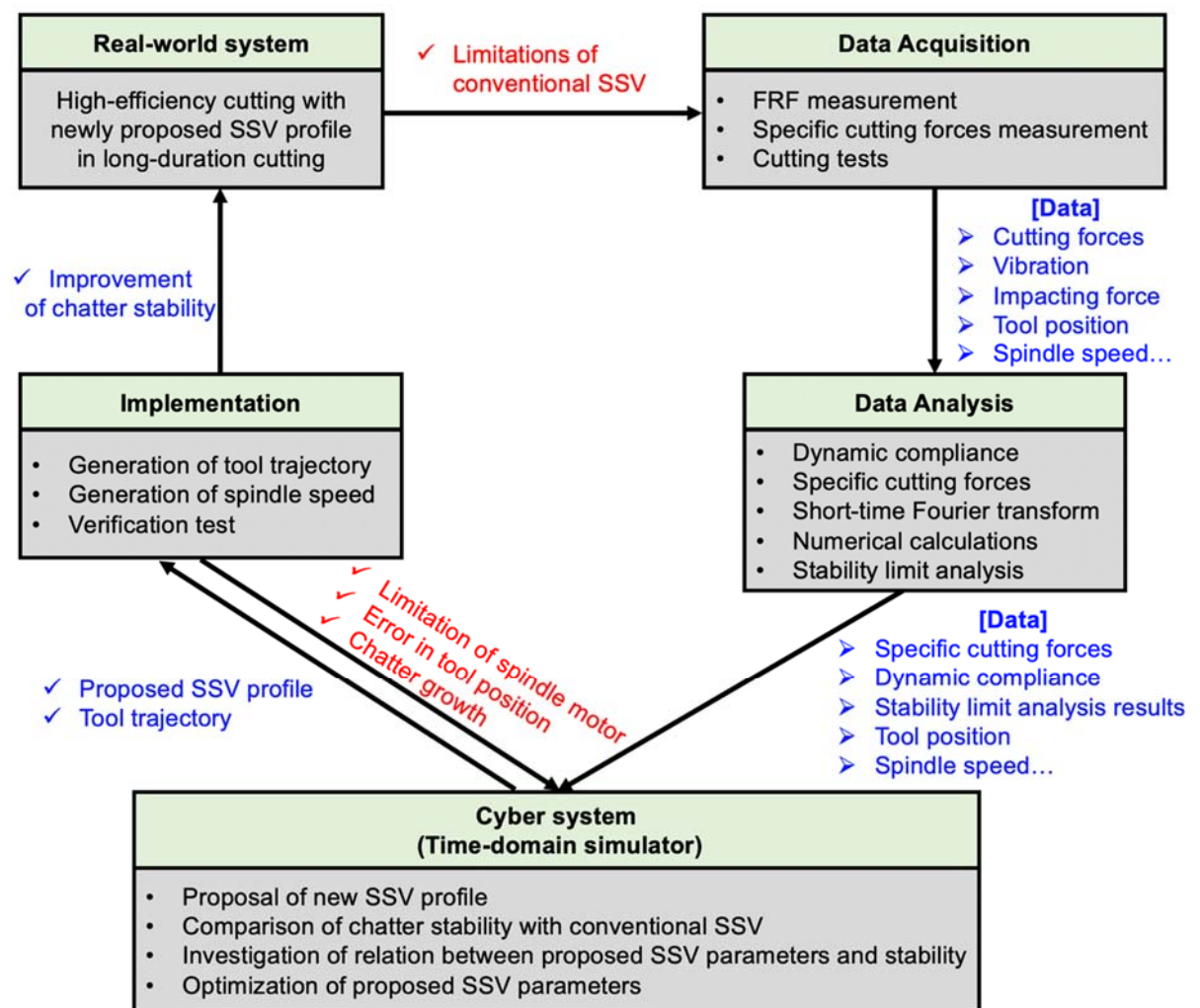


Fig. 6.3. Illustration of RWDC in Chapter 4.

5.3 Imagined future Real-World Data Circulation of researches in thesis

In this section, the imagined future RWDC for wide application and greater contribution to the manufacturing site of the researches described in the thesis is introduced. As described in [Section. 1.3](#), the integrations between information technologies, e.g., big data, information analytics, IoT, and monitoring technologies, and manufacturing technologies are encouraging the advent of the smart factory of Industry 4.0 [\[54\]](#). Through the appropriate design of Cyber-Physical Systems (CPS), the physical system to take proper action according to a certain purpose.

The previous studies that can show a better synergy effect by combining with the researches in the thesis were investigated. Spence et al. [\[94\]](#) presented CAD assisted adaptive control method for cutting process. It was possible to prevent the force overshoots during sudden part geometry changes by providing online information to the controller from the CAD model of part. Specifically, the maximum cutting force was predicted based on the geometric information obtained from the CAD of part model and cutting force model. Meanwhile, many kinds of methodologies to achieve the path planning of the cutting tool have been proposed. The most commonly utilized method is utilizing the recurrences of the trial-and-error cycle between the CAM data and real-world machining until it is competent. Unlike only geometric computational analysis of commercial CAM systems, Lazoglu et al. [\[95\]](#) introduced a new methodology to determine the optimum tool paths for free form surfaces. For optimizing the tool paths, it was included the mechanic of cutting process for minimizing the average cutting forces. By combining those technologies with the newly proposed SSV profile or accelerative cutting, it is expected that setting appropriated speed variation parameters can be selected based on the CAD/CAM and optimized tool path information and anticipated stability limit from speed variation techniques. The integration of virtual and on-line

machining process control and monitoring system was proposed [96]. In this research, the cutting forces were extracted from the feed and spindle drive motor current commands by compensating the distortion caused by the structural dynamics between the cutting and motor locations. By utilizing the techniques, it was possible to detect the tool failure and control the process more robustly. By integrating the real-time monitoring technologies [96-98] and the proposed speed variation techniques, it is expected that the condition of the cutting process, e.g., occurrence of chatter, excessive tool wear, and breakage of tool, can give real-time feedback for not only adjusting the speed variation parameters but also for changing the tool at the right time. Meanwhile, a neural network approach for predicting accurately both surface roughness and tool wear [99] as well as for optimizing the cutting parameters [100] were also studied. Specifically, as for the former, the experimental data of measured surface roughness and tool flank wear were utilized to train the neural network models, and the trained neural network models were used in predicting surface roughness and flank wear for various different cutting conditions [99]. As for the latter, the total time and cost for production, permissible range of cutting conditions, volume to be removed were utilized as input data, and then optimized cutting conditions such as spindle speed, feed rate, and depth of cut were outputted from the training [100]. There are tremendous data from the many machining tools and various types of the cutting process in the manufacturing sites. By utilizing those data effectively into the neural network models, the advanced cutting process can be realized. By incorporating the neural network model with the proposed technologies, it is expected that the more accurate speed variation parameters can be set by training to minimize the error between the expected stability and the actual stability.

Imagined future RWDC of researches in the thesis is shown in Fig. 6.4. First, based on the CAD/CAM information and the speed variation profile/tool trajectory generated from the cyber system, e.g., simulator and code generator, the input parameters are created. Second, the input parameters are mounted on a Real-world system, i.e., machine tool. By utilizing the sensors and

monitoring technologies, outputs during the cutting process such as the vibration cutting forces, and internal data of machine tool are acquired. Third, the acquired data are analyzed based on appropriate methods, whereby the cutting process is evaluated. Here, the generated profiles, input/output parameters, machine construction, machine dynamics, evaluated cutting process, and the estimated stability from the cyber system are all collected and analyzed using big data processing technology and neural network models. When troubles occur in the cutting process or chatter stability is insufficient, the input parameters and the speed variation profile are corrected by using artificial intelligence to give feedback to the machine tool and simulator. Particularly, the simulator can quickly modify the speed variation parameters based on the clarified relation between the stability and the parameters. By iterating those series of processes, it is expected that the optimized parameters setting method can be automatically designed. Therefore, it is speculated that the future RWDC of researches in the thesis can make a great contribution to the manufacturing sites for achieving high-efficiency, high-precision, low-cost, unmanned, and long tool life.

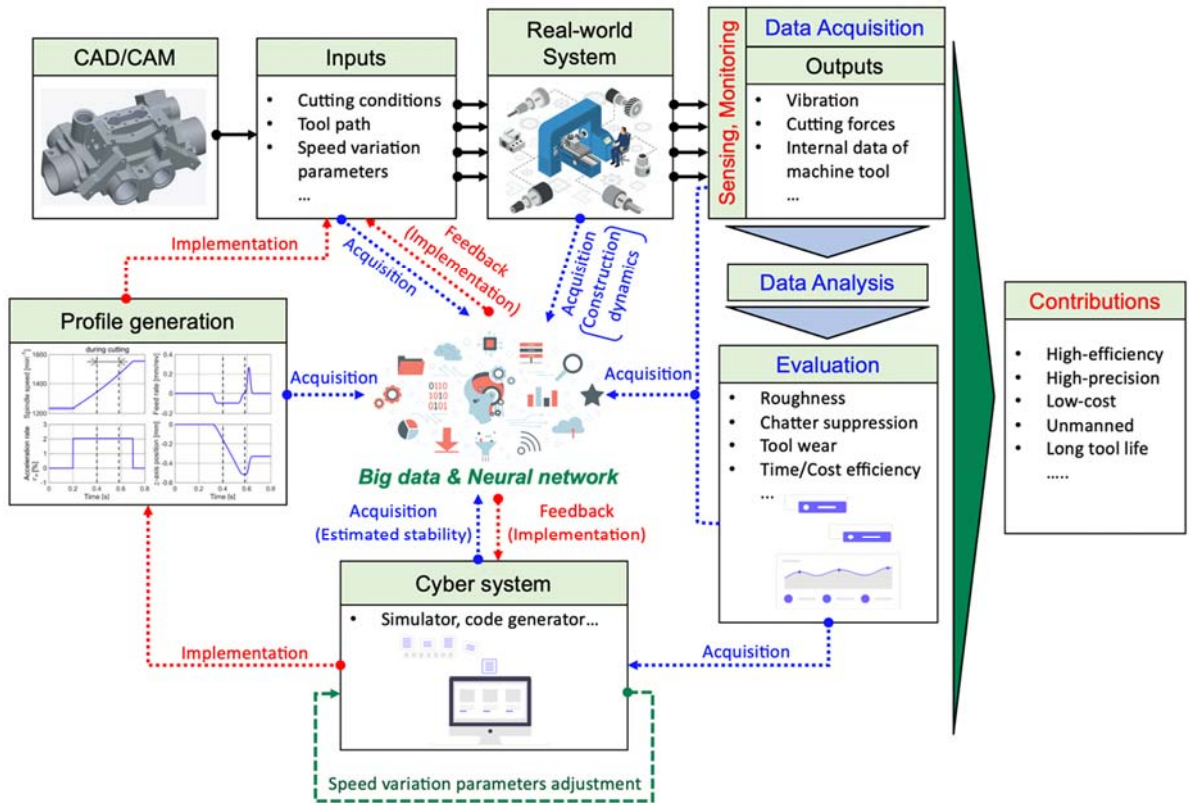


Fig. 6.4. Imagined future RWDC of researches in thesis

Chapter 6

Conclusions

For the suppression of the regenerative chatter without sacrificing the machining efficiency, the spindle speed variation (SSV) has been studied, where the speed is varied around the nominal spindle speed. This technique has been developed to utilize in production sites. Meanwhile, since the stability of SSV varies greatly depending on the SSV parameters, it is quite a complicated problem to determine the parameters properly. Furthermore, the temporal growth of chatter occurs even if SSV is applied and its reason was not clarified. For this problem, despite the fact that SSV is an effective technique, the industrial application has been limited because there is no simple and logical methodology to determine the parameters properly for the suppression of chatter and the improvement of the machining efficiency. To overcome these limitations and expand its applications in the industry, research on high-efficiency cutting with spindle speed variation is carried out in this thesis. The aims of this thesis are clarifying the characteristics of the chatter growth in SSV, proposing the chatter stability indices in SSV, proposing the novel spindle speed variation profile for improvement of chatter stability, and proposing new technology with speed variation for utilizing in the short-duration cutting process. The main contributions and findings are summarized as follows:

In [Chapter 1](#), the various types of chatter vibrations and the chatter suppression techniques were introduced. The past researches related to spindle speed variation were briefly overviewed. Subsequently, the motivation and objectives of this thesis were described. The meanings and roles of the Real-World Data Circulation to the manufacturing sites were also introduced.

In [Chapter 2](#), the chatter growth characteristics in SSV were revealed, and the suppression effect of SSV was newly explained focusing on the

fluctuation of the time chatter frequency. Even when SSV is applied, the regenerative chatter can grow with a considerably flexible structure. It was found in this study that the regenerative chatter generally grows at a constant spatial frequency in SSV (the first chatter growth characteristic). Therefore, when chatter occurs, the time chatter frequency changes at the same ratio in which the spindle speed changes, meaning that the spatial frequency is kept constant, and it brings out change of the magnitude of the dynamic compliance. Due to the change of the magnitude, the chatter can be suppressed since the dynamic compliance usually reduces as the chatter frequency changes. It was found that the chatter is likely to grow during a period where the absolute acceleration rate is small in SSV (the second chatter growth characteristic). Based on the reduction of the compliance, the average of the absolute acceleration rate in one period of SSV (the first stability index) and the number of revolutions in a unidirectional acceleration section (the second stability index) were proposed as novel indices to evaluate the chatter stability in SSV. Through the analytical investigations with time-domain simulation, it was proved that the revealed chatter growth characteristics are valid. In addition, the relations between the stability and the proposed stability indices were investigated, and the results denoted the effectiveness of proposed stability indices. Specifically, it was observed that the influence of the first stability index on the chatter stability is more dominant in comparison with the second stability index. Therefore, it is important to set appropriate SSV parameters so that the average of the absolute acceleration rate in one period of SSV is larger than the critical value which is required for the suppression of chatter throughout the cutting. Next, the influence of SSV parameters to stability were clarified. The chatter suppression effect of TSSV and SSSV decreases in high-speed region, and thus remarkable improvement of machining efficiency cannot be realized unfortunately. A series of experiments were carried out to verify the validity of the revealed chatter growth characteristics in SSV and to confirm the effectiveness of the proposed stability indices. The experimental results showed same tendency with the results in the time-domain simulations.

In [Chapter 3](#), a new SSV profile, which was named CAR-SSV (SSV with constant acceleration rate), was proposed to overcome the limitation of the chatter stability improvement in conventional SSV. Since the absolute acceleration rate is maintained a constant, chatter suppression throughout the cutting could be achieved. Analytical investigations were carried out to reveal the potential of the proposed profile. Firstly, the relations between the stability limit and the proposed stability indices in SSSV, TSSV, and CAR-SSV were investigated. From the results, the higher stability was confirmed in CAR-SSV under the same conditions of the stability indices. Secondly, the relations between the parameters of CAR-SSV and the chatter stability were revealed. Thirdly, the machining efficiency against the thermal load of the spindle motor in CAR-SSV was compared with the conventional SSV profiles to verify the effectiveness of CAR-SSV considering its applicability to the actual industry. From the results, it was confirmed that the higher machining efficiency can be achieved by utilizing CAR-SSV when the thermal load of the spindle motor is the same. A series of experiments were carried out to confirm the relations between the parameters of CAR-SSV and the stability as well as to verify the effectiveness of CAR-SSV. The experimental results were consistent with the results of the simulation. Therefore, CAR-SSV is an effective solution to overcome the limitation of conventional SSV and it denotes higher applicability to the industry.

In [Chapter 4](#), the ‘accelerative cutting’ was proposed to improve the chatter stability in short-duration cutting process. Due to the nature of SSV, the transitions from acceleration to deceleration exists regardless of the type of SSV. In these sections, the chatter easily grows since the absolute acceleration rate decreases. In accelerative cutting, the spindle is accelerated/decelerated in a unidirectional manner, and hence the direction of acceleration does not change. Thus, there is always a sufficient speed difference between the present and previous revolutions. In addition, the spindle is accelerated/decelerated so that the absolute acceleration rate is kept constant. Particularly, the set acceleration rate is kept above the critical

rate to achieve chatter suppression effect throughout the cutting. The time-domain simulations were conducted, and it was proved that the stability increases drastically by the accelerative cutting. Specifically, the increase of the set acceleration rate realized a great increase of the critical stability. Cutting experiments were carried out to verify the effectiveness of the accelerative cutting. It was validated that the stable cutting can be conducted at large widths of cut, e.g., 7 times larger than that of constant speed cutting. Therefore, it is expected that accelerative cutting can be utilized for short-duration plunge cutting and increase the stability drastically in practice.

In [Chapter 5](#), the utilized data and the applied Real-World Data Circulation in this thesis were described. In addition, the imagined future RWDC for wide application and greater contribution to the manufacturing site of the researches was introduced.

Based on the researches in the thesis, the chatter growth characteristics in SSV and the chatter stability indices were clarified for the first time. By proposing the new SSV profile and the accelerative cutting, the high-efficiency cutting without chatter in both long-duration and short-duration cutting can be achieved. Hence, this study is significantly contributed to expanding the applicability of cutting with speed variation techniques because of clarified understandings of chatter in those techniques and verified high-efficiency in proposed techniques.

References

- [1] Wiercigroch M, Budak E. Sources of nonlinearities, chatter generation and suppression in metal cutting. *Philosophical Transactions of the Royal Society of London. Series A: Mathematical, Physical and Engineering Sciences*. 2001 Apr 15;359(1781):663-93.
- [2] Munoa J, Beudaert X, Dombovari Z, Altintas Y, Budak E, Brecher C, Stepan G. Chatter suppression techniques in metal cutting. *CIRP Annals*. 2016 Jan 1;65(2):785-808.
- [3] Quintana G, Ciurana J. Chatter in machining processes: A review. *International Journal of Machine Tools and Manufacture*. 2011 May 1;51(5):363-76.
- [4] Arnold R. Cutting tools research: report of subcommittee on carbide tools: the mechanism of tool vibration in the cutting of steel. *Proceedings of the institution of mechanical engineers*. 1946 Jun;154(1):261-84.
- [5] Hahn RS. Metal-cutting chatter and its elimination. *Trans. ASME*. 1953 Aug;75(6):1073.
- [6] Doi S, Kato S. Chatter vibration of lathe tools. ASME, 1955.
- [7] Tobias S. The chatter of lathe tools under orthogonal cutting conditions. *Trans ASME*. 1958; 80:1079-85.
- [8] Tobias SA, Fishwick W. Theory of regenerative machine tool chatter. *The engineer*. 1958 Feb;205(7):199-203.
- [9] Altintas Y, Weck M. Chatter stability of metal cutting and grinding. *CIRP annals*. 2004 Jan 1;53(2):619-42.
- [10] Tlusty J. *Manufacturing Processes and Equipment*. (Prentice Hall, NJ). 2000.
- [11] Arnold R. Cutting tools research: report of subcommittee on carbide tools: the mechanism of tool vibration in the cutting of steel. *Proceedings of the institution of mechanical engineers*. 1946 Jun;154(1):261-84.
- [12] Hayasaka T, Jung H, Azuma K, Shamoto E. Consolidated chatter stability prediction model considering material removing and ploughing processes. *Precision Engineering*. 2019 Sep 1;59:120-33.
- [13] Tlusty J, Polacek M. The stability of the machine tool against self-excited vibration in machining. *Proc. Int. Res. in Production Engineering, Pittsburgh, ASME*. 1963;465-474.
- [14] Altintas Y, Ber AA. Manufacturing automation: metal cutting mechanics, machine tool vibrations, and CNC design. *Appl. Mech. Rev.* 2001 Sep 1;54(5):121-135.
- [15] Altintas Y, Eynian M, Onozuka H. Identification of dynamic cutting force coefficients and chatter stability with process damping. *CIRP annals*. 2008 Jan 1;57(1):371-4.
- [16] Budak E, Tunc LT. Identification and modeling of process damping in turning and milling using a new approach. *CIRP annals*. 2010 Jan 1;59(1):403-8.

- [17] Kaneko T, Sato H, Tani Y, O-hori M. Self-excited chatter and its marks in turnin. 1984: 222-228.
- [18] Marui E, Kato S, Hashimoto M, Yamada T. The Mechanism of Chatter Vibration in a Spindle-Workpiece System: Part1-Properties of Self-Excited Chatter Vibration in Spindle-Workpiece System. 1988: 236-241.
- [19] Marui E, Kato S, Hashimoto M, Yamada T. The Mechanism of Chatter Vibration in a Spindle-Workpiece System: Part2-Characteristics of Dynamic Cutting Force and Vibration Energy. 1988: 242-247.
- [20] Marui E, Kato S, Hashimoto M, Yamada T. The mechanism of chatter vibration in a spindle-workpiece system: Part3-Analytical considerations. 1988: 248-253.
- [21] Merritt H.E. Theory of self-excited machine-tool chatter: Contribution to machine-tool chatter research-1. 1965: 447-454.
- [22] Chandiramani NK, Pothala T. Dynamics of 2-dof regenerative chatter during turning. Journal of sound and vibration. 2006 Feb 21;290(1-2):448-64.
- [23] Dassanayake AV, Suh CS. On nonlinear cutting response and tool chatter in turning operation. Communications in Nonlinear Science and Numerical Simulation. 2008 Jul 1;13(5):979-1001.
- [24] Altintas Y, Budak E. Analytical prediction of stability lobes in milling. CIRP annals. 1995 Jan 1;44(1):357-62.
- [25] Tarnq YS, Kao JY, Lee EC. Chatter suppression in turning operations with a tuned vibration absorber. Journal of materials processing technology. 2000 Sep 7;105(1-2):55-60.
- [26] Marui E, Ema S, Hashimoto M, Wakasawa Y. Plate insertion as a means to improve the damping capacity of a cutting tool system. International Journal of Machine Tools and Manufacture. 1998 Oct 1;38(10-11):1209-20.
- [27] Xiao M, Karube S, Soutome T, Sato K. Analysis of chatter suppression in vibration cutting. International Journal of Machine Tools and Manufacture. 2002 Dec 1;42(15):1677-85.
- [28] Dombovari Z, Stepan G. The effect of helix angle variation on milling stability. Journal of Manufacturing Science and Engineering. 2012 Oct 1;134(5).
- [29] Otto A, Radons G. Frequency domain stability analysis of milling processes with variable helix tools. In9th International Conference on High Speed Machining 2012 Mar 7.
- [30] Altintas Y, Engin S, Budak E. Analytical stability prediction and design of variable pitch cutters. 1999: 173-178.
- [31] Budak E. An analytical design method for milling cutters with nonconstant pitch to increase stability, part I: theory. J. Manuf. Sci. Eng.. 2003 Feb 1;125(1):29-34.

- [32] Budak E. An analytical design method for milling cutters with nonconstant pitch to increase stability, part 2: application. *J. Manuf. Sci. Eng.*. 2003 Feb 1;125(1):35-8.
- [33] Hayasaka T, Ito A, Shamoto E. Generalized design method of highly-varied-helix end mills for suppression of regenerative chatter in peripheral milling. *Precision Engineering*. 2017 Apr 1;48:45-59.
- [34] Budak E, Ozturk E. Dynamics and stability of parallel turning operations. *CIRP annals*. 2011 Jan 1;60(1):383-6.
- [35] Brecher C, Epple A, Neus S, Fey M. Optimal process parameters for parallel turning operations on shared cutting surfaces. *International Journal of Machine Tools and Manufacture*. 2015 Aug 1;95:13-9.
- [36] Shamoto E, Mori T, Nishimura K, Hiramatsu T, Kurata Y. Suppression of regenerative chatter vibration in simultaneous double-sided milling of flexible plates by speed difference. *CIRP annals*. 2010 Jan 1;59(1):387-90.
- [37] Shamoto E, Fujimaki S, Sencer B, Suzuki N, Kato T, Hino R. A novel tool path/posture optimization concept to avoid chatter vibration in machining—proposed concept and its verification in turning. *CIRP annals*. 2012 Jan 1;61(1):331-4.
- [38] Tunc LT, Budak E. Effect of cutting conditions and tool geometry on process damping in machining. *International Journal of Machine Tools and Manufacture*. 2012 Jun 1;57:10-9.
- [39] Alan S, Budak E, Ozguven HN. Analytical prediction of part dynamics for machining stability analysis. *International Journal of Automation Technology*. 2010 May 1;4(3):259-67.
- [40] Zelinski P. How to Machine Aircraft Titanium: The 8-to-1 Rule for Finishing Walls and Ribs. *Modern Machine Shop*. 2009;2(4).
- [41] Takemura T. Active suppression of chatter by programmed variation of spindle speed. *J. JSPE*. 1975;41(5):489.
- [42] Inamura T, Sata T. Stability analysis of cutting under varying spindle speed. *J. Fac. Eng. Univ. Tokyo*. 1975 May;33(1):13-29.
- [43] Hoshi T, Sakisaka N, Moriyama I, Sato M, Higashimoto A, Tokunaga T. Study for practical application of fluctuating speed cutting for regenerative chatter control. *Annals of the CIRP*. 1977 Jan;25(1):175-9.
- [44] Sexton JS, Stone BJ. The stability of machining with continuously varying spindle speed. *Annals of the CIRP*. 1978 Jan;27(1):321-6.
- [45] Yamato S, Ito T, Matsuzaki H, Fujita J, Kakinuma Y. Self-acting optimal design of spindle speed variation for regenerative chatter suppression based on novel analysis of internal process energy behavior. *International Journal of Machine Tools and Manufacture*. 2020 Oct 15:103639.

- [46] Al-Regib E, Ni J, Lee SH. Programming spindle speed variation for machine tool chatter suppression. *International Journal of Machine Tools and Manufacture*. 2003 Sep 1;43(12):1229-40.
- [47] Seguy S, Insperger T, Arnaud L, Dessein G, Peigné G. On the stability of high-speed milling with spindle speed variation. *The International Journal of Advanced Manufacturing Technology*. 2010 Jun 1;48(9-12):883-95.
- [48] Yilmaz A, Al-Regib E, Ni J. Machine tool chatter suppression by multi-level random spindle speed variation. *J. Manuf. Sci. Eng.*. 2002 May 1;124(2):208-16.
- [49] Bediaga I, Munoa J, Hernández J, De Lacalle LL. An automatic spindle speed selection strategy to obtain stability in high-speed milling. *International Journal of Machine Tools and Manufacture*. 2009 Apr 1;49(5):384-94.
- [50] Urbikain G, Olvera D, de Lacalle LL, Elías-Zúñiga A. Spindle speed variation technique in turning operations: Modeling and real implementation. *Journal of Sound and Vibration*. 2016 Nov 24;383:384-96.
- [51] Otto A, Radons G. Application of spindle speed variation for chatter suppression in turning. *CIRP Journal of Manufacturing Science and Technology*. 2013 Jan 1;6(2):102-9.
- [52] Hayasaka T, Nam S, Jung H, Shamoto E, Saito K. Proposal of 'accelerative cutting' for suppression of regenerative chatter. *CIRP Annals*. 2018 Jan 1;67(1):401-4.
- [53] Sexton JS, Stone BJ. An investigation of the transient effects during variable speed cutting. *Journal of Mechanical Engineering Science*. 1980 Jun;22(3):107-18.
- [54] Wang S, Wan J, Li D, Zhang C. Implementing smart factory of industrie 4.0: an outlook. *International journal of distributed sensor networks*. 2016 Jan 19;12(1):3159805.
- [55] Shrouf F, Ordieres J, Miragliotta G. Smart factories in Industry 4.0: A review of the concept and of energy management approached in production based on the Internet of Things paradigm. In 2014 IEEE international conference on industrial engineering and engineering management 2014 Dec 9 (pp. 697-701). IEEE.
- [56] Lee J, Bagheri B, Kao HA. A cyber-physical systems architecture for industry 4.0-based manufacturing systems. *Manufacturing letters*. 2015 Jan 1;3:18-23.
- [57] Baheti R, Gill H. Cyber-physical systems. *The impact of control technology*. 2011 Mar;12(1):161-6.
- [58] Stone BJ. The effect on the chatter behavior of machine tools of cutters with different helix angles on adjacent teeth. In *Proc. 11th Int. MTDR Conf.* 1970 (pp. 169-180).
- [59] Sims ND, Mann B, Huyanan S. Analytical prediction of chatter stability for variable pitch and variable helix milling tools. *Journal of Sound and Vibration*. 2008 Nov 11;317(3-5):664-86.

- [60] Shamoto E, Kageyama K, Moriwaki T. Suppression of Regenerative Chatter Vibration With Irregular Pitch End Mill: Construction of Analytical Model and Optimization of Pitch Angle. In JSME Kansai Branch Annual Meeting 2002 (pp. 3-5).
- [61] Takemura T, Kitamura T, Hoshi T, Okushimo K. Active suppression of chatter by programmed variation of spindle speed. *CIRP Annals*. 1974; 23(1):121-122.
- [62] Tsao TC, McCarthy MW, Kapoor SG. A new approach to stability analysis of variable speed machining systems. *International Journal of Machine Tools and Manufacture*. 1993 Dec 1;33(6):791-808.
- [63] Insperger T, Stepan G. Stability analysis of turning with periodic spindle speed modulation via semidiscretization. *Journal of vibration and control*. 2004 Dec;10(12):1835-55.
- [64] Jayaram S, Kapoor SG, DeVor RE. Analytical stability analysis of variable spindle speed machining. *J. Manuf. Sci. Eng.*. 2000 Aug 1;122(3):391-7.
- [65] Albertelli P, Musletti S, Leonesio M, Bianchi G, Monno M. Spindle speed variation in turning: technological effectiveness and applicability to real industrial cases. *The International Journal of Advanced Manufacturing Technology*. 2012 Sep 1;62(1-4):59-67.
- [66] Suzuki N, Nishimura K, Shamoto E, Yoshino K. Effect of cross transfer function on chatter stability in plunge cutting. *Journal of Advanced Mechanical Design, Systems, and Manufacturing*. 2010;4(5):883-91.
- [67] Altintas Y. *Manufacturing Automation*. Cambridge University Press. 2012; p.139-142.
- [68] Zhu L, Liu C. Recent progress of chatter prediction, detection and suppression in milling. *Mechanical Systems and Signal Processing*. 2020 Sep 1;143:106840.
- [69] Lin SC, Hu MR. Low vibration control system in turning. *International Journal of Machine Tools and Manufacture*. 1992 Oct 1;32(5):629-40.
- [70] Mei Z, Yang S, Shi H, Chang S, Ehmann KF. Active chatter suppression by on-line variation of the rake and clearance angles in turning—principles and experimental investigations. *International Journal of Machine Tools and Manufacture*. 1994 Oct 1;34(7):981-90.
- [71] Wan S, Li X, Su W, Yuan J, Hong J. Active chatter suppression for milling process with sliding mode control and electromagnetic actuator. *Mechanical Systems and Signal Processing*. 2020 Feb 1;136:106528.
- [72] Dohner JL, Lauffer JP, Hinnerichs TD, Shankar N, Regelbrugge M, Kwan CM, Xu R, Winterbauer B, Bridger K. Mitigation of chatter instabilities in milling by active structural control. *Journal of sound and vibration*. 2004 Jan 6;269(1-2):197-211.

- [73] Nam S, Hayasaka T, Jung H, Shamoto E. Proposal of novel chatter stability indices of spindle speed variation based on its chatter growth characteristics. *Precision Engineering*. 2020 Mar 1;62:121-33.
- [74] Kondo Y, Kawano O, Sato H. Behavior of self-excited chatter due to multiple regenerative effect. 1981; 324-329.
- [75] Tlustý J. A method of analysis of machine tool stability. In *Proc. 6th MTDR 1965 (Vol. 5)*.
- [76] Slavicek J. The effect of irregular tooth pitch on stability of milling. In *Proceedings of the 6th MTDR Conference 1965 Sep (Vol. 1, pp. 15-22)*.
- [77] Hahn RS. Design of Lanchester damper for elimination of metal cutting chatter. *Trans. ASME*. 1951;73:331.
- [78] Insperger T, Stepan G, Namachchivaya SN. Comparison of the dynamics of low immersion milling and cutting with varying spindle speed. In *Proceedings of the ASME 2001 Sep (pp. 333-345)*.
- [79] Sexton JS, Milne RD, Stone BJ. A stability analysis of single-point machining with varying spindle speed. *Applied Mathematical Modelling*. 1977 Sep 1;1(6):310-8.
- [80] Jemielniak K, Widota A. Suppression of self-excited vibration by the spindle speed variation method. *International Journal of Machine Tool Design and Research*. 1984 Jan 1;24(3):207-14.
- [81] Otto A, Kehl G, Mayer M, Radons G. Stability analysis of machining with spindle speed variation. In *Advanced Materials Research 2011 (Vol. 223, pp. 600-609)*.
- [82] Bossmanns B, Tu JF. A thermal model for high speed motorized spindles. *International Journal of Machine Tools and Manufacture*. 1999 Sep 1;39(9):1345-66.
- [83] Mayr J, Jedrzejewski J, Uhlmann E, Donmez MA, Knapp W, Härtig F, Wendt K, Moriwaki T, Shore P, Schmitt R, Brecher C. Thermal issues in machine tools. *CIRP annals*. 2012 Jan 1;61(2):771-91.
- [84] Gautschi GH. Cutting Forces in Machining and Their Routine Measurement with Multi-Component Piezo-Electric Force Transducers. In *Proceedings of the Twelfth International Machine Tool Design and Research Conference 1972 (pp. 113-120)*. Palgrave, London.
- [85] Li X. Development of current sensor for cutting force measurement in turning. *IEEE Transactions on Instrumentation and Measurement*. 2005 Jan 17;54(1):289-96.
- [86] Chang YC. Cutting force estimation of spindle motor. *Journal of Control Systems and Technology*. 1995;3(2):145-52.
- [87] Haber RE, Peres CR, Alique A, Ros S, Gonzalez C, Alique JR. Toward intelligent machining: hierarchical fuzzy control for the end milling process. *IEEE Transactions on Control Systems Technology*. 1998 Mar;6(2):188-99.

- [88] Huh K, Jung JJ, Lee KK. A cutting force monitoring system based on AC spindle drive. In Proceedings of the 1998 American Control Conference. ACC (IEEE Cat. No. 98CH36207) 1998 Jun 26 (Vol. 5, pp. 3013-3017). IEEE.
- [89] Altintas Y, Peng J. Design and analysis of a modular CNC system. Computers in industry. 1990 Mar 1;13(4):305-16.
- [90] Altintas Y. Prediction of cutting forces and tool breakage in milling from feed drive current measurements. 1992; 386-392.
- [91] Lee JM, Choi DK, Kim J, Chu CN. Real-time tool breakage monitoring for NC milling process. CIRP annals. 1995 Jan 1;44(1):59-62.
- [92] Smith S, Tlustý J. Stabilizing chatter by automatic spindle speed regulation. CIRP annals. 1992 Jan 1;41(1):433-6.
- [93] Smith S, Tlustý J. Stabilizing chatter by automatic spindle speed regulation. CIRP annals. 1992 Jan 1;41(1):433-6.
- [94] Spence A, Altintas Y. CAD assisted adaptive control for milling. 1991; 444-450.
- [95] Lazoglu I, Manav C, Murtezaoglu Y. Tool path optimization for free form surface machining. CIRP annals. 2009 Jan 1;58(1):101-4.
- [96] Altintas Y, Aslan D. Integration of virtual and on-line machining process control and monitoring. CIRP Annals. 2017 Jan 1;66(1):349-52.
- [97] Liang SY, Hecker RL, Landers RG. Machining process monitoring and control: the state-of-the-art. J. Manuf. Sci. Eng.. 2004 May 1;126(2):297-310.
- [98] Rehorn AG, Jiang J, Orban PE. State-of-the-art methods and results in tool condition monitoring: a review. The International Journal of Advanced Manufacturing Technology. 2005 Oct 1;26(7-8):693-710.
- [99] Ozel T, Karpat Y. Predictive modeling of surface roughness and tool wear in hard turning using regression and neural networks. International journal of machine tools and manufacture. 2005 Apr 1;45(4-5):467-79.
- [100] Zuperl U, Cus F. Optimization of cutting conditions during cutting by using neural networks. Robotics and Computer-Integrated Manufacturing. 2003 Feb 1;19(1-2):189-99.

Publications Originated from this Thesis

JOURNAL PAPER

1. T. Hayasaka., **S. Nam.**, H. Jung., E. Shamoto., and K. Saito., Proposal of 'accelerative cutting' for suppression of regenerative chatter, *CIRP Annals*, Vol. 67, No. 1, pp. 401-404, (2018).
2. **S. Nam.**, T. Hayasaka., H. Jung., and E. Shamoto., Proposal of novel chatter stability indices of spindle speed variation based on its chatter growth characteristics, *Precision Engineering*, Vol. 62, pp. 121-133, (2020).
3. **S. Nam.**, T. Hayasaka., H. Jung., and E. Shamoto., Proposal of Novel Spindle Speed Variation Profile with Constant Acceleration Rate for Improvement of Chatter Stability, *Precision Engineering*, 2020 (Accepted).

INTERNATIONAL CONFERENCE

1. T. Hayasaka., **S. Nam.**, H. Jung., E. Shamoto., and K. Saito., Proposal of 'accelerative cutting' for suppression of regenerative chatter, *The 68th CIRP General Assembly*, Aug. 19-25, Tokyo, Japan, M10, (2019).
2. **S. Nam.**, T. Hayasaka., H. Jung., E. Shamoto., Proposal of novel chatter stability indices of spindle speed variation based on its chatter growth characteristics, *The 8th international conference on Virtual Machining Process Technology*, Apr. 23-25, Vancouver, Canada, #32 (2019).

Other publications

JOURNAL PAPER

1. **S. Nam.**, B. Eren., T. Hayasaka., B. Sencer., and E. Shamoto., Analytical Prediction of Chatter Stability in Low Frequency Vibration Assisted Turning, *International Journal of Machine Tools and Manufacture*, 2020 (Under review).

INTERNATIONAL CONFERENCE

1. **S. Nam.**, K. Lee., T. Hayasaka., E. Shamoto., One-dimensional chatter stability analysis and simplified FRF measurement for three-dimensional cutting, *The 20th Machining Innovations Conference for Aerospace Industry (MIC 2020)*, Dec. 2, Garbsen, Germany, (2020).

Acknowledgements

I here thank all the people who have supported me in any kind of way to complete my thesis research.

First of all, I would like to express my sincere gratitude and appreciation to my research supervisor, Dr. Eiji Shamoto for his invaluable inspiration and motivation throughout this thesis work. He has given me the chance to work on together when I was struggling with some troubles. He always instructed me with valuable and appropriate instruction, and always welcomed me whenever I want to discuss my research project as wells as personal issues. I have able to learn from him not only extensive knowledge but also the desirable attitude and think of way as a researcher. The teachings from him will be a great lesson in my entire life.

Next, I would like to express my sincere gratitude to Dr. Takehiro Hayasaka for his warming care of my life in the laboratory and helpful advice on conducting the research projects. He is one of the most passionate people I have ever met, he has always been willing to dedicate his time and effort to discussions with all the students. Every student including me have been able to make steady progress in their research activities thank to his dedication, and his close care makes a great support for a healthy research life. He was the best mentor during my doctoral course.

I will forever be thankful to Dr. Hongjin Jung for his great help not only in my laboratory life but also private life. He has always been exemplary as a senior in my laboratory, and he has been inspired me from the lots of conversations related to the research. Working with him has made my life in the laboratory enjoyable.

Besides my advisors, I am grateful to Dr. Kenji Fukuzawa, Dr. Daisuke Tsubakino, Dr. Tatsuya Suzuki, and Dr. Takashi Nakamura for their help in accomplishing my thesis. They have helped me brush up on my thesis and

gave me essential comments on my research, which helps to think about my research in different ways.

I wish to thank Dr. Takashi Ueda, Mr. Shunsuke Fujimaki, and Mr. Yudai Mizutani for their help in my laboratory life and precious comments and discussions in and out of the research. I would like to heartily thank to Mr. Takahiro Sakai for his assistance in experiments. Not to mention, I would like to express my sincere thanks to Ms. Tomoko Ishihara, Ms. Megumi Takaya, and Ms. Rieko Itoh for their kind supports in many ways including office procedures needed at the university and also their warming words.

My sincere thanks also go to Mr. Katsuhisa Saito and Mr. Shoichiro Manda from Denso-Daishin Corp. for their technical support in experiments on the research project of 'proposal of accelerative cutting'. Next, I am grateful to Mr. Akihide Hamaguchi and Mr. Noriyuki Fujise for their dedicated support in experiments on the research project of 'proposal of new SSV profile'. I also sincerely thanks to Dr. Mitsunori Hirose for the numerous discussions and technical support in the current research project.

It is needless to say that I am thankful to all of my colleagues in the Manufacturing Engineering Research Group for not only sharing their knowledge and experience with me and encouraging me in laboratory life. I particularly would like to thank Mr. Kota Aoyama, Mr. Keigo Miyagawa, Mr. Kentaro Hisanaga, Mr. Kensuke Suzuki, and Mr. Kyunki Lee for the conversations they held with me about research and private life, which have made my life in the laboratory enjoyable.

I am grateful to the funding not only for my research but other valuable activities from the graduate program for "Real-World Data Circulation Leaders" in Nagoya University as they hired me as a research assistant. I would like to particularly thank Dr. Kazuya Takeda, Dr. Katashi Nagao, Dr. Hiromi Nakaiwa, Dr. Ichiro Ide, Dr. Leo Iijima, Dr. David Wong, and Dr. Nagoki Nishida for their valuable time and effort to give me the helpful advices for being a leader. I could learn lots of knowledge and have experienced through the excellent

curriculum not only focused on the coursework but combined with lots of real-world works such as industry internship and oversea study.

I am very grateful to Dr. Burak Sencer for letting me study at the University of Oregon State University in the United States for 7 months. I also would like to sincerely thanks Mr. Eren Bora and Mr. Eddy Lee for not only their kind supports in many ways for life in the United States but also for helping to conduct research at Oregon State University.

Finally, words cannot express the feelings I have for my father Mr. Kiwon Nam, my mother Mrs. Miok Son, and my brother Mr. Woohyun Nam for their endless unconditional love, encouragement, and supports at every step of my personal and academic life.